TR- 60
1974

An Investigation of the Return Flow from Irrigated Land

K.W. Brown
C.J. Gerard
D.W. DeMichele
P.J.H Sharpe
B.W. Hipp

Texas Water Resources Institute

Texas A&M University

RESEARCH PROJECT COMPLETION REPORT

Project Number B-148-Tex

July 1, 1972 - January 31, 1974

Agreement Number

14 - 31 - 001 - 3940

AN INVESTIGATION OF THE RETURN FLOW FROM IRRIGATED LAND

Principal Investigators

K. W. Brown
C. J. Gerard
D. W. DeMichele
P. J. H. Sharpe
B. W. Hipp

The work upon which this publication is based was supported in part by funds provided by the United States Department of the Interior, Office of Water Resources Research, as authorized under the Water Resources Research Act of 1964.

Technical Report No. 60
Water Resources Institute
Texas A&M University

September 1, 1974

TABLE OF CONTENTS

Appendix D: Supplemental Information for Chapter 4

CHAPTER 3

Model of Soil Moisture Movement

Contribution
by
Charles N. Schroeder
Don DeMichele

SUMMARY

The emphasis of this research was directed to the problem of developing an optimal, yet comprehensive, model for the transfer of heat and moisture within soils. Also modeled were the surface-atmosphere interface and the effects of the atmosphere on soil conditions.

The basic equations of de Vries [8] were used for the subsurface heat and moisture flow. These basic equations, along with the properties of soil physics and numerical techniques, were used in modeling the soil surface. The model does not neglect any known properties affecting heat and moisture transfer.

A unique solution technique was developed for solving the system of equations involved. The second derivative terms involved were not approximated using the classical finite difference approach. Instead, the Divergence Theorem was applied to the second order terms, reducing these terms to first order derivatives. Approximations were then used for evaluating these first-order terms.

Verification of the model was done using the results of a study done by Philip [28]. Further verification was done using sample data collected by the Soil Science Department at Texas A&M University to the extent that this data was valid. In each case, the model proved to be quite accurate in its predictions and expected results.

Throughout the programming phase of the model, execution time efficiency was emphasized. Where possible, calculations from previous steps were saved for future use to prevent repetition of calculations. Arrays of pointers were used extensively to prevent recalculation of these values at each iteration. Multiple subscripts were not used and care was exercised in eliminating unnecessary steps. Execution efficiency was sacrificed on a few occasions to make modifications and initialization easier for the user.

Included in Appendix C-7 and C-4 are a complete program listing and a comprehensive User's Guide. Included in the User's Guide is a detailed example, with suggestions to the user and a guide to the initilization of required values. A description of the logic used is given in Appendix C-2.

Although the study of soil properties has advanced rapidly during the past few years, further research is needed, especially in the area of the soil-atmosphere interface. Other investigations that would improve the accuracy and reliability of the model developed would include further studies on the soil surface and the effects of this layer on moisture movement.

Among the "whistles and bells" which could be added to the developed model are the following:

1. During rainfall or surface irrigation, the occurrence of puddles on the soil surface could be calculated and the effects of these water sources on the moisture and heat content could be included in the resulst of the model.

2. Specific inclusions of the effects of a crop above the soil surface. This is currently handled by the model via user-provided values for solar input and boundary layer resistance, and air temperature.

3. For bare soils, the location of the sun with respect to the soil surface could be included. The model developed assumes the solar input is perpendicular to the soil surface.

4. The output of this model can be used in conjunction with chemical models for obtaining a complete simulation of all soil characteristics. If another phase of crop development, specifically the simulation of crop development above the surface and the root development in the soil, could be modeled, it is plausible that a model for all phases of crop growth and development could developed.

1. INTRODUCTION

The recent trend toward improvement of the environment and the necessity for increased productivity of the land to meet requirements of ever-increasing population has stimulated renewed interest in soil physics. This interest is especially noticeable with respect to the areas of crop production and the proper disposal of waste material. One phase of soil physics of particular interest to both of these areas involves the movement of water in the soil and the effects of temperature gradients upon this movement.

The need of a good computer model for predicting the flow of water is twofold. First, a predictive model can be used for management decisions in crop production. Such decisions are concerned with the quantity and timing of irrigation. In environmental control, predictions with respect to water and waste transport within the soil are needed.

Secondly, predictive information about water and heat transfer are important in scientific studies. An area of interest where there is particular activity at this time is in analysis of the transfer of chemicals in the soil in conjunction with water movement. This is of special interest with respect to fertilizer applications as well as the chemical processes which take place in the soil via waste products, both treated and untreated.

There have been some attempts to model the flow of moisture and heat. However, most of these models appear to be very inefficient and very restrictive with respect to the variety of conditions what can be simulated. Specific examples include neglect of temperature influences, assuming uniform soil (i.e., no soil layers), and neglecting the effects of atmospheric condition.

The simulation model developed in this research is a user-oriented experimental tool. It was specifically designed for use in research and is far more comprehensive than any model developed to date.

The model itself is for two-dimensional flow

of moisture and temperature. It permits the user to define an irregular shaped surface and has an automatic grid routine which fits a grid to the shape of the surface. The model is set up to handle the influences of rainfall, subsurface sources or sinks, wind, sunshine, and solar energy. Multiple soil layers are also allowed and the user has the option of specifying the surface temperature or having these values calculated. The user may also set specific widths for the rows in the grid which are below the soil surface.

The code has been optimized in an effort to reduce execution time and to save space as much as possible. Time steps for calculations are determined by the program based on the amount of temperature and moisture changes which occurred in the previous iteration. If the time step chosen is too large to handle large moisture or temperature gradients, a routine for overlaying the rows having the large gradients with a much finer grid has been developed. This routine conserves moisture and heat in determining the new temperature and moisture values associated with the elements in the fine grid network set up.

This routine would normally be necessary only if a moisture or temperature front is moving through the soil as a result of rainfall or large sources and sinks. After the overlay routine has been used, all rows are restored to their previous size for further calculations.

The object code for a grid network with 40 rows and 30 columns can be run using less than 132 K of core on the IBM 360/65. Using symmetry and the provision for special layer sizes, this grid could represent an area of 60 cm. x 90 cm. Execution time to simulate both heat and moisture transfer for 1 full day would be around 30 minutes. A similar network with 40 rows and 90 columns can be run using less than 200 K of core.

1.1 Heat and Moisture Flow

Within the soil, the transfer of heat and moisture is a highly complex phenomenon. Not only does the quantity of water present, in both liquid and

vapor form, and the temperature of the soil affect this flow, but further effects are realized from the moisture and temperature gradients. Other factors, such as soil type, surface characteristics, the existance of subsurface sources and sinks (roots), as well as gravity have some effect on the overall movement of moisture and temperature. Environmental factors such as net radiation, air temperature, humidity and wind also enter the total picture.

De Vries [8] has presented a most comprehensive study of the transfer of heat and moisture in porous media. His fundamental approach is an extension of an earlier paper by Philip and De Vries [29] that involves a system of non-linear partial differential equations. These equations incorporate the major influencing factors that influence heat and moisture flow. However, sources and sinks and the environmental factors mentioned above are not included.

1.2 Computer Simulation

The simulation of a system, where, according

to Gordon [15], a system is an aggregation of objects joined in some regular interaction or interdependence, can take many forms. In general a simulation is either a physical or mathematical model. Mathematical models involve the use of variables and functions that inter-relate the variables under consideration [15]. Generally, physical models are considered as being scale models. Models can be further classified as either deterministic or stochastic. Deterministic models are those models where the results can be determined completely in terms of the input. When results of an activity vary randomly over various outcomes, the model is referred to as a stochastic model [15].

System simulation involves determining changes, usually considered with respect to time, which take place in the response of a mathematical model due to either internal or external stimuli. Systems may also be classified as either discrete or continuous. Continuous systems involve continuous equations which illustrate changes of system attributes with respect to time. Discrete systems in-

volve discontinuous changes in the state of the system and are concerned with events producing these changes.

1.3 Efficient Programming Techniques

One of the main goals in programming this model was to minimize the execution time. By optimizing the code and thereby reducing the execution time, it becomes feasible to have a more complex model than has been developed to date without imposing additional costs upon the user.

2. REVIEW OF THE LITERATURE

Klute [23] summarized the importance of the influence of the moisture and energy of soil water on the physical and chemical processes, taking place in the soil, by noting that this influence is important to anyone interested in the formation and the development of soils, the growth and development of plants in soils, or the mechanical and engineering properties of the soil. He further stated that the water content and associated energy state of the soil water at a given location are generally determined by the physical processes of water movement, as well as by other processes (i.e., biological, physical, or chemical) which locally produce or consume water. Since water transport influences so many processes within the soil, an understanding of these phenomena is of importance [23].

Philip and de Vries [29] discussed the movement of water in porous media under the influence of gradients of temperature and moisture content. They presented a set of partial differential equations describing simultaneously heat and moisture

transfer. These equations are summarized in Table 1. In a subsequent paper, de Vries [8] extended the approach, and developed simultaneous differential equations for the transfer of heat and moisture in porous media under the combined influence of gravity and gradients of temperature and moisture. The noticeable difference in the two papers is the inclusion of the effects of moisture content in the vapor phase assumed to be negligable in the first paper. See Table 2 for the summary of the equations used by de Vries.

Rubin [36] carried out a Darcian-approach analysis (i.e., based on Darcy's law for the flow of water through soils) of two-dimensional water transfer in unsaturated and partially unsaturated soils. He demonstrated the significance of the vertical flow component occuring in horizontal moisture infiltration and the effect of gravity on hydraulic conductivity. Klute [23], however, noted that the Darcian-approach is strictly applicable to a very idealized medium and not useful for the general soil model. In Table 3 the equations used by Rubin are summarized.

TABLE I. Equations of Philip and de Vries [29]

Equation describing moisture movement

$$\frac{\partial \theta}{\partial t} = \nabla\cdot(D_T \quad \nabla T) + \nabla\cdot(D_\theta \quad \nabla\theta) + \frac{\partial K}{\partial z}$$

Equation for heat conduction

$$C\frac{\partial T}{\partial t} = \nabla\cdot(\lambda\nabla T) - L\nabla\cdot(D_{\theta vap}\nabla\theta)$$

Symbols used

C	volumetric heat capacity of the soil
D_θ	isothermal moisture diffusivity
$D_{\theta vap}$	isothermal vapor diffusivity
L	heat of vaporization of water
D_T	thermal moisture diffusivity
∇	gradient
K	hydraulic conductivity
θ	liquid moisture content
T	temperature
λ	thermal conductivity (including the thermal distillation effect)
z	vertical coordinate

TABLE II. Equations of de Vries [8]

Equation for moisture movement

$$(1 + \frac{D_{\theta v}}{\alpha \nu D_{atm}} - \frac{\rho_v}{\rho_\ell}) \frac{\partial \theta_\ell}{\partial t} + \frac{(S - \theta_\ell) h \beta}{\rho_\ell} \frac{\partial T}{\partial t}$$

$$= \nabla \cdot (D_\theta \nabla \theta_\ell) + \nabla \cdot (D_T \nabla T) + \frac{\partial K}{\partial z}$$

Equation for heat transfer

$$(C + L(S - \theta_\ell) h \beta) \frac{\partial T}{\partial t} + (\frac{L \rho_\ell D_{\theta v}}{\alpha \nu D_{atm}} - L \rho_v + \rho_\ell j^{-1} g (\psi - T \frac{\partial \psi}{\partial T})) \frac{\partial \theta_\ell}{\partial t}$$

$$= \nabla \cdot (\lambda_* + L \rho_\ell D_{Tv} \nabla T) + L \rho_\ell \nabla \cdot (D_{\theta v} \nabla \theta_\ell)$$

$$+ \rho_\ell c_p ((D_{\theta v} \nabla \theta_\ell + D_{Tv} \nabla T) \nabla T)$$

$$+ \rho_\ell c_\ell ((D_{\theta \ell} \nabla \theta_\ell + D_T \nabla T + Kk) \nabla T)$$

Symbols used

a	volumetric air content
c_p	specific heat of water vapor at constant pressure
c_ℓ	specific heat of liquid water
C	volumetric heat capacity of moist porous medium
C_d	volumetric heat capacity of dry porous medium
D_{atm}	molecular diffusion coefficient of water vapor in air
$D_T = D_{T\ell} + D_{Tv}$	thermal moisture diffusivity
$D_{T\ell} = K\gamma\psi$	thermal liquid diffusivity
$D_{Tv} = fD_{atm}\nu\beta h(\nabla T)_a / \rho_\ell \nabla T$ (with $f = S$ for $\theta_\ell < \theta_{\ell K}$, $f = a + a\theta_\ell/(S - \theta_{\ell K})$ for $\theta_\ell > \theta_{\ell K}$)	thermal vapor diffusivity
$D_\theta = D_{\theta\ell} + D_{\theta v}$	isothermal moisture diffusivity
$D_{\theta\ell} = K(\frac{\partial \psi}{\partial \theta_\ell})$	isothermal liquid diffusivity

TABLE II. Equations of de Vries (Continued)

Symbols used

$D_{\theta v} = \alpha a D_{atm} \nu g \rho_v (\partial \Psi / \partial \theta_\ell) \rho_\ell RT$ isothermal vapor diffusivity

E rate of evaporation

g acceleration due to gravity

h relative humidity

j mechanical equivalent of heat

k unit vector in vertical direction

K unsaturated hydraulic conductivity

L heat of vaporization

p partial pressure of water vapor

P total gas pressure

R gas constant of water vapor

S porosity

t time

T absolute temperature

x horizontal coordinate

z vertical coordinate

α tortuosity factor for diffusion of gases in soils

$\beta = d\rho_0 / T$

γ temperature coefficient of surface tension of water

θ_ℓ volumetric liquid content

$\theta_{\ell K}$ value of θ_ℓ at which liquid continuity fails

λ thermal conductivity

λ^* hypothetical thermal conductivity

$\nu = P/(P-p)$ mass flow factor

ρ_v density of water vapor

ρ_0 density of saturated water vapor

ρ_ℓ density of liquid water

Ψ water pressure, with atmospheric pressure as datum

TABLE III. Equations of Rubin [36]

Flow of water equation

$$C(H - z)\frac{\partial H}{\partial t} = \frac{\partial}{\partial x}(K(H - z)\frac{H}{x}) + \frac{\partial}{\partial z}(K(H - z)\frac{\partial H}{\partial z})$$

Symbols used

$C(H - z) = \frac{\partial w}{\partial h}$ = slope of the soil's water-retention curve

H = hydraulic head

t = time

x = horizontal coordinate

z = vertical coordinate

K = soil's hydraulic conductivity

h = water pressure head

w = w(h) = volumetric water content

Fitzsimmons [11] developed a numerical model for simulating unsteady radial flow in partially saturated soils. His solution, based on a non-linear, parabolic differential equation, included the effects of imbibition (i.e., a wetting process). The results of this model when compared with laboratory results, indicated close agreement. See Table 4 for the equation of Fitzsimmons.

Rose [35], using the basic equations of de Vries [8], isolated terms in the equation which had little effect on the overall moisture flow and neglected these terms in his calculations. His results, compared with the results of laboratory experiments, indicated that daytime temperature and pressure gradients are steeper than at night and that for shallow depths the water content in the soil by day is less than by night. He also noted that the vapor flux reversed direction from downward by day to upward by night. The basic equations used by Rose for his comparisons with the laboratory results are presented in Table 5.

Other models developed deal with some of the "other" influences upon heat and moisture flow.

TABLE IV. Equations of Fitzsimmons [11]

Equation for moisture flow

$$\frac{\partial S}{\partial t} = \frac{1}{r} \frac{\partial}{\partial r} \left(rD \frac{\partial S}{\partial t} \right)$$

Symbols used

$D = - \frac{K \rho g}{\mu f} \frac{\partial h_c}{\partial S}$ = diffusivity coefficient

K = effective permeability of the soil

ρ = fluid density

g = acceleration due to gravity

μ = fluid viscosity

f = porosity of the soil

h_c = capillary pressure head

S = liquid saturation value

r = horizontal coordinate

t = time

Specifically, de Vries [9] performed a theoretical analysis of the effect of irrigation on the temperature of the lower air layers and on the energy balance of the surface. It should be emphasized that his estimates, although theoretical, include the importance of irrigation. Similarly, Hanks, et al. [18], investigated the effects of evaporation of water from soils and the effects of drying by wind and radiation. The effects of wind in cooling and radiation in heating the soil were included in this latter study.

Bouwer [2], in another theoretical study, investigated the aspects of unsaturated flow in drainage and subirrigation. This two-dimensional flow analysis included the hypothetical conductivity-tension relationship, as well as the effect of subirrigation flow.

Rose [34], using a one-dimensional model, considered the uptake of moisture from the atmosphere by dry soil. In this paper he included both theoretical as well as experimental results relating to water transport resulting from temperature gradients, soil water suction and gravitational

TABLE V. Equations of Rose [35]

Moisture flow equation

$$\nabla\cdot(D_\Theta \nabla\Theta_\ell) + \nabla\cdot(D_{T\ell}\nabla T) + \nabla\cdot(D_{Tv}\nabla e_s) - \frac{\partial K}{\partial z}$$

$$= \left(1 + \frac{D_{\Theta v}\varepsilon_T}{\xi f(\varepsilon) D_a} - \frac{\rho_v}{\rho_\ell}\right)\frac{\partial\Theta_\ell}{\partial t} + \frac{(\varepsilon_T - \Theta\ell)h_r\beta}{\rho_\ell}\frac{\partial T}{\partial t}$$

Symbols used

T = temperature
∇ = gradient
D_Θ = $D_{\Theta\ell} + D_{\Theta v}$
Θ_ℓ = volumetric water content
$D_{T\ell}$ = thermal liquid diffusivity
D_{Tv} = thermal vapor diffusivity
$f(\varepsilon)$ = ratio of diffusion coefficients
e_s = saturation vapor pressure of water
K = hydraulic conductivity
z = vertical coordinate
$D_{\Theta\ell}$ = isothermal liquid diffusivity
$D_{\Theta v}$ = isothermal vapor diffusivity
ε_T = total porosity of dry soil
ξ = vapor flux factor
D_a = molecular diffusion coefficient of water vapor in air
ρ_v = density of water vapor
ρ_ℓ = density of liquid water
h_r = relative humidity
β = $\frac{d\rho_0}{dT}$
t = time

potential. It should be noted, however, that this model is a highly artificial approach to more realistic events within the soil.

Nimah and Hanks [5] presented a complex model for estimating soil water, plant and atmospheric interrelationships. This model included a numerical solution for predicting water content profiles, evapotranspiration, water flow from or to the water table and the effects of plant roots, however, ignoring hysteresis and layered soil. This model was tested under field conditions, with some minor disagreement between water content profiles over 24 and 72 hour periods, however, the measured and predicted values were in almost complete agreement after longer time periods.

Dutt, et al. [10] developed a computer simulation model for some of the environmental and managerial factors on soil-water plant systems. A specific purpose of this model was to determine and predict the effects of irrigation over long periods of time. While this model is useful in predicting very general results using monthly and semi-monthly time periods, it is much too general

to predict moisture and heat transfer over shorter periods of time. The model, restricted to only linear flow for simplicity, is valuable for long range predictions of the effects of irrigation.

Computers have been used in several other developed models, however, in most cases the computer usage has been chiefly for ease of calculation (e.g., Remson, et al. [30]). Hanks and Bowers [17], however, developing one of the first general computer models utilizing the IBM 650, included provisions for non-homogeneous soil (two layers), gravity, two-dimensional moisture flow, and varying initial moisture content. A major drawback of this model is that no effects of temperature were considered, making the solution rather artificial. The results of the model compared favorably with the results of Scott, et al. [37] and Philip [28] although no experimental evidence was used to verify the model. The model developed by Scott, et al. [37] is a linear model while the model of Philip [28] treated vertical infiltration, making the latter comparison perhaps more valuable.

3. DESIGN OF THE MODEL

3.1 Simulation Models

The interest of this research was in the development of an efficient simulation model for predicting the physical state of soils under various interrelated and dependent conditions. Gordon [15] pointed out that the "simulation" technique observes the way in which the variables of a model change with time. The relationship of these variables must be derived from such observations, therefore, making simulation essentially an experimental problem-solving technique.

In the particular type of model developed for this research, the analysis and description of soil water flow involved the following procedure [23]:

(1) Selection of approach to use in building the model.

There have been several approaches tried and suggested, as mentioned in the literature survey. The broadest and most comprehensive approach was then used in developing this particular model.

(2) Modification of chosen system of equations. The most comprehensive system of equations found did not allow for all properties which were desirable in the model. For completeness, all known factors were included in the model.

(3) Selection of boundary conditions. The systems of equations used were adapted to actual situations by choosing appropriate boundary conditions and assuming symmetry wherever appropriate.

(4) Determination of assumptions to simplify the model, producing an efficient model. After the model was developed and tested using all possible variables involved, approximations were made for many values used in the model. These were not a priori assumptions, but were done only after extensive testing had been performed.

After the model has been developed and tested, simulated results must be verified. Gordon [15] noted that inferences made in establishing the model can be checked by observing if the model behaves as expected. Similarly, the results of the simulation model may be compared with

analytical results, or, as is the case in this study, results of controlled experiments (e.g., laboratory studies) may be compared with simulated results.

3.2 Code Optimization

The practicality of a simulation process in day-to-day applications depends, to a large extent, upon the cost of such utilization. At the same time, the user of tools of this type expects to exert a minimum effort in preparing the necessary information (initial values, parameters, etc.) to be input to the model; hence the programming effort has somewhat conflicting interests, viz, minimization of computer memory-space and execution time as opposed to convenience of use.

The code for this simulation model was written following the rules of USA Standard FORTRAN IV [1]. This choice automatically eliminated machine-dependent optimization techniques. The optimization techniques which follow were intended to generate, as much as possible, optimal object code with respect to execution time and memory requirements.

3.2.1 Program Design

The objectives include [14]:

(1) A well-designed program that is easy to modify, maintain and update by the programmer as well as by other users.

(2) A well-designed program that is more efficient with respect to execution time and memory usage.

(3) A well-designed program that has a "well-ordered" logic structure.

As an example of "good" program design, consider Figure 1 and Figure 2. It is obvious that the program logic in Figure 2 is superior to that in Figure 1 in terms of the logic as well as programming ease. Careful program design and logic structure, as illustrated in Figure 2, can be used as an aid in producing optimal execution code.

3.2.2 Efficiency Techniques

Cohn [7] noted that efficient programming techniques are generally not included in programming texts and that many programmers, both pro-

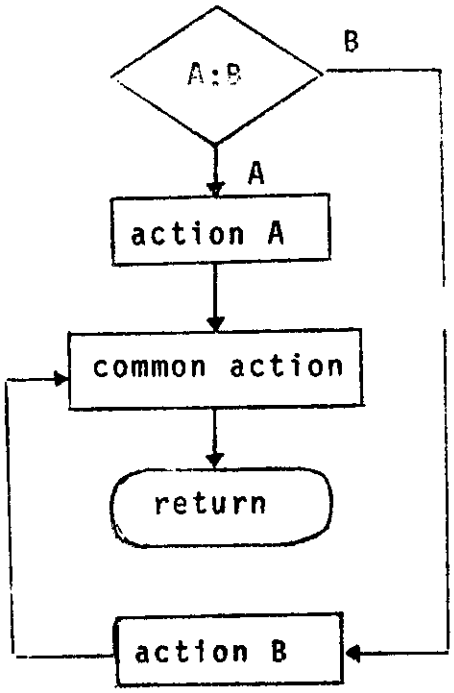

Fig. 1. Poor program design

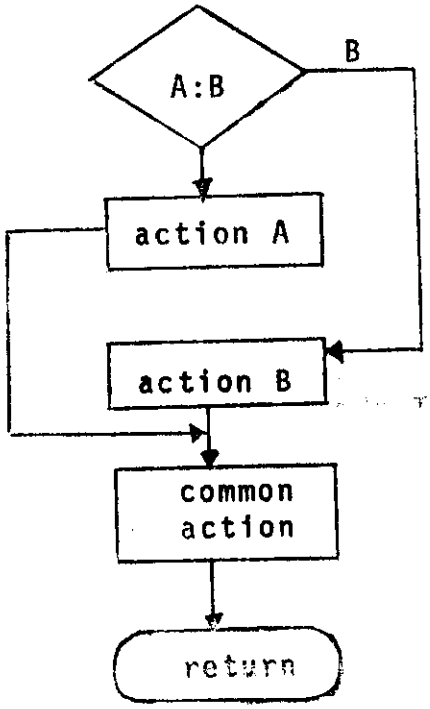

Fig. 2. Good program design

NAME	DESCRIPTION	SAVINGS MEM.	SAVINGS TIME	SUB-SECTION
Redundant Subexpressions	Perform calculations which occur repeatedly and save result until needed.	No	Yes	A
Polynomial Factorization	Rewrite polynomial expressions to reduce number of calculations performed.	Yes	Yes	B
Simple-Store Elimination	Eliminate expressions which assign values not requiring calculations to a variable, where the variable is used in later calculations.	Yes	Yes	C
Folding	Perform arithmetic operations on constants before writing expressions.	Yes	Yes	D
Integer Power Elimination	Write expressions with small integer exponents as repeated multiplication.	Yes	Yes	E
EQUIVALENCE	Use the same memory space for different purposes.	Yes	-	F
Subscripted Variables	Reduce references to subscripted variables and reference multi-dimensioned arrays using single dimensions.	No	Yes	G
Subprograms	References to subprograms should be made only under certain conditions.	Varies		H
Miscellaneous	Other standard optimization techniques.	Varies		I

Fig. 3. Optimization Techniques

fessional and amateur, are not aware of them. Several discussions of efficient programming techniques have been found [3, 4, 7, 16, 19, 24, 39]. A summary of the time and/or space savings tactics used in this research is illustrated in Figure 3. The column labeled "SAVINGS" in Figure 3 indicates changes in memory space or execution time for the various techniques under discussion.

3.3 Equations

During the development of the model, decisions were made regarding the variables and solution technique used. These decisions were made based upon previous models developed and the results obtained by these models, realizing that independent decisions had to be made in many cases due to the dissimilarity of this model from those previously developed. Also, during program development, it was found that, for many of the variables used, better estimates of the values could be found using variations of suggested equations cited in the literature. The equations used for these values are discussed in Appendix C - 5 and the solution techniques attempted are in Section 4.

The basic simultaneous differential equations for heat and moisture transfer in porous media (soil) under the influence of gravity and gradients of temperature and moisture, as presented by de Vries [8], were chosen as the skeleton equations of the model developed. These equations, which are extensions of previous equations developed by Philip and de Vries [11] over 15 years ago, still remain today as the basis of our understanding of water movement in soils.

The derivations of equations (3.1) and (3.2) below are given by de Vries [8] and are not included in this dissertation. Appendix C-1 contains a description of all variables used.

Basic equations for interior rectangular elements

The basic equation for the transfer of moisture, in terms of the volumetric liquid content θ_ℓ and the temperature T, is

$$\left(1 + \frac{D_{ev}}{\alpha_v D_{atm}} - \frac{\rho_v}{\rho_\ell}\right) \frac{\delta \theta_\ell}{\delta t} + \frac{(s-\theta_\ell)\, h\, \beta}{\rho_\ell} \frac{\delta T}{\delta t}$$

$$= \nabla\cdot(D_\theta \nabla\theta_\ell) + \nabla\cdot(D_T \nabla T) + \frac{\delta K}{\delta z} \qquad (3.1)$$

The terms on the right hand side of equation (3.1) deal with the liquid flux due to moisture gradients, due to the temperature gradient, and due to gravity, respectively. The coefficient of $\frac{\delta\theta_\ell}{\delta t}$ in equation (3.1) is close to one (1) for most calculations, the latter two terms in this coefficient being negligible (included only for completeness). The coefficient of $\frac{\delta T}{\delta t}$ was determined assuming equilibrium of water in the liquid and vapor phases.

Similarly, the equation for heat (energy) transfer, again in terms of θ_ℓ and T, is

$$\begin{aligned}
&(c + L(s-\theta_\ell)\, h\cdot\beta)\, \frac{\delta T}{\delta t} + \left(\frac{L\rho_\ell D_{atm}}{\alpha v}\right) \frac{v}{} - L\rho_v \\
&\quad + \rho_\ell j^{-1} g\, (\psi - T\tfrac{\delta\psi}{\delta T}))\, \frac{\delta\theta_\ell}{\delta t} \\
&\quad = \nabla\cdot\left((\lambda^* + L\rho_\ell D_{Tv})\, \nabla T\right) + L\rho_\ell\, \nabla\cdot(D_{\theta v}\nabla\theta_\ell) \\
&\quad + \rho_\ell c_\ell\, ((D_{\theta v}\nabla\theta_\ell + D_{Tv}\, \nabla T)\, \nabla T) \\
&\quad + \rho_\ell c_\ell\, ((D_{\theta\ell}\nabla\theta_\ell + D_{T\ell}\, \nabla T + Kk)\, \nabla T)
\end{aligned} \qquad (3.2)$$

In equation (3.2), the first term on the right side involves the effects of the volumetric vapor content on the heat movement; the second term concerns the liquid and vapor flux densities; and the third term represents the sensible heat transfer by vapor movement. The last term on the right side of equation (3.2) describes the heat transfer by liquid movement.

The coefficient of $\frac{\delta T}{\delta t}$ in equation (3.2) includes the effects of the volumetric liquid content in relation to the porosity of the soil. The coefficient of $\frac{\delta \Theta_\ell}{\delta t}$ includes terms for liquid and vapor diffusivity and the affects of the differential heat of wetting.

Equation (3.1) has no provisions for water sources such as rainfall or irrigation, nor does it provide for sinks such as plant roots. The addition or loss of water at the surface due to transpiration or evaporation is also excluded in equation (3.1). Equation (3.2) similarly excludes the effects of surface influences such as heat, radiation, air temperature and related atmospheric conditions. The method for including

these parameters is included in the following sections.

3.4 Solution Technique

A classic technique for approximating the solution of partial differential equations with initial and boundary conditions is an explicit method utilizing a network of grid points. A discussion of this technique may be found in any numerical analysis text, e. g., Carnahan, et. al. [5]. The solution technique used in this research also utilizes a grid network, however the actual solution technique differs considerably from the finite difference approach. The following sections contain a complete discussion of the solution technique used.

3.4.1 Setting Up the Grid

The first step is to set up a network of grid points throughout the region under consideration. The classical example generally involves equal grid spacings which are fixed (but not necessarily equal) in both the horizontal and vertical directions. Similarly, most grid solution techniques commonly refer to only rectangular grid elements. The model developed in this research has variable size grid spacings in both the horizontal and vertical directions

and uses both rectangular and triangular grid elements.

The grid set up would then resemble the following.

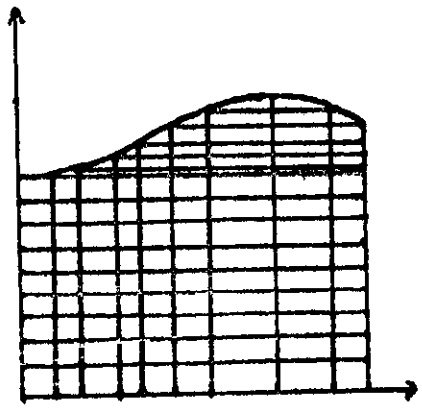

Fig. 4. Typical grid

Figure 5 is an enlarged view of one of the interior rectangular elements, where Δx and Δz are subject to maximum values depending upon the number of grid elements desired and upon the shape of the surface function. In the particular model developed, the grid element reference point was moved to the center of each element, hence, a reference to element (J,I) refers to the center of the grid element in row J, column I, as illustrated in Figure 6.

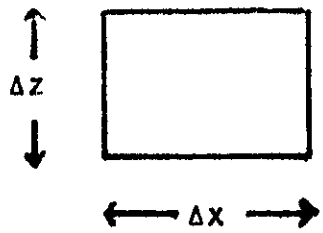

Fig. 5. Interior element

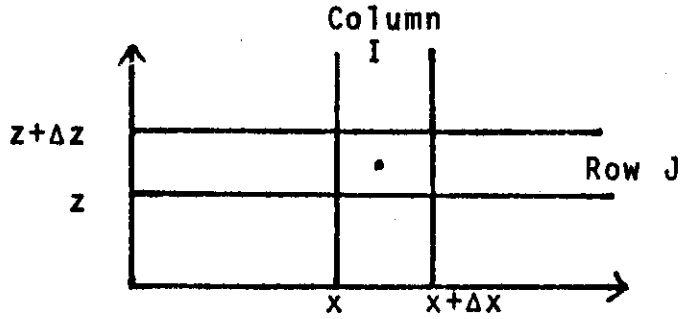

Fig. 6. Reference to center of element

3.4.2 Equation Manipulations

To illustrate the solution technique used, consider the following simple equation:

$$A \frac{\delta \Theta}{\delta t} = \nabla \cdot (B \nabla \Theta) + C \ , \qquad (3.4)$$

where A, B and C are the appropriate functions of Θ, x, z and T.

The operator ∇ is a vector operator, and $B\nabla\Theta$ is a vector of the form

$$\vec{V} = B \frac{\delta \Theta}{\delta x} \vec{i} + B \frac{\delta \Theta}{\delta z} \vec{k},$$

where $\vec{i}$ and $\vec{k}$ are unit orthogonal vectors. Hence, equation (3.4) may be written as

$$A \frac{\delta \Theta}{\delta t} = \nabla \cdot \vec{V} + C \ . \qquad (3.5)$$

Integrating both sides of equation (3.5) over an arbitrary volume,

$$\int_{vol} A \frac{\delta \Theta}{\delta t} dv = \int_{vol} \nabla \cdot \vec{V} dv + \int_{vol} C dv \ . \qquad (3.6)$$

Consider the following theorem:

1) If $\vec{V} = P\vec{i} + Q\vec{j} + R\vec{k}$ and its partial derivatives are continuous in an open region D in space;

2) S is a regular surface in D, forming the boundary of a bounded closed region T in D; and

3) $\vec{N}$ is the outer unit normal vector to S; then

$$\iiint_T \nabla \cdot \vec{\phi}\, dv = \iint_S \vec{\phi} \cdot \vec{N}\, da.$$

The above is known as the Divergence Theorem and is found in most vector analysis books, e.g., McCamy, et al. [25].

Assuming the term $\vec{V}$ and its partial derivatives are continuous over the entire soil area, and using a rectangular volume element, the Divergence Theorem may be applied to the term

$$\int_{vol} \nabla \cdot \vec{V}\, dv \text{ in equation (3.6).}$$

Hence the first term on the right in equation (3.6) was evaluated as

$$\int_{vol} \nabla \cdot \vec{V}\, dv = \int_{area} \vec{V} \cdot \vec{N}\, da, \text{ where } \vec{N} \text{ is the unit}$$

vector orthogonal to the volume surface. Making the above substitution in equation (3.6) results in the following equation:

$$\int_{vol} A \frac{\delta Q}{\delta t}\, dv = \int_{area} \vec{V} \cdot \vec{N}\, da + \int_{vol} C\, dv. \qquad (3.7)$$

Now consider only the term $\int_{\text{area}} \vec{V} \cdot \vec{N}\, da$ in equation (3.11). Since

$\vec{V} = B \frac{\delta O}{\delta X} \vec{i} + B \frac{\delta O}{\delta Z} \vec{k}$, $\vec{k}$ and $\vec{i}$ unit orthogonal vectors,

$$\int_{\text{area}} \vec{V} \cdot \vec{N}\, da \approx \left[\bar{B} \left.\frac{\delta O}{\delta X}\right|_{X+\Delta X} \Delta Z - \bar{B} \left.\frac{\delta O}{\delta X}\right|_{X} \Delta Z \right.$$

$$\left. + \bar{B} \left.\frac{\delta O}{\delta Z}\right|_{Z+\Delta Z} \Delta X - \bar{B} \left.\frac{\delta O}{\delta Z}\right|_{Z} \Delta X \right]. \qquad (3.12)$$

Here $\bar{B}$ indicates evaluation at the surface and at the midpoint of the side being evaluated. Also, $\frac{\delta O}{\delta X}$ and $\frac{\delta O}{\delta Z}$ are evaluated at the midpoint on the surface, in contrast to the other terms in equation (3.11) which are evaluated at the center of the element. Note that this solution technique evaluates all terms of $\int_{\text{area}} \vec{V} \cdot \vec{N}\, da$ along the surface. This is significant since these terms will be the diffusion coefficients in equations(3,1) and (3.2). These terms are dominant and are evaluated using exact techniques while the terms where approximations are used have only small effects on the solution.

The following evaluations were used in equation (3.12)

$$\left.\frac{\delta \Theta}{\delta x}\right|_{x+\Delta x} = \frac{\Theta\left(x+\Delta x+\frac{\Delta x}{2}\right) - \Theta\left(x+\frac{\Delta x}{2}\right)}{\Delta x}$$

and $\left.\frac{\delta \Theta}{\delta x}\right|_{x} = \frac{\Theta\left(x+\frac{\Delta x}{2}\right) - \Theta\left(x-\frac{\Delta x}{2}\right)}{\Delta x}$.

Similar evaluations were used for $\left.\frac{\delta \Theta}{\delta z}\right|_{z+\Delta z}$ and $\left.\frac{\delta \Theta}{\delta z}\right|_{z}$.

To illustrate the difference between the above solution technique with a finite difference approximation consider:

$$\frac{\delta}{\delta z}\left(B \frac{\delta \Theta}{\delta z}\right).$$

The forward difference approximation for this term is the following:

$$\frac{B(z+\Delta z)\cdot\frac{\delta \Theta(z+\Delta z)}{\delta z} - B(z)\cdot\frac{\delta \Theta(z)}{\delta z}}{\Delta z} .$$

But $\frac{\delta \Theta(z+\Delta z)}{\delta z} = \frac{\Theta(z+2\Delta z) - \Theta(z+\Delta z)}{\Delta z}$

and $\frac{\delta \Theta(z)}{\delta z} = \frac{\Theta(z+\Delta z) - \Theta(z)}{\Delta z}$.

So $\frac{\delta}{\delta z}\left(B \frac{\delta \Theta}{\delta z}\right)\Big|_{z} =$

(continued)

$$\frac{B(z+\Delta z)\left[\frac{(z+2\Delta z)-\Theta(z+\Delta z)}{\Delta z}\right]-B(z)\left[\frac{\Theta(z+\Delta z)-\Theta(z)}{\Delta z}\right]}{\Delta z}$$

The technique used in this research would result in this latter term being evaluated as

$$B(z+\Delta z)\cdot\left(\frac{\Theta(z+\Delta z+\frac{\Delta z}{2})-\Theta(z+\frac{\Delta z}{2})}{\Delta z}\right)$$

$$-B(z)\cdot\left(\frac{\Theta(z+\frac{\Delta z}{2})-\Theta(z-\frac{\Delta z}{2})}{\Delta z}\right).$$

This last result is exact for linear (or constant) arguments. Note that in the finite difference approximation, the Θ values used are displaced by $\frac{\Delta z}{2}$. Also, the finite difference method does not allow for discontinuities at the surface while the method used in this research isolates the flux along each side. Hence where discontinuities occurred at the surface, it was possible to calculate the fluxes along 3 sides as discussed above and then use other evaluations along the surface edge.

The method of evaluation used in this research for the term $\nabla\cdot(B\Delta\Theta)$ differs from a finite difference method in that the finite difference method approximates a second derivative term. The former method applies the Divergence Theorem (an exact technique) and uses approx-

imations for evaluating a first derivative term. Approximations of first derivative terms would invoive less error than an approximation of second derivative terms. The application of the above technique to equations (3.1) and (3.2) is in Appendix C-5, as is the extension to surface elements.

For grid elements having a side on the soil surface, equation (3.12) would be written as

$$\overline{A}\frac{\delta\Theta}{\delta t}\Delta x\Delta z = \left(\overline{B}\left.\frac{\delta\Theta}{\delta x}\right|_{x+\Delta x}\Delta z - \overline{B}\left.\frac{\delta\Theta}{\delta x}\right|_{x}\Delta z - \overline{B}\left.\frac{\delta\Theta}{\delta z}\right|_{z}\Delta x\right) + \overline{C}\,\Delta x\Delta z + D \qquad (3.13)$$

where D represented the transfer of moisture at the soil surface. D essentially replaced the effects of the term $\overline{B}\left.\frac{\delta\Theta}{\delta z}\right|_{z+\Delta z}\Delta x$.

3.4.3 Further manipulations

During the development of the model, it was found that extremely small time steps were necessary in the temperature calculations in order to prevent divergence. In an effort to increase time step size and to reduce the number of iterations required, the first terms of Taylor's series expansions were used as approximations for some terms.

Specifically, in the temperature equations,

the term $T^4 = \frac{T^4(t=t) + T^4(t=t+\Delta t)}{2}$ appeared on the right side of the equation. The equation was linear on the left side in terms of $T(t=t+\Delta t)$ and non-linear on the right. A Taylor's series approximation was used to express the temperature at $t=t+\Delta t$ in terms of $T(t=t)$, where $T(t=t)$ was known, as follows.

$$T^4 \quad T^4(t=t) + 4T^3(t=t)\cdot(T(t=t+\Delta t) - T(t=t)).$$

Thus a linear approximation was used to approximate $T^4(t=t+\Delta t)$ in terms of $T(t=t)$. Hence

$$T^4 \quad \frac{T^4(t=t) + T^4(t=t) + 4T^3(t=t)\cdot T(t=t+\Delta t)}{2}$$

$$-T^4(t=t)$$

$$= -T^4(t=t) + 2T^3(t=t)\cdot T(t=t+\Delta t).$$

Since the equation being used was to be solved for $T(t=t+\Delta t)$, the non-linear term involving $T^4(t=t+\Delta t)$ was approximated in terms of $T(t=t)$ and the resulting linear term was carried to the left side of the equation, giving the solution technique more stability.

In a similar manner, the term

$$= \frac{\rho(t=t) + \rho T}{2}$$ appeared in the equation discussed

above, where $\bar{T} = \frac{T(t=t+\Delta t) + T(t=t)}{2}$. Again using Taylor's series approximations,

$$\rho_{\bar{T}} \approx \rho_o + \beta \cdot \frac{(T(t=t+\Delta t) - \bar{T})}{2}$$, where

$\rho_o = \rho$ at $\bar{T}$ and $\beta = \frac{d\rho_{\bar{T}}}{dt}$. As in the preceding case, the linear term involving $T(t=t+\Delta t)$ was taken to the left side of the equation. Similar expansions were used in other terms.

4. SIMULATION LOGIC

The simulation model developed is based upon the equations and solution technique discussed in the previous section.

4.1 The Grid

One of the unique aspects of this model is the inclusion of various shaped surfaces (i.e., mound shaped or strictly increasing), and the effects of such surfaces on the overall moisture-temperature movement in the soil. In order to accurately model the effects of the surface contour, an accurate method had to be devised to set up the grid network in the surface region. The method requires the user to define a function (FTOP) which gives the shape of the surface. The user is also required to provide the range of the abscissa (x) values to be modeled, as well as the depth or ordinate (z) value at the left-most, right-most and maximum points on the surface.

Using the above mentioned information, a grid network is set up automatically to cover the entire region to be modeled. To assure accuracy, both

rectangular and triangular grid elements are used on the surface, while only rectangular elements are used below the surface. The grid network is set up by starting at the left-most boundary of the region and incrementing by a maximum allowable Δx value, yielding a new x value at $x + \Delta x$. The values of $f(x)$ and $f(x + \Delta x)$ are then calculated and a check is made to determine if the resulting Δz value exceeds the pre-determined maximum, DZMAX. If $f(x + \Delta x) - f(x) < DZMAX$, another Δx increment is made, dividing the grid into vertical elements. This process continues until a z value is found which is greater than or equal to ZR (the right-hand side z value) or the resulting Δz is too large (See Figure 7)

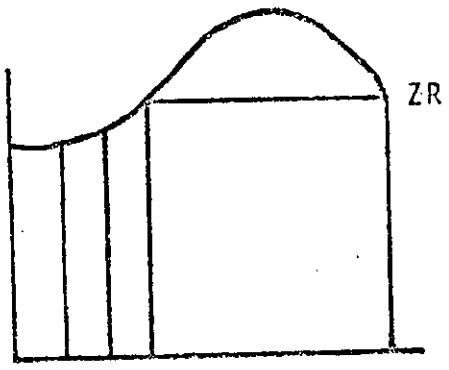

Fig. 7. First step in grid set-up

If a value for f(x) is found which is greater than or equal to ZR, the value of x is found corresponding to ZMAX (See Figure 8). Then, starting at this new value of x, the remainder of the grid is divided into vertical elements using the same techniques as described in the preceding paragraphs. However, when a grid point is found on the left of ZMAX, the element to the right is located at the same height to facilitate setting up the z grid elements. Figure 9 illustrates the location of z values at equal heights on each side of ZMAX.

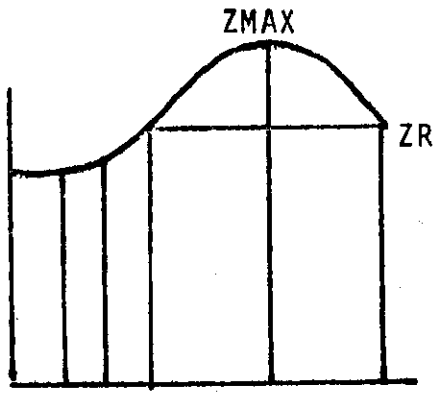

Fig. 8. Maximum Z value

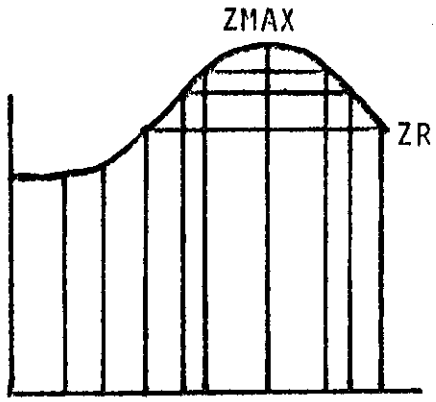

Fig. 9. Equal heights on each side of ZMAX

If the Δz value at any point $x + \Delta x$ exceeds DZMAX, the x value chosen is not used and DZMAX is added to f(x) yielding the z value f(x) + DZMAX, for which the corresponding x value, (i.e., $x + \Delta x$) must be found. This is obtained as follows: given a z value (f(x) + DZMAX), and the range of admissible x values (called XMIN and XMAX), find the corresponding x and Δx values such that $f(x + \Delta x) \approx f(x) + DZMAX$. For the following discussion, assume the function is non-decreasing in the region where the x value is being looked for. A similar technique is used for

decreasing functions. This process involves picking a guess value GU for the correct x value. If the guess value yields a z value greater than f(x) + DZMAX but outside the chosen range of accuracy, the value of XMAX is set to GU. If f(GU) > XMIN and f(GU) < f(x) + DZMAX, XMIN is set to GU. In either case, a new GU value is picked as (XMIN + XMAX)/2. This technique continues until the required x value is within the desired range of accuracy.

Alternatively, if the soil surface is flat, provisions have been made to divide the surface region into equal size rectangular surface elements. This procedure by-passes the complex procedure mentioned above for non-flat surfaces.

Having set up the required vertical elements, the horizontal elements are then set using the Δz values calculated in each step. Since care was taken to use the same Δz values for elements on either side of ZMAX (for mound shaped surfaces) there is no conflict in setting up the z grid elements above the surface. The lower surface area is also divided into a grid using the same Δx values set up at the surface and the entire lower region is divided into Δz increments with the user specifying the number

and size of these increments. This allows larger soil layers deeper in the soil where soil properties change very slowly, if at all.

The surface elements are then classified as either rectangular or triangular. The first element on each row is set to be triangular to avoid a surface of the shape illustrated in Figure 10. The inclusion of triangular elements on each row gives the surface a shape as illustrated in Figure 11. If the surface is flat over some interval, the surface elements (except those on the end) are designated as rectangular surface elements.

After the entire grid network has been set up as described above, all reference points are moved to the center of the grid element. This is done because this simulation program is to determine the heat and moisture values at various points in the soil. The value at the center represents the average values for the elements, assuming the heat and moisture values are linear.

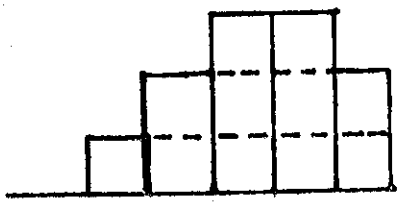

Fig. 10. Grid before adding triangular elements

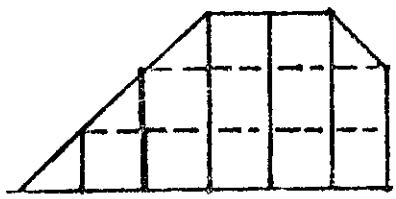

Fig. 11. Grid after adding triangular elements

4.2 Initialization

After the entire grid network has been set up as described in section 4.1, initial values for moisture content and temperature of the soil at each grid point are required. This information is supplied by a user-written subprogram called INITAL which gives the temperature and moisture values in terms of their location. Also required is the temperature of the air, as well as other atmospheric conditions. Since as many as 6 soil layers are allowed, soil parameters must also be provided by subroutine INITAL in terms of these soil layers.

The user may also specify two sources and/or two sinks to be present in the grid network. These elements may be sources (sinks) with respect to both moisture and temperature, as would be the case with subsurface irrigation, or they may each be sources

(sinks) of only one type. The latter approach could be used to represent plant roots which are subsurface sinks with respect to moisutre but take on the temperature of the surrounding soil. Figure 12 illustrates the concept of sources and sinks with respect to a grid network.

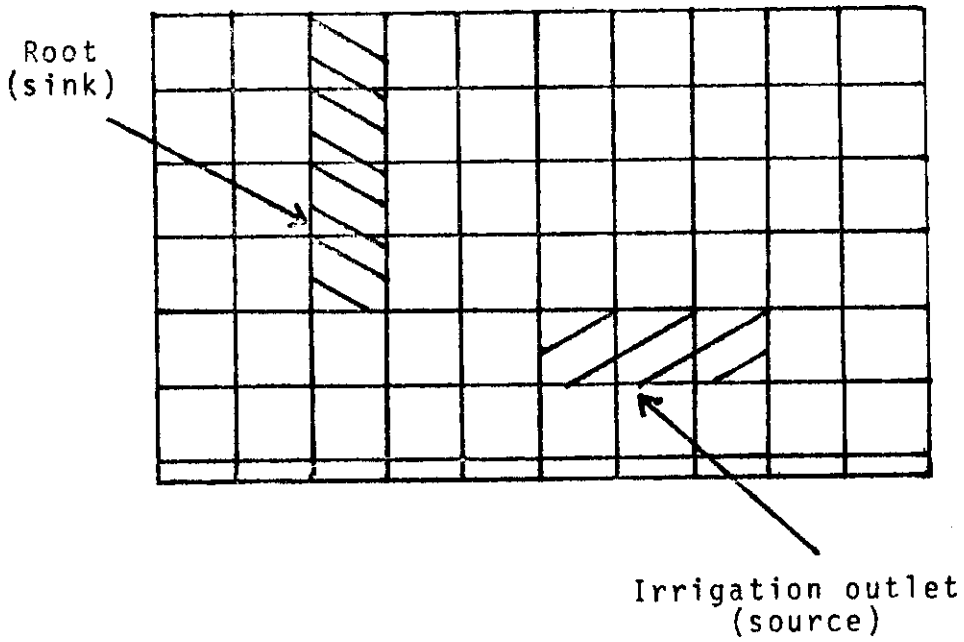

Fig. 12. Grid with sources and sinks

Further simulation of actual conditions is permitted on the soil surface. In addition to allowances for rain on the soil surface, the model also allows for variations in the atmosphere such as temperature, relative humidity and the effects of radiation from the sky and sun. These values are

provided as input parameters to the model and may be measured or predicted from appropriate equations. The effects of the wind upon the surface elements may also be entered into the model in the calculation of the terms SH/RB, where wind speeds affect this boundary layer resistance.

The user has many options available to him in determining what situations are to be simulated. The user determines whether the soil surface is to be flat, sloping or mound shaped. It is also possible to specify what size grid elements are to be used by the model to allow for larger elements where little heat or moisture flow normally occurs or to specify smaller grid sizes in the upper soil layers and in the areas of sources or sinks. All soil properties (bulk density, porosity, diffusivity and conductivity, etc.) are input to the model. Sources and sinks may be present or may be omitted.

Environmental conditions are also input to the model. Factors such as the air temperature, air relative humidity, radiation effects, presence or absence of rain, and the effects of wind on the boundary layer resistance are all used by the model.

In the presence of rainfall, the soil surface layer is assumed to be saturated and the temperature of this layer assumes the temperature of the rain.

The values to be provided by the user's subroutine are included in Appendix C-3. Suggested values for many of the parameters which remain constant or vary little under most conditions are included in the appendix.

4.3 Changes in Moisture and Temperature

Using the temperatures and the moisture content of the grid elements at the starting time for the simulation model ($t = 0$) as initial values, a first approximation for the values of the temperature (T) and the moisture (θ_ℓ) content are calculated for time $t + \Delta t$ for each element in the grid. The approximations used for solving the system of equations involved is discussed in Section 3. Having calculated the T and θ_ℓ values at $t + \Delta t$, each element in the grid is checked to see if the values are within 10% of the previous iteration values before going on to the next time step. It was found that a minimum of three iterations was required by the model to assure that the effects of the fluxes would be transferred to surrounding elements. If further

iterations are required (after the first 3), the convergence test is based upon the percent of change from the previous calculations at time t + Δt.

When T and Θ_ℓ have been calculated to the desired degree of accuracy for all elements, these values are used as the values at time t = 0 for the next iteration, (i.e., the new initial conditions). This process continues for the number of time steps required to satisfy the length of the simulation period.

In order to calculate the moisture and temperature values at successive times, it was necessary to use a scheme for determining optimal time step sizes. The technique utilized involved using the time step size from the previous iteration and the maximum actual change that took place for any one element during the last iteration. Specifically, the new time step DT is found assuming a change of .05 in the moisture content can be handled in any one time step. Then, using the previous time step size DT and the actual largest change in Θ for any one element, a new DT is found using the relation DT = .05·DT/(Max. Θ change). This same procedure was used for determining the time step DTT for temperature calculations, assuming a 1°K change in temp-

erature was allowable. Specifically, the relation DTT = 1.-DTT/(Max. T change) was used.

In both cases, it was found that at least three iterations were required by the solution technique in order for the predicted values to closely coincide with the test data (discussed in Section 5). A maximum time step of 3600 seconds was set for both temperature and moisture calculations since more accurate values could normally be expected from the smaller (and more frequent) time steps. This added accuracy results since each iteration after the first reflects the moisture or temperature movement due to the fact that the solution technique uses an average of initial values and values found in the previous iteration in the current time step.

Another major execution-time consideration involves calling in a special routine, MESH, if convergence has not been reached within 10 iterations using the current time step size. MESH (described in detail in Appendix C-6) is a routine to divide rows involving large gradients into smaller grid elements. This routine must calculate numerous values to be used in further calculations and

also requires these rows to be restored after convergence is reached. This routine is quite expensive, time wise, and is used only as an emergency measure.

Upon arriving at the appropriate time step size for both moisture and heat transfer, values for the moisture content at time $t + \Delta t$ were calculated first. Since the effect of temperature on moisture transfer is relatively insignificant within a few degrees, the temperature value is held constant for these calculations.

The values for the elements on the soil surface were calculated first. Then these values were calcluated for all interior elements. After 3 iterations, convergence tests are made and if all values converged, the temperature calculations are performed. However, if convergence did not occur for all grid elements, further iterations (up to 10) are carried out until convergence is obtained. If convergence still was not possible, MESH is called, where necessary, to assure convergence.

The temperature calculations are then performed in the same manner using average moisture

values from the beginning of the time step and the value at the end of $t + \Delta t$. It should be mentioned that different size time steps were required for temperature, since the initial equations do not allow for the fact that the heat movement occurs at a much faster rate than does moisture movement. Hence, several sets of calculations might be required in the heat transfer portion of the model in order to determine the temperature values at time $t + \Delta t$, since time steps of size DTT = DT/n, n a positive number, would normally be required, where DTT is the time step for the temperature calculations.

4.4 Solution Techniques Attempted

During the development of this dissertation, several solution techniques were attempted in order to select one which would converge to the desired range of accuracy. Not all of the techniques attempted were successful, however, they are mentioned here for completeness, and may be of some help in guiding others attempting similar solution procedures.

The first, and simplest, technique used was a straight-forward solution technique in which no attempt was made to speed up the convergence of the moisture and temperature values. The equations discussed in Section 3 were simply solved simultaneously and in calculations involving partial derivatives of the type $\left.\frac{\delta \Theta_\ell}{\delta x}\right|_{x+\Delta x}$, the approximation

$$\frac{\delta \Theta_\ell}{\delta x} = \frac{\bar{\Theta}_\ell(I+1) - \bar{\Theta}_\ell(I)}{(\Delta x(I) + \Delta x(I+1)) \cdot (.5)}$$

, where $\bar{\Theta}_\ell$ is the average Θ-value between $\Theta_\ell(t=0)$ and $\Theta_\ell(t=t+\Delta t)_{last}$ i.e.,

$$\bar{\Theta}_\ell = \frac{\Theta_\ell(t=0) + \Theta_\ell(t=t+\Delta t)_{last}}{2}$$

, where $\Theta_{\ell\ last}$ was the value of Θ_ℓ obtained in the last iteration of the current time interval. This solution technique was fairly stable, that is, for "small" time steps, convergence was usually satisfied within 10 iterations.

The initial solution procedure also attempted to use the same time step size for both the temperature and moisture calculations. This turned out to

be a most unwise decision, since it was quickly discovered that the flow of moisture through the soil was considerably slower than the heat transfer, hence very small time steps had to be used and in the small time intervals, the moisture movement was almost unnoticeable.

In this initial procedure, the time steps used were on the order of 300 to 600 seconds in order to handle even small temperature gradients. This method was considered to be non-optimal with respect to execution time since the calculations for moisture values were performed repeatedly for small time steps while attempting to get the temperature solution to converge, while larger time steps would have been adequate for the moisture values.

Another solution technique that was attempted was a slight variation to the above procedure. This technique separated the moisture and temperature calculations into distinct parts, allowing for different size time steps. This method was considerably more efficient than the one above since convergence of the moisture equations usually occurred in 4 or 5 iterations for moderate gradients

and time intervals of up to two hours (7200 seconds), while the time steps for the temperature calculations were kept in the neighborhood of 10 minutes. In order to compensate for the fact that moisture values were not calculated for each of the time periods used in the temperature calculations, a moisture value of $\theta_\ell = \theta_\ell(t=o)\cdot k_1 + \theta_\ell(t=o+\Delta t)\cdot k_2$, k_1 and k_2 appropriate (linear) weighting factors, was used in the temperature calculations, where Δt was the time step used in the θ calculations.

Even with the above changes, the convergence of the temperature equation was very slow and, for many time steps, the solution procedure diverged completely, i.e., the temperature values started oscillating away from the solution value.

The next attempt, to speed up convergence, involved a somewhat more complicated procedure involving the θ and T values used. In an attempt to prevent divergence, the calculations involving $\overline{\theta}_\ell$ and $\overline{T}$ were modified as follows.

$$\text{Instead of } \left.\frac{\delta \theta_\ell}{\delta x}\right|_{x+\Delta x} = \frac{\overline{\theta}_\ell(I+1) - \overline{\theta}_\ell(I)}{(\Delta x(I) + \Delta x(I+1))/2}$$

$\overline{\theta}_\ell(I)$ was replaced with

$$\frac{\theta_\ell(t=0) + \frac{\theta_\ell(\text{last}) + \theta_\ell(\text{now})}{2}}{2}$$

where $\theta_\ell(\text{last})$ refers to the θ_ℓ value found in the last iteration for the current time step and $\theta_\ell(\text{now})$ refers to the θ_ℓ value currently seeked. This latter term (along with the appropriate coefficient) was then taken to the left side of the equation before solving for $\theta_\ell(\text{now})$. Similar substitutions were made throughout the moisture and temperature equations.

The results of this technique were disasterous! Since the first approximation of a solution, i.e., $\theta_\ell(\text{last})$, was probably either too large or too small, the introduction of this value along with $\theta_\ell(\text{now})$ caused the current value of $\theta_\ell(\text{now})$ to overcompensate for the previous calculation and hence, instead of insuring convergence, rapid divergence was created.

Graphically, this might be illustrated as follows. The convergence to the solution value should behave roughly as follows.

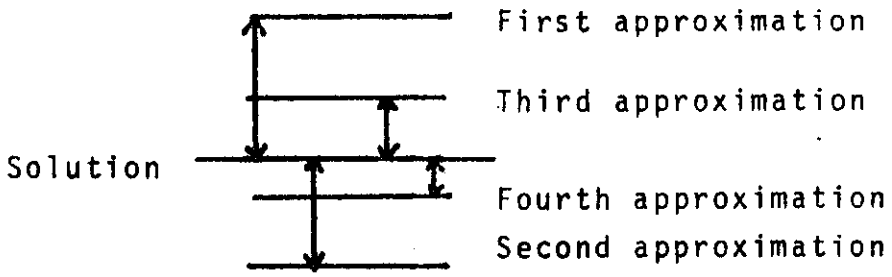

However, the introduction of the 1st approximation into the solution using

$$\frac{\Theta_{\ell}(\text{last}) + \Theta_{\ell}(\text{now})}{2}$$

would mean that $\Theta_{\ell}(\text{now})$ would have to be much larger (i.e., larger in the opposite direction from the $\Theta_{\ell}(\text{last})$ value) in order to offset the first error,

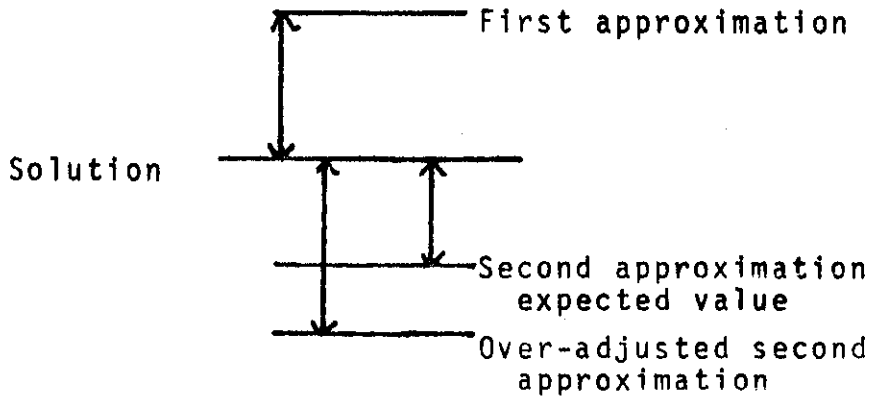

i.e., $\frac{\Theta_{\ell}(\text{last}) + \Theta_{\ell}(\text{now})}{2}$ = correct value can occur only if $\Theta_{\ell}(\text{now})$ = correct value - $\Theta_{\ell}(\text{last})$. But

since Θ_ℓ(last) was too large (or, of course, it could have been to small), and 'correct value', upon convergence, should be very close to the solution value, instead of Θ_ℓ(now) approaching the correct value, it will over-compensate to average out with the value of Θ_ℓ(last).

The final solution technique arrived at used the following substitutions for the approximations of the type

$$\left.\frac{\partial \Theta_\ell}{\partial x}\right|_{x+\Delta x} = \frac{\Theta_\ell(I+1) - \Theta_\ell(I)}{(\Delta x(I) + \Delta x(I+1))/2} \quad \text{, where}$$

$$\Theta_\ell(I) = \frac{\Theta_\ell(t=0) + \Theta_\ell(\text{now})}{2}$$

This solution technique puts a damper on the first approximations and prevents them from differing from the actual solution as much as would be possible were the Θ_ℓ(now) term not used.

Graphically,

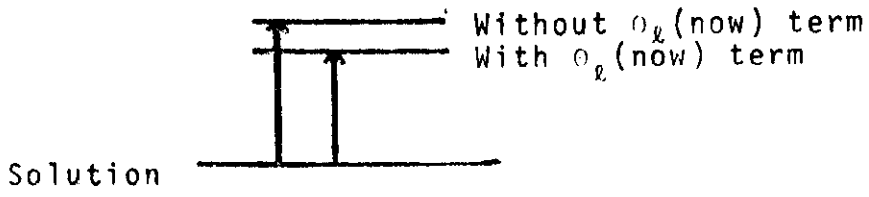

This entire solution technique was discussed in Section 3.

5. RESULTS

Validation of a model of the type developed is extremely difficult due to the very nature of the problem itself. Many of the soil parameters used in the model are highly theoretical, especially those dealing with the soil-atmosphere interface. Not only are many of the parameters not thoroughly understood, but they are practically impossible to measure. Specifically, properties involving the loss or gain of heat at the soil surface, the resistance of the soil layer to give up or receive moisture to/from the atmosphere and the effect of a dry crust on the soil to these phenomenon are among the reactions which defy accurate measurement or calcluation. Hence the attempt to validate the model is based mostly upon "expected" results.

5.1 Philip's results

Since considerable research has been done with respect to the moisture transfer within the soil, an

attempt to compare the results of the solution technique in the model with other results was undertaken. The data and parameters used for this process were those of Philip [28] for infiltration into Yolo light clay. The data and calculations used by Philip were for vertical infiltration only, hence the original model was altered for this special case and test runs were made. The initial conditions used in this run are as follows:

$$\theta = \theta_n, \; t = 0, \; z \geq 0$$

$$\theta = \theta_0, \; z = 0, \; t \geq 0$$

where $\theta_n = .2376$ and $\theta_0 = .4950$. The calculations for the conductivity, K, and the diffusivity, D, were performed using the values presented by Philip.

The general equations of this model, subject to the conditions stated above, reduce to

$$\frac{\partial \theta_\ell}{\partial t} = \nabla \cdot (D_\theta \nabla \theta_\ell) + \frac{\partial K}{\partial z}$$ subject to the initial and boundary conditions given above. The results of the simulation model as compared to the moisture profile of Philip were almost identical when time steps of 600 sec. were used and at least

three iterations were required before convergence was assumed. The model differed by about 15% at a depth of 5 cm. using a fairly large rectangular area (2 cm. x 2 cm.) and time steps of 400 or 600 seconds. The model's predicted moisture values were lower than those predicted by Philip in these cases, however, it is very possible that a considerable part of this error could be introduced from the interpretation of Philip's graph. Using a finer grid (Δz = 1 cm.), the model reduced the difference to about 10% at the 5 cm. depth. At a depth of 10 cm., both models were in agreement about the predicted values.

At the end of 4×10^4 seconds, the difference between the two predicted values were indistinguishable at all depths, indicating that the model had "caught up" with the predicted values of Philip. A moisture profile for the model is given in Figure 13. Also included are the predicted values of Philip for the times of 10^4 sec, 4×10^4 sec. and 10^5 sec. Beyond this time, the profiles appear identical. Beyond 4×10^4 seconds, time steps of 900 seconds were used, since the gradients in the

model had become smaller, permitting these larger time steps to be used without affecting the results.

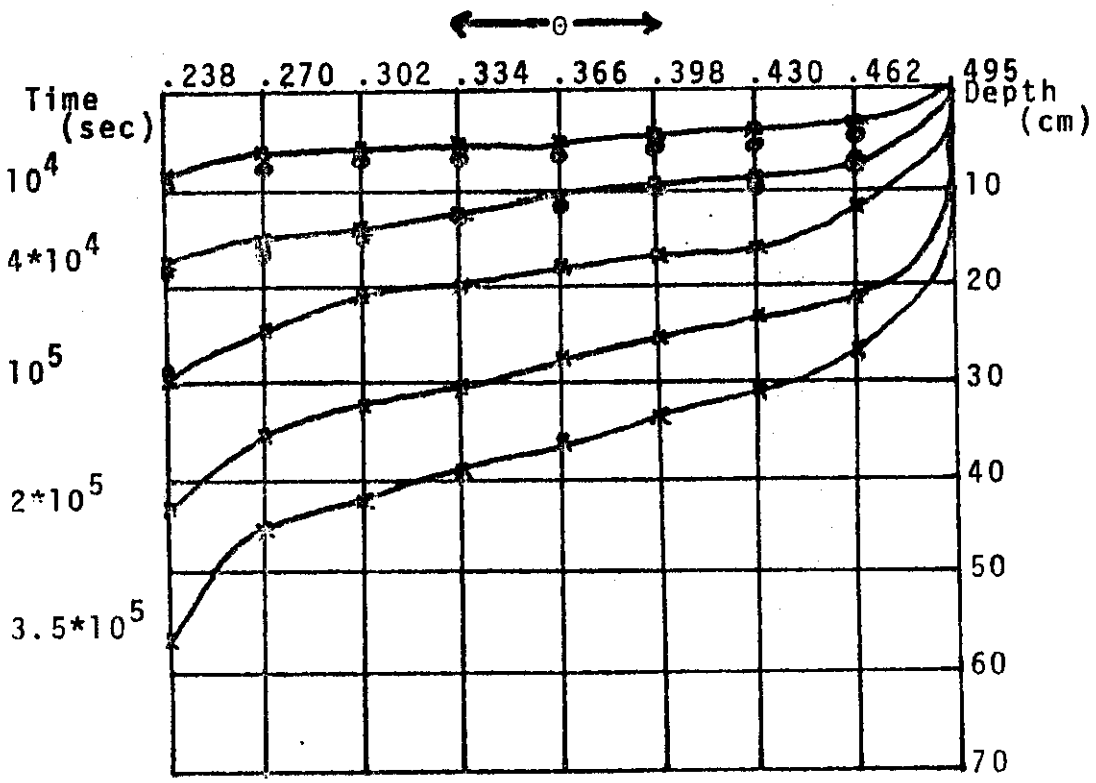

x-represent model predicted values
o-Philip's predicted values

Fig. 13. Comparison of model and Philip's results.

5.2 Further Results

Using the properties of Philip's [28] soil, a Yolo light clay, runs were made to determine the effects of sources and sinks on the moisture content of the soil. A moisture source of roughly 2.5 X 2.36 cm. was located in the soil at a depth of about 10.5 cm. and a moisture sink of the same size was located at the same depth at a distance of about 9.4 cm. from the source. The source was given a constant moisture value of .44 cm^3/cm^3 while the sink had a moisture content of .26 cm^3/cm^3. This soil reaches saturation at about .495 cm^3/cm^3.

The initial conditions of the soil used were $\theta = .34,\ t = 0,\ z \geq 0;\ T = 288.3\ ^\circ K,\ t = 0,\ z \geq 0$. Zero moisture and temperature fluxes were maintained at the bottom of the modeled area, hence giving the effect of an infinite vertical column. A very high boundary layer resistance (2 sec/cm) was used to minimize the effects of the atmosphere on the moisture content. Temperature flux at the soil surface were also near zero. Zero fluxes were also assumed along vertical boundaries.

The above set-up represented a moist soil with additional moisture present at the source. This source was considered to be the equivalent of a slow, constant seepage of water into the soil rather than water running into the soil. Similarly, the sink represented a slow uptake of water from the soil, perhaps like the uptake of water from the soil by a root system.

The following countour map represents the results. (Fig. 4) Each countour outward from the sources and sinks represents the moisture content at one hour intervals. The plot around the source represents moisture values .36 cm^3/cm^3 or greater. The corresponding plot around the sink represents moisture content of .33 cm^3/cm^3 or less. The grid elements have dimensions of Δz = 1.25 cm and Δx = 1.18 cm.

The soil surface layer dried out during this time period from an initial content of .34 cm^3/cm^3 down to .29 cm^3/cm^3 in the area above the sink, while the region on the surface above the source ended with a moisture content of .35 cm^3/cm^3. The drying of the surface layer had some effect on the contour map. It

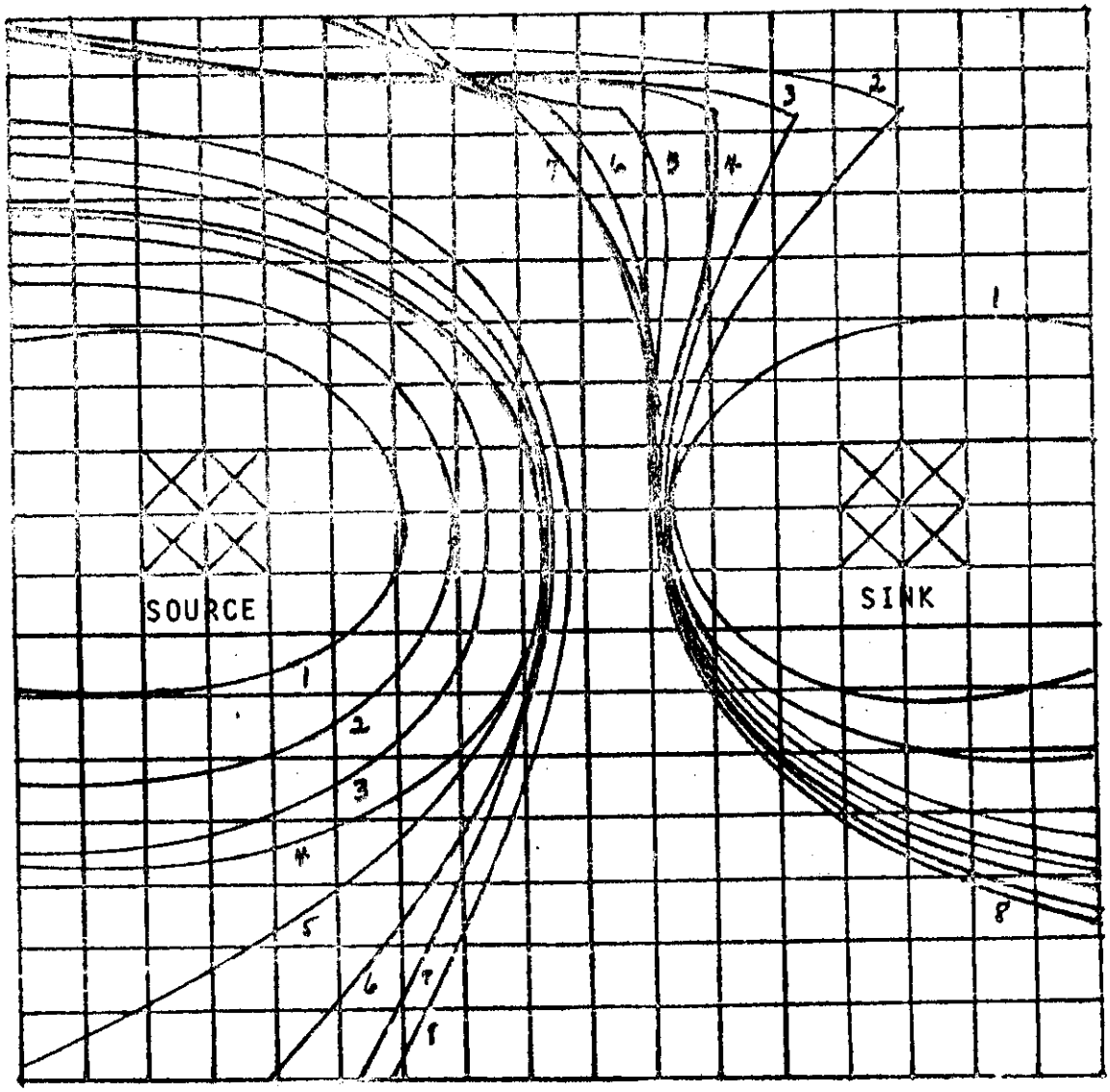

Label	Time	Label	Time
1	$3.6 \cdot 10^3$ sec	5	$1.8 \cdot 10^4$ sec
2	$7.2 \cdot 10^3$ sec	6	$2.16 \cdot 10^4$ sec
3	$1.08 \cdot 10^4$ sec	7	$2.52 \cdot 10^4$ sec
4	$1.44 \cdot 10^4$ sec	8	$2.88 \cdot 10^4$ sec

Fig. 14. Flow with sources and sinks

also appeared that the small region between the wet front and the dry front in the soil acted as a buffer and was merely passing moisture from the wet region into the dry.

The identical initial conditions were used for another complete run, however small temperature sources and sinks were set up corresponding to the moisture sources and sinks. The temperature source on the left was set to a constant value of 285 ° K and the one on the right was set to 292 ° K. These small changes in the temperature had no effect on the moisture profile of the soil.

Another set of runs was made using the same soil properties as in the previous run, i.e., for a Yolo light clay. Zero moisture and temperature fluxes were maintained at the bottom of the modeled region, as in the previous example. Boundary layer resistance of 1 sec/cm was used. Temperature fluxes were present at the soil surface. When rainfall occurs, the saturated value of the soil surface layer was assumed to be $\theta = .45$, giving the effect of a very light rainfall. The temperature of the rain was set at 285 ° K.

The initial conditions of the soil were: $z \geq 0$, $T = 288.3\ ^\circ K$, $t = 0$; $z \geq 0$, $\theta = .4218 - .006 \cdot z$, $t = 0$. The soil surface was an increasing function; specifically the curve $z = 10 + 2 \cdot \sin(\pi/2 \cdot x/6)$ was used.

Figure 15 represents the soil moisture and temperature profile at 9 A. M., 9 hours after the start of the simulation run. Note that the soil had cooled considerably since the beginning of the run at 12 A. M., i. e., at $t = 0$.

At 9 A. M., a light rainfall began and lasted until 10 A. M. The temperature of the rainfall was $285\ ^\circ K$. Figure 16 is the profile of the soil after the rain had fallen for 30 minutes. Note that this rainfall included no run-off and under heavier rainfall conditions, a value of $\theta = .495$ would have been used instead of the value $\theta = .45$.

Figure 17 represents the soil profile at 12:30 P. M., or 2-1/2 hours after the rainfall stopped. During this time, the soil surface began drying slightly, however was still near saturation.

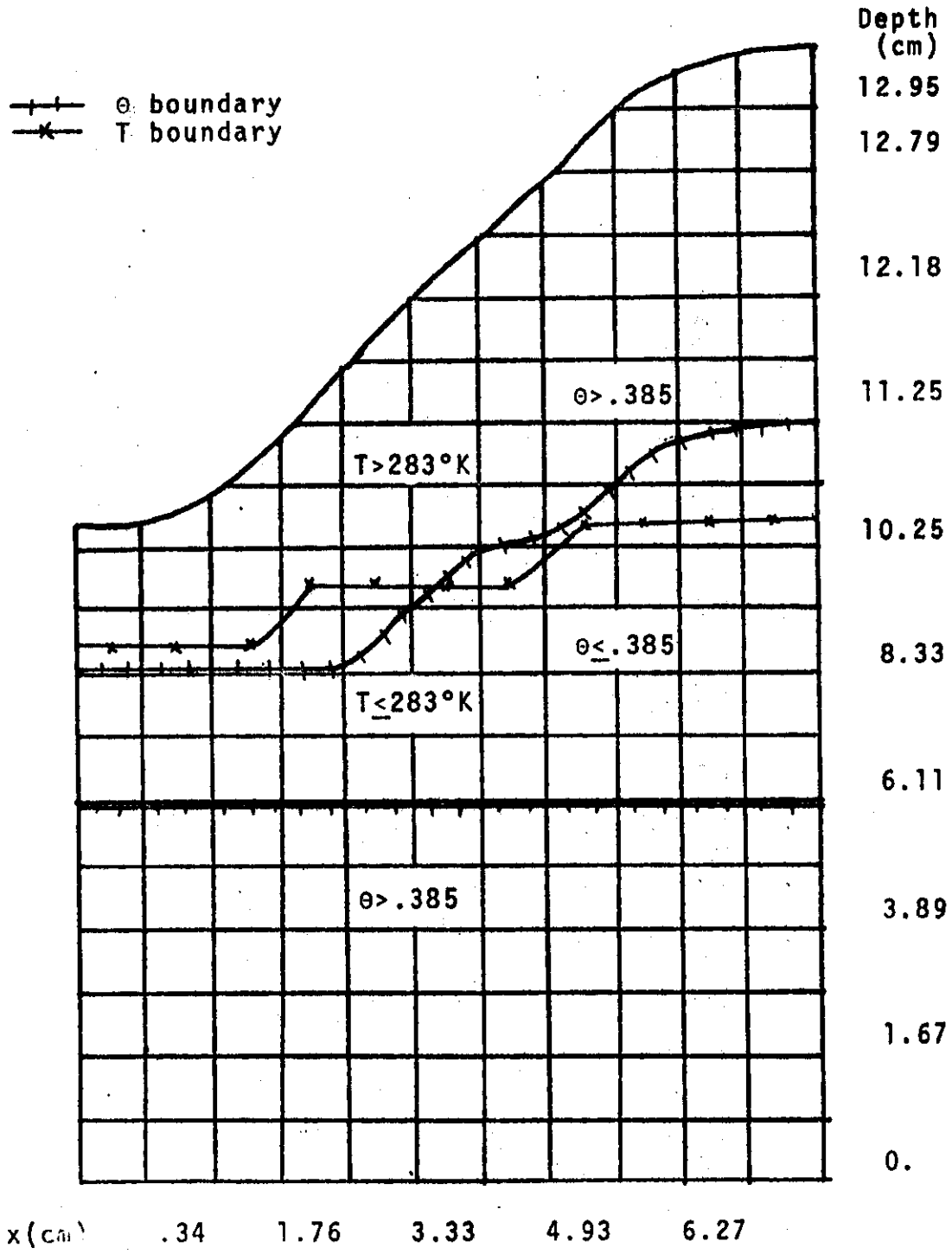

Fig. 16. Profile at 9:30 A. M.

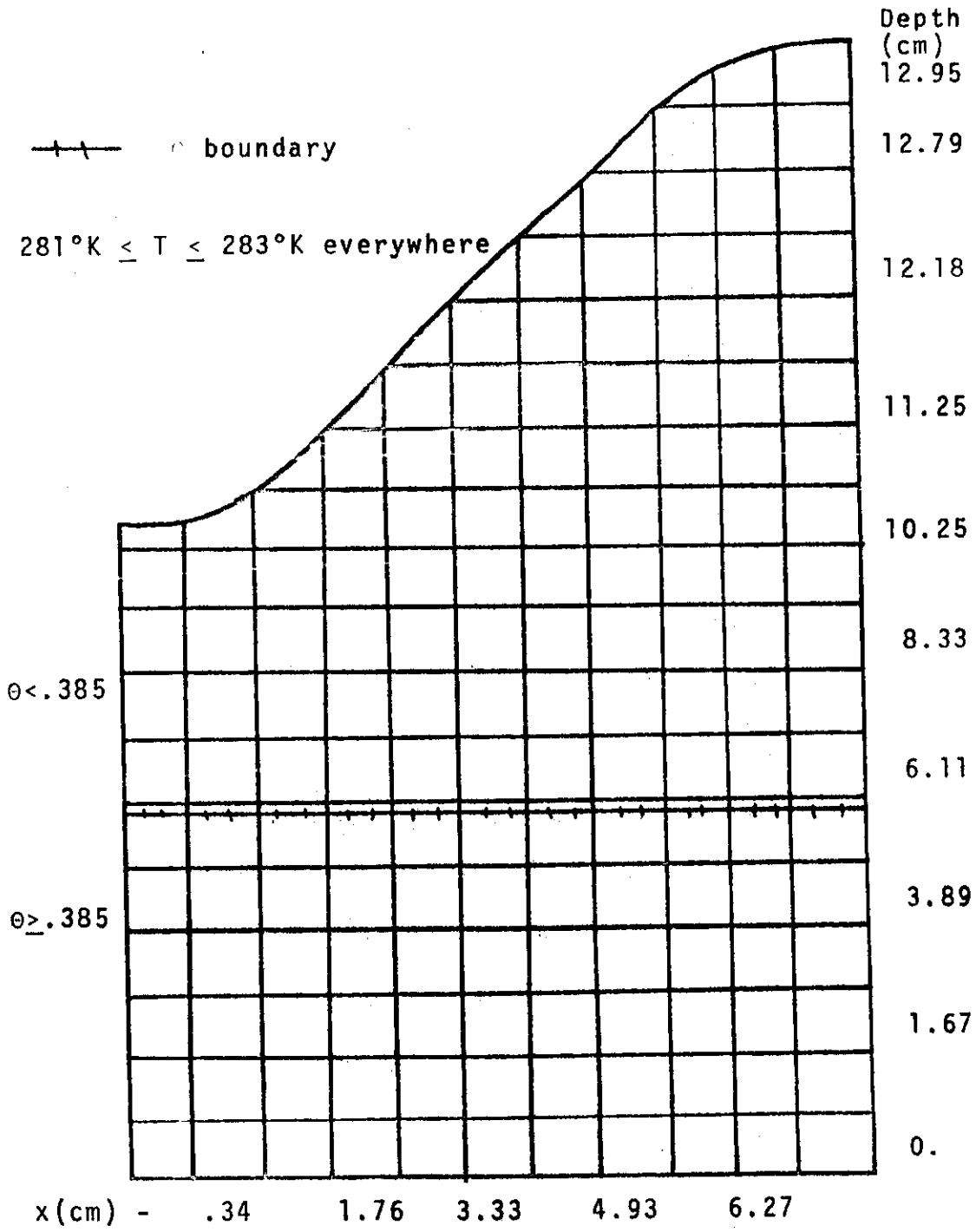

Fig. 15. Profile at 9 A. M.

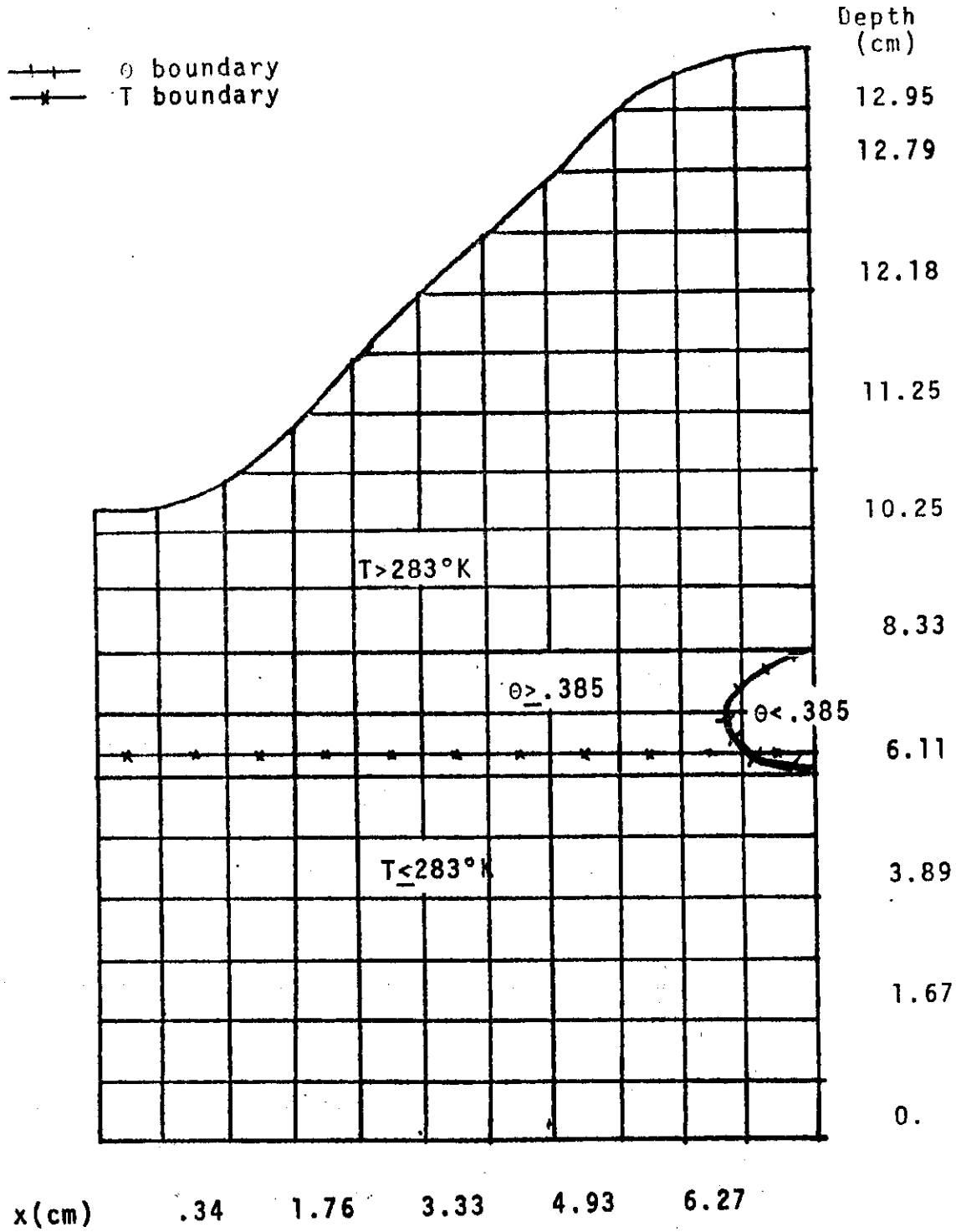

Fig. 17. Profile at 12:30 P. M.

Again using the soil properties of Yolo light clay, a grid was set up having a depth of 10.5 cm. and a width of 20 cm. The soil surface was flat. On top of the soil, a slab (representing a concrete foundation, for instance) was situated covering the right half of the soil surface. This was simulated by eliminating all atmospheric influences for the surface elements under this slab.

At 9 A. M., the entire area had a moisture content of about .35 and a temperature of 288 ° K. As in the previous run, a light rain was allowed to fall for 1 hour (using the saturation value = .45). Then the rain stopped and the soil began drying on the surface area not covered by the slab. Figure 18 represents the moisture profiles of the soil at 10 A. M., 2 P. M., 6 P. M., and 12 midnight. It should be noted that rectangular grid elements of dimensions 1 cm x 1 cm were used, however the grid depicted in Figure 18 was condensed and is actually half the size of the actual grid set up.

In an effort to further validate the model, the model was compared with the linear model developed by Hauk [18] using the properties of Geary Silt Loam. In order to model vertical flow only, a single column was

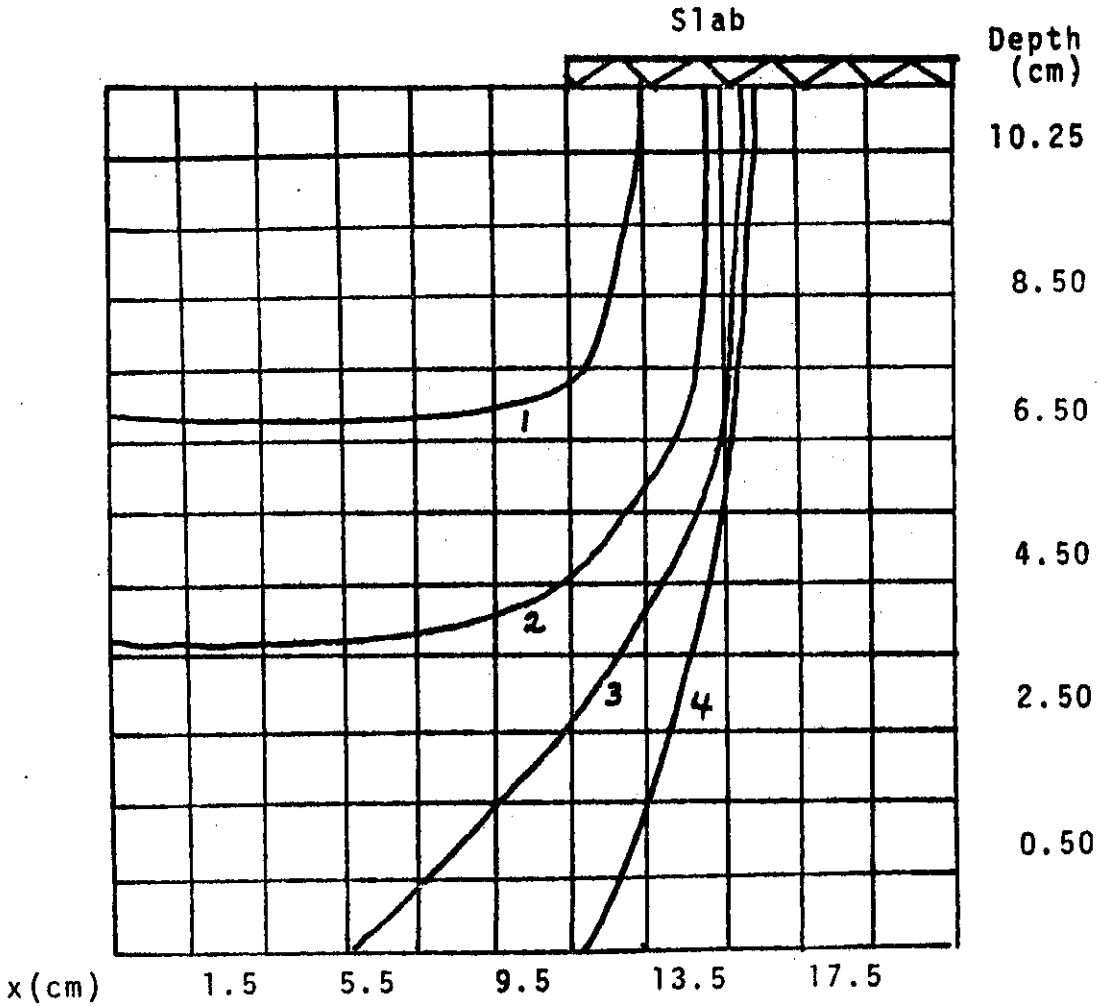

Label	Time	Label	Time
1	$3.6 \cdot 10^3$ sec	3	$3.24 \cdot 10^4$ sec
2	$1.8 \cdot 10^4$ sec	4	$5.40 \cdot 10^4$ sec

Fig. 18. Moisture flow with slab on surface

set up and zero moisture and heat fluxes were used on each side.

Hauk's work included most of the properties of Geary Silt Loam, however not all of the properties needed were available, hence approximations of these values were used. The atmospheric conditions modeled were constant for the duration of the run, simulating heat and moisture flow at noon on a sunny day following a rainfall. This introduced maximum heat fluxes in the soil. The soil was assumed to be near saturation, hence the initial values of [illegible] .36 were used to closely match Hauk's first moisture profile. The soil was given the initial temperature of 280 °K. The air temperature was kept at 294 °K and the relative humidity of the air was set at .5. The comparison of the results of the models is in Figure 19.

Hauk's model predicted only a 1 ° rise (to 281 °K) in the temperature of the soil to a depth of 20 cm after 40 hours, which seems highly unlikely with a difference of 14 ° in the temperatures of the soil and the air. The model of this research predicted a temperature of at least 288 °K at the same depth, which is much more likely in view of the atmospheric conditions.

Note that after 36 hours, the model of Hauk predicted a rewetting of the soil in the 4 to 10 cm range. This model did not predict such a rewetting since the

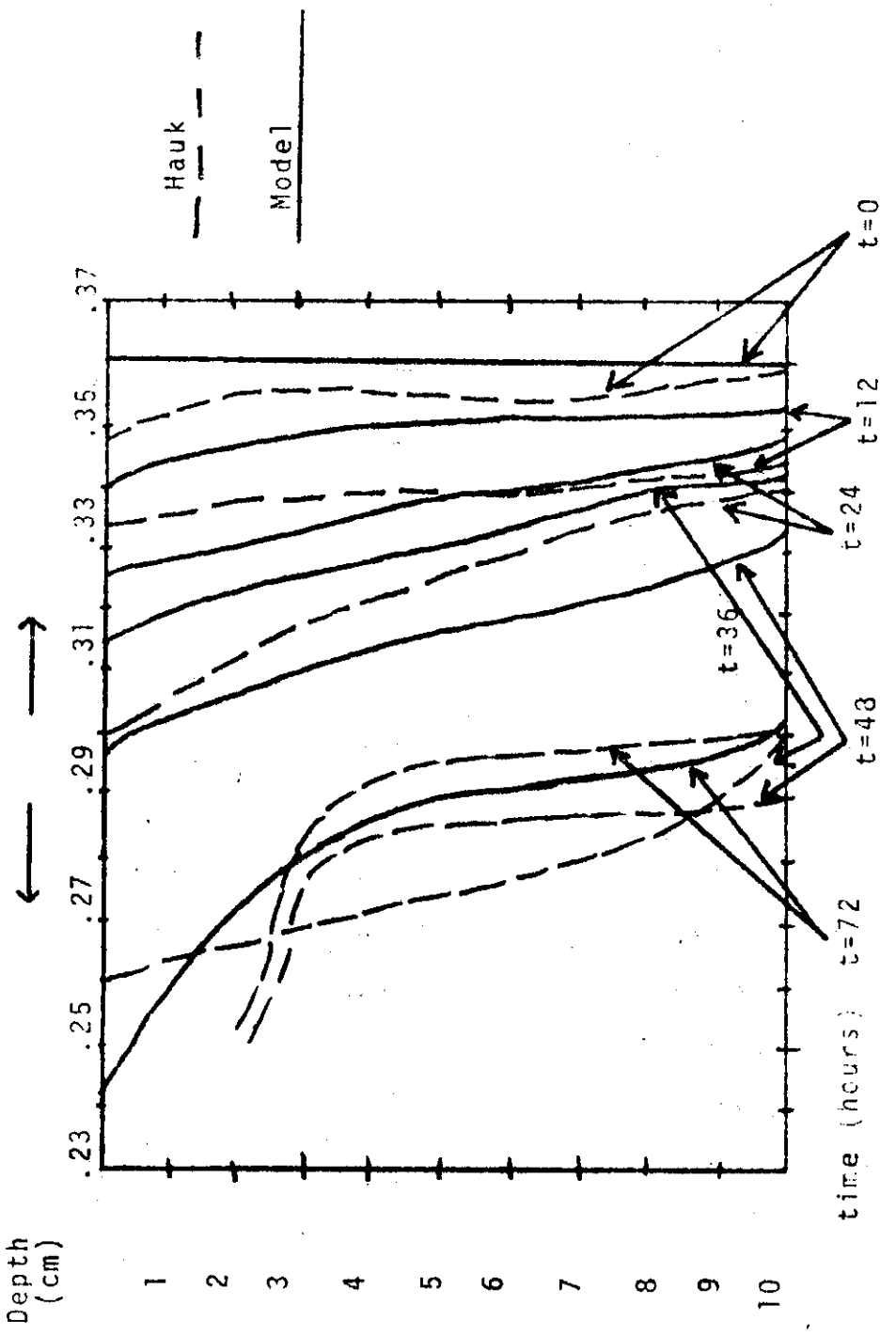

Fig. 19. Comparison of model and Hauk' results.

maximum depth modeled was 20 cm and zero fluxes were maintained at the lower layer, thus preventing the prediction of such rewetting.

Note that although the model developed here did not predict the formation of a dry layer as rapidly as the model of Hauk, the results differ by less than 5 % after 72 hours. These discrepencies could have been caused by the temperature differences mentioned above, by inaccuracies in estimating the soil parameters from the figures of Hauk, by translating the moisture profile of Hauk to the profile in Figure 19, and by the fact that the initial values for moisture used did not allow for the beginning of a dry layer which had already begun forming in the first profile given by Hauk. This last fact alone could cause the model of this research to lag behind Hauk's model by as much as 4 to 8 hours.

Generally, the two models compared quite favorably with respect to predicted moisture values. Seldom are the discrepencies greater than 10 % and the two models are in almost total agreement after 72 hours.

REFERENCES

1. American National Standard Fortran (ANS X 3.9-1966). American National Standards Institute, New York.
2. Bouwer, H. Theoretical Aspects of unsaturated flow in drainage and subirrigation. AG. ENG, 40, 7 (1959), 395 - 400.
3. Breuer, M.A. Generation of optimal code for expressions via factorization. Comm. ACM 12, 6 (June 1969), 333 -340.
4. Busam, V., and Englund, D. Optimization of expressions in FORTRAN. Comm. ACM 12, 12 (Dec. 1969), 666 - 674.
5. Carnahan, B., Luther, H. A., and Wilkes, J. O. Applied Numerical Methods. Wiley, New York, 1969.
6. Chemical Rubber Co. Handbook of Chemistry and Physics. Cleveland, Ohio, 1962.
7. Cohn, C. E. Efficient programming in FORTRAN. Software Age, 2,5 (1968), 22 - 31.
8. De Vries, D. A. Simultaneous transfer of heat and moisture in porous media. Trans. Amer. Geophys. Union, 39, 5 (1958), 909-916.

9. ----. The influence of irrigation on the energy balance and the climate near the ground. J. of Applied Meterology, 16 (1958) 256-270.

10. Dutt, G. R., Shaffer, M. J., and Moore, W. J. Computer simulation model of dynamic biophysio-chemical processes in soils. Technical Bulletin 196, Ag. Experiment Station, Tuscon, Ariz., October 1972.

11. Fitzsimmons, D. S. Simulation of unsteady radial flow in partially saturated soils. ASAE paper no. 71-714 (1971)

12. Fuchs, M. and Tanner, C. B. Evaporation from a drying soil. J. of Applied Meterology, 6 (1967) 852-857.

13. Gardner, W. R. and Mayhugh, M. S. Solutions and tests of the diffusion equation for the movement of water in soil. Proc. Soil Sci. Society 1958, (1958) 197-201.

14. Gordon, D., Dyck, A., and Sesher, S. Good programme design. Report, University of Waterloo.

15. Gordon, G. System Simulation. Prentice Hall, Englewood Cliffs, N. J., 1969.

16. Gries, D. Compiler Construction for Digital Computers. Wiley, New York, 1971.

17. Hanks, R. J., and Bowers, S. A. Numerical solution of the moisture flow equation for infiltration into layered soils. Proc., Amer. Soil Sci. Soc., 26, 6 (1962) 530-534.

18. Hanks, R. J., Gardner, H. R., and Fairbourn, M. L. Evaporation of water from soils as influenced by drying with wind or radiation. Soil Sci. Soc. Amer. Proc., 31, 5 (1967) 593-598.

19. IBM. FORTRAN H Compiler program logic manual. Ref. Man. GC28-6642.

20. Jackson, R. D., Diurnal changes in soil-water content during drying. SSSA Spec. Publ. # 5, Soil Sci. Soc. Amer., Madison, Wisc., 1971.

21. ----, Kimball, B. A., Reginato, R. J., and Nakayama, F. S. Diurnal soil-water evaporation: time-depth-flux patterns. Soil Sci. Soc. Amer. Proc., 37, (1973), 505-508.

22. King, L. G., Hanks, R. J., Nimah, M. N., Gupta, S. C., and Backus, R. B. Modeling subsurface return flow in Ashley Valley. Res. Report, Utah State University.

23. Klute, A. Soil water flow theory and its application field situations. Draft of paper presented at Amer. Agronomy Soc., 1971.

24. Larson, C. The efficient use of FORTRAN. Datamation, (Aug. 1971), 24-31.

25. Mac Camy, R. C., and Mizel, V. J. Linear Analysis and Differential Equations. Macmillan, Toronto, Ontario, 1969.

26. Monteith, J. L., an empirical method for estimating long-wave radiation in the British Isles. Qtrly. J. of the Qtrms. Royal Mlt. Soc., (1961), 171-179.

27. Nimah, M. N., and Hanks, R. J. Model for estimating soil water, plant and atmospheric interrelations. Soil Brief, Utah State University.

28. Phillip, J. R. The theory of infiltration: 1. Soil Sci., 83, (1957), 345-357.

29. ----, and De Vries, D. A. Moisture movement in porous materials under temperature gradients. Trans. Amer. Geophys. Union, 38 (1957), 222-232.

30. Remson, I., Drake, R. L., McNeary, S. S., and Wallo, E. M. Vertical drainage of am unsatruated soil. J. Hy. Div., ASCE, (Jan., 1965), 55-74.

31. Ritchie, J. T. Dryland evaporation in a subhumid climate: I. Agron J. 63(1971), 51-55.

32. ----, and Burnett, E. Dryland evaporation in a subhumid climate: II. Agron J. 63(1971), 56-62.

33. ----, ----, and Henderson, R. C. Dryland evaporation in a subhumid climate: III. Agron J. 64(1972), 168-173.

34. Rose, D. A. Water movement in dry soils, J. of Soil Sci., 19, 1 (1968), 81-93.

35. Rose, C. W. Water transport in soil with a daily temperature wave. Aust. J. Soil Res., 6 (1968), 31-44.

36. Rubin, J. Theoretical Analysis of two-dimensional, transient flow of water in unsaturated and partly unsaturated soils. Proc., Amer. Soil Sci., 32, 5 (1968), 607-615.

37. Scott, E. J., Hanks, R. J., Peters, D. B., and Klute, A. Power series solution of the one-dimensional diffusion equation for exponential and linear diffusivity function. USDA, ARS 41-64. (Sept., 1962).

38. Smithsonian Institution. Smithsonian Meterological Tables, Washington, D. C., 1963.

39. Vogt, C. Optimization with FORTRAN H. Computer Center Newsletter, University of Waterloo.

CHAPTER 4

MODEL OF OXYGEN SUPPLY TO PLANT ROOTS

Contribution by

W. R. Teague
and
K. W. Brown

MODEL OF OXYGEN SUPPLY TO PLANT ROOTS

Introduction

The availability of oxygen at the surface of roots within the soil profile may well regulate the ability of plants to carry on several important functions. Certainly root respiration can not proceed at its optimum rate without an adequate oxygen supply. Without respiration, cell division and elongation will be impaired and thus the roots will not be able to expand into regions where water and essential nutrients may be available. It is well known that root interception is an important mechanism for the uptake of several of the less mobile essential nutrients (Barber, 1966). The possibility also exists that root respiration is necessary to facilitate the uptake of nutrients and water which move to roots. Nutrient difficiencies, and often wilting, occur when the root zone of most crops is flooded.

There is also a growing body of evidence that the supply of oxygen to roots may be limiting for several days after irrigation as showed by Wiegand and Lemon (1958). They found that the oxygen diffusion rate was too low to keep the concentration at the roots above a critical level for up to two days after irrigation even in a sandy soil. Brown and Rosenberg (1970) observed that stomates of irrigated sugar beets had greater resistances to vapor diffusion after irrigation than before. Johnson and Davies (1973) showed that the normal nocturnal expansion of sugar beet roots did not occur for several days after an irrigation. The loss of growth immediately after irrigations may or may not have a significant influence on final yield.

These observations serve to indicate that root water uptake may be limited by the lack of O_2 in the entire profile on certain occasions. Once enough water has been removed from the top of the soil profile, root water uptake may again resume at rates sufficient to meet the demand. Even though the plant needs for water may be met by a particular layer, the ability of the plant to take up water and nutrients at a lower depth may depend on oxygen diffusion to these depths. As additional drying takes place at the top of the soil, the soil water potentials may become too low to allow water uptake. As water is removed from the pores, the greater cross sectional area available for diffusion will increase the supply of O_2 to the air filled soil below. Thus, it is possible that the zone of water uptake, which moves down in the soil as it dries, is bounded above by the surface, or by soil which is too dry to supply water, and below by the depth at which oxygen supply is insufficient to meet the needs of the roots.

The utility of calculating the diffusion of oxygen through the soil profile has been shown by Bakker et al. (1970). They demonstrated the influence of surface sealing on gas diffusion. Lemon (1962) and Lemon et al. (1962) developed a model of the diffusion of oxygen from the air in the soil pores through the water film to the root. Van Bavel (1951) presented a steady-state solution to the diffusion equation utilizing a depth dependent sink term q_s. Papendick, et al. (1965) provided a non-steady-state counterpart to this model, except in this case a uniform sink term was assumed. Covey, et.al. (1962), developed a nonsteady-state model for diffusion into the root. In order to provide insight

into the importance of root oxygen demand, water film thickness around the root and air filled porsity in the soil on the oxygen supply to the roots, and perhaps ultimately to allow calculations of nutrient and water uptake by roots in wet soil, a combined model which takes into account the diffusion of oxygen through both the soil air and the soil water film must be developed.

Theoretical Considerations

An individual active root of a plant consumes oxygen and thus provides an oxygen sink within the soil in which it is growing. If a particular root is idealized as a cylinder; and if the oxygen concentration in the soil air near the root, the oxygen consumption rate of the root, the root diameter and length, water film thickness on the root, and appropriate diffusivities are known; then the oxygen concentration within the root may be determined as a function of distance from the root axis by a steady-state cylindrical diffusion analysis, provided variations of O_2 concentrations in the pores during the time intervals considered are small and provided logitudinal gradients of oxygen consumption rate within the root are not significant. Lemon (1962) and Lemon et al. (1962) have taken this approach in treating root-oxygen use and have given solutions of the equation

$$\frac{1}{r}\frac{\partial}{\partial r}\left(D_r \frac{\partial C}{\partial r}\right) = q \qquad (1)$$

where q is the oxygen consumption rate per unit root volume.

While it may be true that at a given time approximately steady-state prevails under normal conditions, in order to realize the effect that root-consumption, variations in root consumption rate, and varying soil conditions have on oxygen concentrations in the soil and in the roots themselves, an approach that will provide for time-varying concentrations is required. Use of nonsteady-state diffusion analysis seems appropriate.

Due to the complexity of root distributions within the soil it would be difficult to solve even the steady-state problem where boundary conditions were given for each root in a given soil segment. The present model avoids the complexities encountered on a microscopic scale but provides insight into the entire diffusion process.

I. Soil

If it is assumed that roots are uniformly distributed throughout a given soil segment, then the total oxygen consumption by roots in that segment will constitute a diffuse oxygen sink. Therefore, in one dimension for example, the diffusion equation with boundary conditions

$$f \frac{\partial C_s}{\partial t} = \frac{\partial}{\partial z} \left(D_s \frac{\partial C_s}{\partial z} \right) - q_s(z) \qquad (2)$$

$$C_s\ (o,t) = C_a$$

$$\frac{\partial C_s}{\partial z} \Big|_{z = z_D} = 0$$

may be applied to the movement of O_2 from the surface $z = 0$ to some depth z_D where O_2 flux becomes negligible, where the sink term $q_s(z)$ is added to account for the root consumption at intermediate depths. Much literature is available on numerical solutions of equations of this type, but in order to implement a solution, the nature of the function q_s must be known as well as the nature of D_s. The analysis of q_s will be deferred until equation (5) has been discussed.

A number of equations which describe the dependence of D_s on soil aeration porosity are available in the literature (Papendick, et al., 1965 or Bakker, et al., 1970). The following two equations were chosen for use in the model, as use of both equations apparently will provide capability of analysis of a variety of soil conditions:

$$D_s = .66fD_a \quad \text{(Penman, 1940)} \qquad (3)$$

$$D_s = f^{4/3}D_a \quad \text{(Millington, 1959)} \qquad (4)$$

where f = aeration porosity and D_a = diffusion coefficient for O_2 in air ($1.8 \times 10^{-5} cm^2/sec$). Equation (3) takes into account the effect of changes in diffusion cross-section with changes in porosity (multiplication by f) and the effect of tortuosity (multiplication by 0.66). Equation (4) introduces a non-linear reduction in cross-section (or increase in tortuosity) with decreasing aeration porosity. This equation may be more suitable for analysis of clay soils having a larger proportion of pores which do not contribute significantly to diffusion cross-section at higher water contents.

II. Water Film

Water films occur on plant roots in varying thicknesses, depending on the soil moisture potential. The relationship between the water film thickness and soil moisture potential depends on the soil under analysis. Wiegand et al. (1958) have presented data taken on Miller clay that enables the determination of this functional relationship for a limited range of soil moisture potentials (Ψ). It was found, using their data, that the water film thickness could be expressed:

$$S = 0.0365\ (\exp(3.68 \times 10^{5}(7.5 \times 10^{-6}-((\log(-\Psi) + 2.489) \times 10^{-6})/0.285))-1.) \qquad \text{(cm)}$$

The equation which describes the diffusion process within the water film is:

$$\frac{\partial C}{\partial t} = \frac{1}{r}\frac{\partial}{\partial r}\left(D_w\, r \frac{\partial C}{\partial r}\right) \qquad R \le r \le R + S \qquad (5)$$

where R is the root radius and S is the water film thickness

III. Oxygen Diffusion in Water

The value of D_w in (5) is 2.6×10^{-5} cm^2 sec^{-1} at 25°C. For other temperatures Wiegand et al. (1958) reported a linear relationship between D_w and the temperature T:

$$D_{w_T} = D_{w_{25}}\ (1. + .03\ (T-25)). \qquad (6)$$

This relationship is utilized in the model.

IV. Solubility of O_2 in water

In order to relate the oxygen concentration in the water film to that in the soil atmosphere, the solubility of oxygen in water must be taken into account. Henry's Law was used for this purpose. This relationship, which describes the relationship of a solute in dilute solution to the partial pressure of the vapor of the solute above the solution, can be stated for oxygen and water as:

$$PO_2 = h \cdot XO_2 \qquad (7)$$

where PO_2 is the partial pressure of oxygen in the soil air, XO_2 is the mole fraction of the dissolved oxygen, and h is Henry's Law constant.

PO_2 can be obtained from the concentrations of oxygen and nitrogen and the partial pressure of nitrogen in the soil air:

$$PO_2 = \frac{0.8\ C_s/32}{N_2 \text{ concentration (air)}/28.}$$

Assuming no change in N_2 concentration with depth, the quantity in the denominator can be obtained from the density of air and is:

$$N_2 \text{ concentration (air)}/28 = 3.5 \times 10^{-5}\ m/cm^3.$$

Therefore:

$$PO_2 = \frac{0.8\ C_s}{32 \times 3.5 \times 10^{-5}} \qquad (8)$$

The mole fraction XO_2 of oxygen is obtained:

$$XO_2 = \frac{[O_2]}{[O_2] + [H_2O]} \simeq \frac{[O_2]}{[H_2O]} = \frac{[O_2]}{55.6.} \qquad (9)$$

Substituting (7) and (8) into (6), we get:

$$[O_2] = \frac{55.6 \cdot 0.8}{h \cdot 32 \cdot 3.5 \times 10^{-5}} \cdot C_s .$$

Since the quantity $[O_2]$ has units (moles/liter), multiplying by the factor 32/1000 yields the desired quantity (in gm/cm^3):

$$O_2 \text{ concentration at water film surface} = 1270 \frac{C_s}{h}.$$

At 23°C h has the value, 4.187×10^4; therefore, the oxygen concentration at the water film surface can be expressed:

$$C(\text{water film surface}) = k \cdot C_s$$

where

$$k = \frac{1270}{h}$$

Examination of values of h for different temperatures (Int. Crit. Tab.) revealed an approximately linear relationship between these quantities. The equation used in the model was:

$$h = (2.0 + .0514\ T) \times 10^7/760.0.$$

V. Microbial Respiration Rate

The rate of microbial respiration in the soil is assumed, for the present purpose, to depend on the temperature of the soil and, under limiting conditions, the oxygen concentration in the soil. The data available for making reasonable quantifications of consumption rate is limited, but an effort has been made to make estimates of rates on the basis of values determined by observers and to take into account the effects of temperature and limiting oxygen supply in a rational way. The possible influence of dessication at low potentials will not be included, since our work will be concentrated in the replication of high potentials. The influence of other parameters such as substrate concentration are also not included.

The rate at which microbes multiply has been related to temperature via thermodynamics (Hattori, 1973). For modeling purposes it was assumed that respiration rate would increase or decrease in proportion to the rate of increase or decrease of the multiplication rate; thus, the equation:

$$TEMF = .01CT \exp(-\Delta H_1/RT)/(1 + \exp(+\Delta S/R)\exp(-\Delta H_2/RT))$$

$C = .3612 \exp(24.04)$ R = Universal Gas Constant (2.0 cal°K^{-1})

ΔH_1 = 15,000 cal T = Temperature (°K)

ΔH_2 = 150,000 cal S = 476.46 cal °K^{-1}

was developed from data on the relative rate of multiplication of Escherichia coli (Hattori, 1973), and used to modify the optimum oxygen consumption rate RESM.

The influence of oxygen concentration on microbial activity is approximately linear between zero concentration and concentration of 4% (Hattori, 1973 and Griffin, 1972). Between this concentration and 21% they found the level of activity to be independent of O_2 concentration.

In practice a value of O_2 consumption rate (RESM), which was considered to be optimum for the soil being modeled, was introduced as input. For testing purposes, values in the range 1.2 to 12 µℓ (gm soil)$^{-1}$ hour^{-1} Grable, et al., 1968) were used for RESM. This in turn was multiplied by the factor TEMF and modified according to the O_2 concentration C_s to obtain the value q_m for the microbe respiration rate.

VI. Soil Sink Term

The flux of oxygen across the water film surface is expressed as:

$$q_{wfs} = \int_{\text{Root}} \left(\frac{\partial C}{\partial t} + q_r\right) dv + \int_{\substack{\text{Water} \\ \text{film}}} \frac{\partial C}{\partial t}\, dv$$

This value is multiplied by the root density (γ_R) and divided by the aeration porosity (f) to obtain the consumption rate by roots. The value of the soil sink term q_s is obtained:

$$q_s = q_m + q_{wfs} \times \gamma_R$$

VII. Root

The following equation is solved to obtain concentrations of oxygen within the root

$$\frac{\partial C}{\partial t} + q_r = \frac{1}{r}\frac{\partial}{\partial r}(D_i \; r \frac{\partial C}{\partial r}) \qquad 0 < r < R \qquad (10)$$

$$\left.\frac{\partial C}{\partial R}\right|_{r = 0} = 0$$

A value of 9.0×10^{-6} cm^2/sec (25°C) has been reported for D_i for onion root tips (Berry and Norris, 1949). As the diffusion was assumed to occur primarily in the liquid phase within the root, the linear equation used to describe the temperature dependence of D_w was also used here, except in this case D_w (25) has been replaced by D_i (25).

The term q_r in equation (10) represents the oxygen consumption rate (gm cm^{-3} sec^{-1}) of the root. Values for different species of plants are available in the literature (Lemon and Wiegand, 1962) and most of these lie in the range 10^{-8} to 10^{-6} gm cm^{-3} sec^{-1}. It has been shown (Huck, et al., 1962) that the consumption rate is not necessarily constant, but may vary diurnally. For the present, q_r is calculated as a periodic function

$$q_r = U_1 + U_2 \sin \tau$$

where U_1 and U_2 are inputs to the program, and τ is a normalized time

argument.

General Discussion of Solution Technique Used for Obtaining O_2 Concentration in Soil Layers, Roots, and Water Films

This discussion is applicable to finite- difference solution of the diffusion equation in the following areas:

Area		
1. Soil	$f\frac{\partial C}{\partial t} = \frac{\partial}{\partial z}(D \cdot \frac{\partial C}{\partial z}) - q_s$	(11)
2. Roots in any one of the N soil layers considered	$\frac{\partial C}{\partial t} = \frac{1}{R}\frac{\partial}{\partial R}(D \cdot R \cdot \frac{\partial C}{\partial R}) - q_r$	(12)
3. Water film on roots in any one of the soil layers	$\frac{\partial C}{\partial t} = \frac{1}{R}\frac{\partial}{\partial R}(D \cdot R \cdot \frac{\partial C}{\partial R})$	(13)

In each case, C, D, and q represent the concentration, diffusion coefficient, and sink term appropriate to the given area.

There are basic parts of the solution format for these equations which are common to all three areas. For convenience of comparison with the program the equations used here will be written in Fortran.

In each case the particular media is segmented into subareas depending on the geometry and dimensions characteristic of that media. For the soil, the segments are bounded by parallel planes on the order of cms apart. For the root and water film, the segments are bounded by concentric cylinders usually on the order of $\Delta R = 10^{-2}$cm. Figure 1 gives schematics which illustrate the segmentations and the program names of the concentrations in each area.

Moreover, in each case, concentrations are obtained as functions of time dated from a starting time t_0, by successive updates of concentrations over finite size time steps Δt. There are two such time steps

utilized; one is for the roots and water films for a given layer (Δt = DT1(I)), and the other is for the soil layers (Δt = DTAU). DT1(I) is chosen to divide DTAU an integral number of times, and both are chosen to insure stability of the finite difference scheme. As DT1(I) is usually necessarily smaller than DTAU, DTAU/DT1(I) computations are done for the roots and water films in layer I for each DTAU time step for the soil in layer I. The stability criterion for DTAU and DT1(I) will be discussed later.

Except in the case of CO(I) (Concentration at root axis), C(N) (Concentration at the bottom of the soil profile), CW1(I, KMAX(I)) (Concentration at water film surface), or CR(I) (Concentration at root surface) when there is no water film, the updating process consists of calculating a particular concentration at the end of a time-step as a weighted average of three quantities (the concentration under consideration and the concentrations at points adjacent to the point under consideration, e.g. CS(I), CS(I-1), CS(I+1), at the beginning of the time step) plus a sink term, where applicable. For example:

$$C(I) = AS1(I) * CS(I-1) + AS2(I) * CS(I) + AS3(I) * CS(I+1) + DTAU * QS(I) \quad (14)$$

where AS1(I) + AS2(I) + AS3(I) = 1.

CS(I-1) + AS2(I) * CS(I) + AS3(I) * CS(I+1) + DTAU * QS(I)

where AS1(I) + AS2(I) + AS3(I) = 1.

The coefficients AS1, AS2, and AS3 in this case, and corresponding coefficients in other cases, depend on the relative diffusivities and

sizes of the segments adjacent to the point where C(I) is calculated. Derivations of these coefficients for particular cases will be given below. This form of the equation was chosen for the sake of economy of computer time. The coefficients, which need be calculated only once, replace numerous operations that would otherwise be needlessly repeated.

The basic tools used in calculating the coefficients for computation of a given concentration are:

(A) application of the appropriate diffusion equation at the point in question,

(B) use of one-dimensional Taylor's Approximation for determining the finite-difference expression for $\frac{\partial^2 C}{\partial z^2}$ or $\frac{\partial^2 C}{\partial R^2}$, and

(C) application of continuity of flux at the point in question.

To illustrate the use of these principles, the coefficients AS1(I), AS2(I), and AS3(I) are derived for 2 <I<N-1 for the case where there is no abrupt change in diffusion properties of the soil in the vicinity of the point Zi where C(I) is to be computed. Expanding C in a Taylor's Series about the point Zi, we have:

$$C(I-1) = C(I) - \Delta z \frac{\partial C}{\partial z}\Big|_{Z_i} + \frac{\Delta z^2}{2} \frac{\partial^2 C}{\partial z}\Big|_{Z_i} + \ldots$$

or

$$C(I-1) = C(I) - \Delta z \frac{\Delta C}{\Delta z}\Big|_{Z_i} + \frac{\Delta z^2}{} \frac{\partial^2 C}{\partial z^2}\Big|_{Z_i} - \ldots$$

Solving for $\frac{\partial^2 C}{\partial z^2}\Big|_{Z_i}$ and dropping the $|_{Z_i}$ for brevity, yields

$$\frac{\partial^2 C}{\partial z^2} = \frac{2}{\Delta z^2}\,(C(I) - C(I)) + \frac{2}{\Delta z}\,\frac{\partial C}{\partial z} \qquad (15)$$

In a similar manner, the approximation

$$\frac{\partial^2 C}{\partial z^2} = \frac{2}{\Delta z^2}\,(C(I+1) - C(I)) - \frac{2}{\Delta z}\,\frac{\partial C}{\partial z} \qquad (16)$$

is obtained.

Application of the diffusion equation (11) at Z_1 and substitution of (15) and (16) results respectively in the two equations:

$$f(I) \cdot \frac{\partial C}{\partial t} = D\left(\frac{2}{\Delta z^2}\,(C(I-1) - C(I)) + \frac{2}{\Delta z}\right) + \frac{D}{\partial z}\,\frac{C}{\partial z} - q_s \qquad (17)$$

and

$$f(I) \cdot \frac{\partial C}{\partial t} = D\left(\frac{2}{\Delta z^2}\,(C(I+1) - C(I)) - \frac{2}{\Delta z}\,\frac{\partial C}{\partial z}\right) + \frac{\partial D}{\partial z}\,\frac{\partial C}{\partial z} - q_s \qquad (18)$$

Rearranging (17) and (18) to obtain the flux at Z_1 yields:

$$D\frac{\partial C}{\partial z} = \left((f(I) \cdot \frac{\partial C}{\partial t} + q_s) - \frac{2D}{\Delta z^2}\,(C(I-1) - C(I))\right) / \left(\frac{1}{D}\,\frac{\partial D}{\partial z} + \frac{2}{\Delta z}\right) \qquad (19)$$

and

$$D\frac{\partial C}{\partial z} = ((f(I)\cdot \frac{\partial C}{\partial t} + q_s) - \frac{2D}{\Delta z^2}(C(I+1) - C(I)))/(\frac{1}{D}\frac{\partial D}{\partial z} + \frac{2}{\Delta z}). \quad (20)$$

Setting (11) and (12) equal to obtain continuity of flux and rearranging, we get:

$$f(I)\cdot \frac{\partial C}{\partial t} = (-.5\,\frac{\partial D/\partial z}{\Delta z} + \frac{D}{\Delta z^2})\,C(I-1) - (\frac{D}{\Delta z^2} + \frac{D}{\Delta z^2})C(I)$$

$$+ (.5\,\frac{\partial D/\partial z}{\Delta z} + \frac{D}{\Delta z^2})C(I+1) - q_s \quad (21)$$

The program name for D in soil layer I is DS(I). By assuming D varies continuously and smoothly, $\frac{\partial D}{\partial z}$ can be replaced by $\frac{DS(I+1) - DS(I-1)}{2\ DZ}$ where DZ is the program name for Δz. By denoting the concentration at the beginning of the time step by CS(I) and at the end by C(I) and using the program name DTAU for Δt, $\frac{\partial C}{\partial t}$ can be replaced by $\frac{C(I)-CS(I)}{DTAU}$. Substitution into (10) and using CS(I), CS(I-1) and CS(I+1) on the right hand side leads to the finite difference approximation (14) where

AS1(I) = DTAU * (DS(I) + .25 * (DS(I+1) - DS(I)))/(DZ**2*F(I))

AS3(I) = DTAU * (DS(I) + .25 * (DS(I+1) - DS(I)))/(DZ**2*F(I))

AS2(I) = 1. - AS1 (I) - AS3(I).

Although similar coefficients are used throughout for calculation of concentrations, different conditions, which prevail in certain instances, require the modification of the assumptions used to calculate AS1, AS2, and AS3. These conditions and the assumptions made will be

discussed, but the coefficients will not be derived in each case, since derivations in all cases are similar.

Layered Soil and Wetting Fronts

In the case of an abrupt change in aeration porosity of the soil between two depths Z_i-1 and Z_i, due either to an abrupt change in bulk density or to the presence of a wetting front, the resulting discontinuity in DS and its derivative $\frac{\partial(DS)}{\partial z}$ is taken into account by the calculation of an auxillary concentration CT(I) at the mid-point Z_i-1/2 between Z_i-1 and Z_i. In the case of a layered soil, the network of concentrations {C(J)} can be superimposed so that such boundaries lie midway between the points where the {C(J)} are calculated. In the case of wetting fronts, which are nonstationary, the error introduced by missing the position of the front can be controlled by the choice of the depth increment Δz = DZ The value .5(CS(I-1) + CS(I)) is assigned to CT(I) as a starting value, as no initial value is available for CT(I). Updates are then made in accord with the method already discussed. The following changes are implemented in the application of equations (17) and (18).

In equation (17) D is replaced with DS(I-1) and in equation (18), with DS(I). $\frac{\partial D}{\partial z}$ is assigned the value (DS(I-1) - DS(I-2))/D in equation (17), and in equation (18) it has the value (DS(I+1) - DS(I))/DZ. The counterpart of equation (14) in this case is

$$CT(I) = AT1(I) * CS(I-1) + AT2(I) * CTS(I) + AT3(I) * CS(I) - (F(I-1)*q_s(I-1) + F(I)*q_s(I))/(F(I-1) + F(I))$$

```
AT1(I) = (8. * F(I-1) * DTAU * DS(I-1)/(F(I-1) + F(I))) * (DS(I+1)/
         DS(I) - 5.)/(DS(I+1)/DS(I) + DS(I-2)/DS(I-1) - 10.)
AT3(I) = (8. * F(I) * DTAU * DS(I)/(F(I-1) + F(I))) * (DS(I-2)/DS(I-1)
         - 5.)/(DS(I+1)/DS(I) + DS(I-2)/DS(I-1) - 10.)
AT2(I) = 1. - AT1(I) - AT3(I).
```

Note that CT(I) is the concentration calculated for the boundary above Z_i (where C(I) is calculated), as this will be the case in the discussion that follows. (See Figure (2) for illustration of concentrations at boundaries.)

A modification of the coefficients AT1, AT2, AT3 occurs if two abrupt changes in aeration porosity occur consecutively with respect to depth, as might be the case for a pan of depth DZ.

The term $D\frac{\partial C}{\partial z}$ in equations (17) and (18) has been ignored in the derivation of the coefficients for this case since there is no way of estimating $\frac{\partial D}{\partial z}$ within the pan (where the thickness is only DZ) since the knowledge of the medium is restricted to the value of DS(I) obtained at the center Z_i. However, it seems reasonable to expect that any variation in DS within the pan may be assumed negligible compared to changes at the boundaries, Z_i-1/2 and Z_i+1/2. If CT(I) is the concentration at the lower boundary of such a pan, ((b) in Figure 2) the coefficients are:

```
AT1(I) = (8. * F(I-1) * DTAU * DS(I-1)/(F(I-1) + F(I))) * (DS(I+1)/
         DS(I) - 5.)/(DS(I+1)/DS(I) + DS(I-2)/DS(I-1) - 10.)
AT3(I) = 32. * DTAU * DS(I) * F(I)/((9. - DS(I+1)/DS(I)) * DZ **
         2 * (F(I-1) + F(I)))
AT2(I) = 1. - AT1(I) = AT3(I),
```

corresponding to concentrations CS(I-1), CIS(I) and CS(I) respectively. For the upper boundary ((a) in Figure 2).

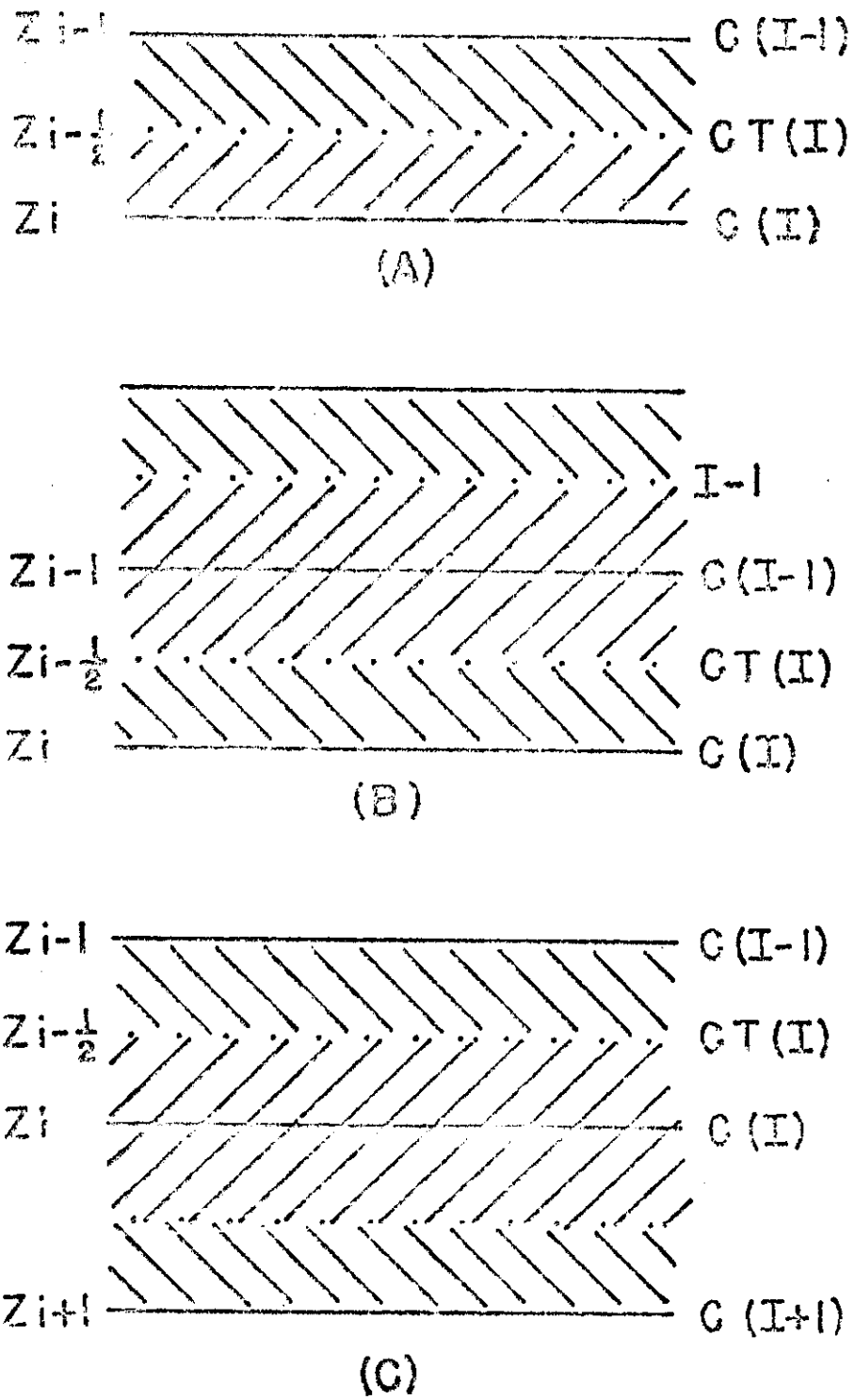

Figure 2. Schematic of finite-difference segmentation near boundaries between wet and dry or compacted and non-compacted layers. A. Adjacent layers of thickness greater than DZ. B. and C. A layer of thickness DZ. Dotted lines represent boundaries between layers. Solid lines represent point of calculation of concentrations in the original network.

```
AT1(I) = 32. * DTAU * DS(I) * F(I)/((9. - DS(I+1)/DS(I)) * DZ **
         2 * (F(I-1) + F(I)))
AT3(I) = (8. * F(I-1) * DTAU * DS(I-1)/(F(I-1) + F(I))) * (DS(I+1)/
         DS(I) - 5.)/(DS(I+1)/DS(I) + DS(I-2)/DS(I-1) - 10.)
AT2(I) = 1. - AT1(I) - AT3(I).
```

Computation of coefficients corresponding to concentrations C(I-1) and C(I+1) in (C) of Figure 2 directly above or below such boundaries must also be modified. Three cases are handled as follows:

Case 1: If C(I) is the concentration at Z_i directly above the point of discontinuity, the coefficients are:

```
AS13(I) = 8. * DTAU * DS(I) * (3. - DS(I-1)/DS(I))/(( 7. -
          DS(I-1)/DS(I)) * DZ ** 2* F(I))
AS11(I) =  8. * DTAU * DS(I)/(( 7. - DS(I-1)/DS(I)) * DZ ** 2* F(I))
AS12(I) = 1. - AS11(I) - AS13(I).
```

corresponding to CS(I-1), CTS (I+1), and CS(I).

Case 2: If C(I) is calculated at Z_i directly below the point of discontinuity,

```
AS23(I) =  8. * DTAU * DS(I)/(( 7. - DS(I+1)/DS(I)) * DZ ** 2* F(I))
AS21(I) = 8. * DTAU * DS(I) * (3. - DS(I+1)/DS(I))/(( 7. -
          DS(I+1)/DS(I)) * DZ ** 2* F(I))
AS22(I) = 1. - AS21(I) - AS23(I),
```

corresponding to CTS(I), CS(I), CS(I+1) respectively.

Case 3: If C(I) is the concentration for the center of the pan layer,

AS31(I) = 4. * DTAU * DS(I)/(DZ ** 2 * F(I))

AS33(I) = AS31(I)

AS32(I) = 1. - 2 * AS31(I).

In all three of the above cases, as well as in the calculation of CT(I), $\frac{\partial D}{\partial z}$ has been included where an estimate was available, although the term may add little in comparison to the contribution of the discontinuities at the boundaries.

The means for invoking the special case calculations of the coefficients is, for the present, comparison of adjacent values of DS(I). For example, if DS(I)/DS(I-1) > 5. or if DS(I-1)/DS(I) > 5., CT(I) is calculated and the appropriate set of coefficients is used for the calculation of concentrations near or at the boundaries.

Root Concentration

Equation (12) is the basis for determining concentrations in the root interior; there are two such concentration calculated, namely, CO(I) and CI(I), as indicated in figure 1. The determination of the coefficients for CI(I) is a straight-forward application of the principles (a), (b), and (c); thus

AI1(I) = 2. * DT1(I) * DI/RRT(I) ** 2

AI3(I) = 6. * DT1(I) * DI/RRT(I) ** 2

AI2(I) = 1. - AT1(I) - AI3(I), where,

CI(I) = AI1(I) * COS(I) + AI2 * CIS (I) + AI3(I) * CRS(I) -

DT1(I) * QR(I).

To obtain coefficients for CO(I), the boundary condition $\frac{\partial C}{\partial R}$ R=0

must be applied. The term $\frac{D}{R}\frac{\partial C}{\partial R}$ in the expanded form of equation (12) is indeterminate at R = 0, but L'Hospital's rule yields:

$$\lim_{R\to 0} \frac{\partial C}{\partial} /R = \lim_{R\to 0} \frac{\partial^2 C}{\partial R^2} = \frac{\partial^2 C}{\partial R^2}\Big| R = 0$$

Therefore at the root axis equation (12) becomes

$$\frac{\partial C}{\partial t} = 2D \frac{\partial^2 C}{\partial R^2} - q_r.$$

Use of Taylor's approximation and proper arrangement yields

```
AR1(I) = 16. * DT1(I) * DI/RRT(I) ** 2
AR2(I) = 1. - AR1(I)
```

where,

```
CO(I) = AR1(I) * COS(I) + AR2(I) * CIS(I) - DT1(I) * QR(I).
```

The root surface provides a boundary between the root interior and the water film. Determination of coefficients for calculation of CR(I) proceeds again with application of (a), (b), and (c), but in this case the term QR(I) is included in the equation that would correspond to (17) for the soil case, while in the equation that would correspond to (18) it is not included. There is also a difference in the diffusivities in the two equations as DI is used in the first while DW is used in the second. The coefficients are:

```
BR1(I) = 2. * DI * DT1(I) * (4./WFT1(I,1) - 1/RRT(I))/
         ((1./RRT(I) + 1./WFT1(I,1)) * RRT(I) ** 2)
```

$$BR3(I) = 10. * DW * DT1(I)/(RRT(I) * (1/WFT1(I,1) + 1/RRT(I)))$$

$$BR2(I) = 1. - BR1(I) - BR3(I)$$

$$BR4(I) = .25 * DT1(I) * (1./RRT(I)-4/WFT1(I,1))/(1./RRT(I) + 1./WFT1(I,1))$$

where

$$CR(I) = BR1(I) * CIS(I) + BR2(I) * CRS(I) + BR3(I) * CWS(I) + BR4(I) * OR(I).$$

Water Film

Analysis of the finite difference scheme derived for calculation of concentrations within the water film reveal that a minimal amount of caution must be observed in making these calculations. If a calculation is to be made corresponding to RZ + ΔR cm (radially) from the root axis, where RZ represents the distance from the root axis of the neighboring location of calculation (nearer to the root axis), then ΔR must satisfy $\Delta R < 4 \times RZ$. To insure the satisfaction of this constraint and to provide a reasonable degree of uniformity of layer thickness, water film layers were allowed to be no greater than ΔR = 2. * RRT. For the first water film layer an additional calculation, CW(I), is made at the cylinder of the first water film layer (see Figure 1). In summary, after water film thickness has been calculated, layers are developed according to the above constraint. Then, as long as the water film thickness does not change, calculations of concentration (CW1(I,k)) are made at the outer boundary of each layer. For the first layer, an additional calculation (CW(I)) is made corresponding to the radial center of this layer.

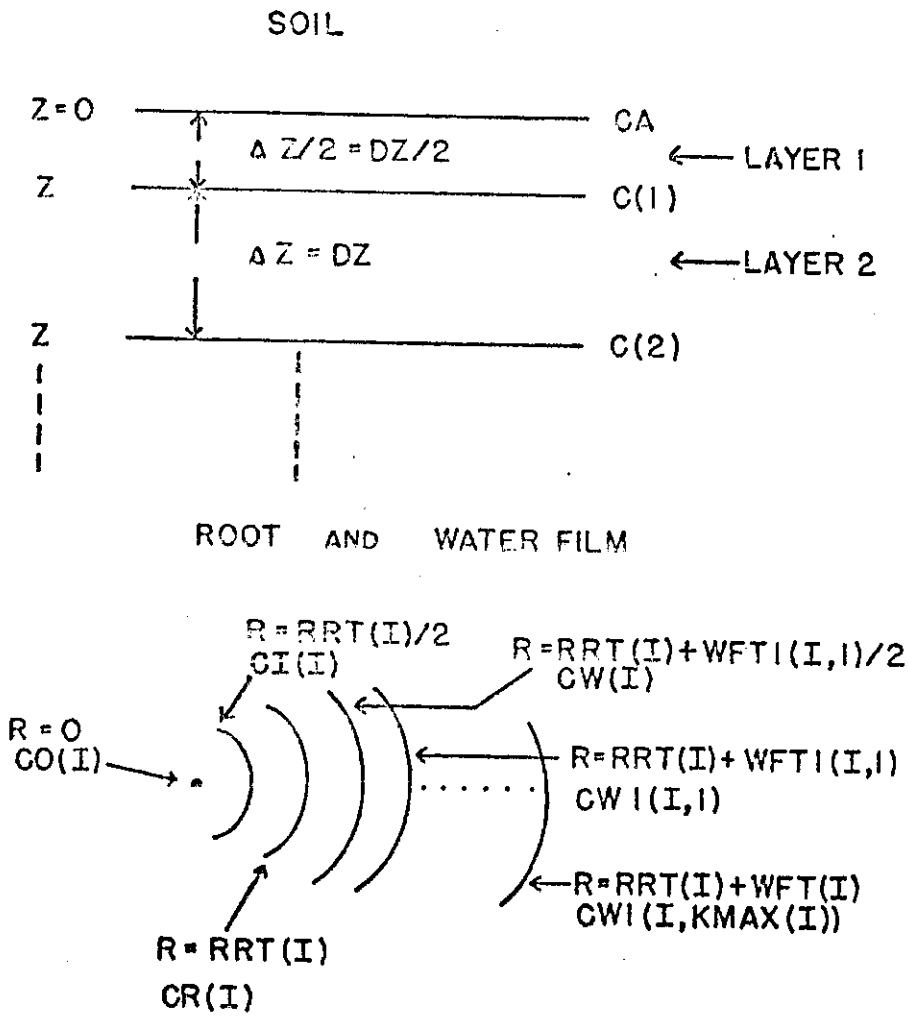

Figure 1. Top: Schematic of finite-difference segmentation of soil. Bottom: Schematic of root and water-film layering.

The concentration CW1(I,KMAX(I)) corresponding to the outer most layer is set at

CW1(I,KMAX(I)) = HK * CS(I).

The coefficients for the calculation of the remaining concentrations CW1(I,K) are:

CW1(I,K) are:

AWF1(I,K) = DW * DT1(I) * (1./WFT1(I,K) ** 2 - .5/(WFT1(I,K) * RZ))

AWF3(I,K) = AWF1(I,K) + DW * DT1(I)/(WFT1(I,K) * RZ)

AW2(I,K) = 1. - AWF1(I,K) - AWF3(I,K) $2 \leq K \leq KMAX(I) - 2$

Slight modifications of these coefficients are used for the cases, K = 1 and K = KMAX(I) - 1. The above coefficients are utilized in the equation

CW1(I,K) = AWF1(I,K) * CW1S(I,K-1) + AWF2(I,K) * CW1S(I,K) + AWF3(I,K+1) * CW1S(I,K+1).

The equation

CW(I) = AW1(I) * CPS(I) + AW2(I) * CWS(I) + AW3(I) * CW1S(I,1)

is used to yield CW(I), where,

AW1(I) = DW * DT1(I) * (4./WFT1(I,1) ** 2 - 1./((RRT(I) + .5 * WFT1(I,1)) * WFT1(I,1)))

AW3(I) = DW * DT1(I) * (4./WFT1(I,L) ** 2 + 1./((RRT(I) + .5 * WFT1(I,1)) * WFT1(I,1)))

AW2(I) = 1. - AW1(I) - AW3(I).

Validation of Numerical Procedure

Due to the complexity of the model, validation was carried out in two steps. For diffusion through the soil, comparison was made with results presented by Papendick and Runkles (1965). They showed oxygen concentration with time and depth in a 150 cm soil column, where a constant sink term, q_s, a uniform initial concentration, and atmospheric concentration at the surface were assumed. Using depth increments of 10 cm, our calculations differed from theirs at 135 cm, after 16 hours, by 2 to 3%. The agreement was better near the surface.

For testing diffusion across the water film and root, comparison was made with results presented by Carslaw and Jaeger (1947) for radial diffusion in an infinite cylinder. To do this, the diffusion coefficients in the root and water film were set equal, and the root consumption rate was assumed to be 0. Initial concentrations were set to zero, and a concentration corresponding to atmospheric (as modified by Henry's Law) was assumed at the water film surface. The results are shown in figure 3. For a root radius of 0.3 cm and water film thickness of .13 cm, nearly perfect agreement was obtained between our results and Carslaw and Jaeger's. A more severe test with a root radius of 0.5 cm and water film thickness of .4 cm, the calculated curve led the exact solution curve slightly, but never more than 2% of the time required to reach equilibrium (in this case, about 2 minutes in 100).

Such a test was not made with a non-zero root consumption rate, but tests made on the mass-balance of the root and water film indicated this

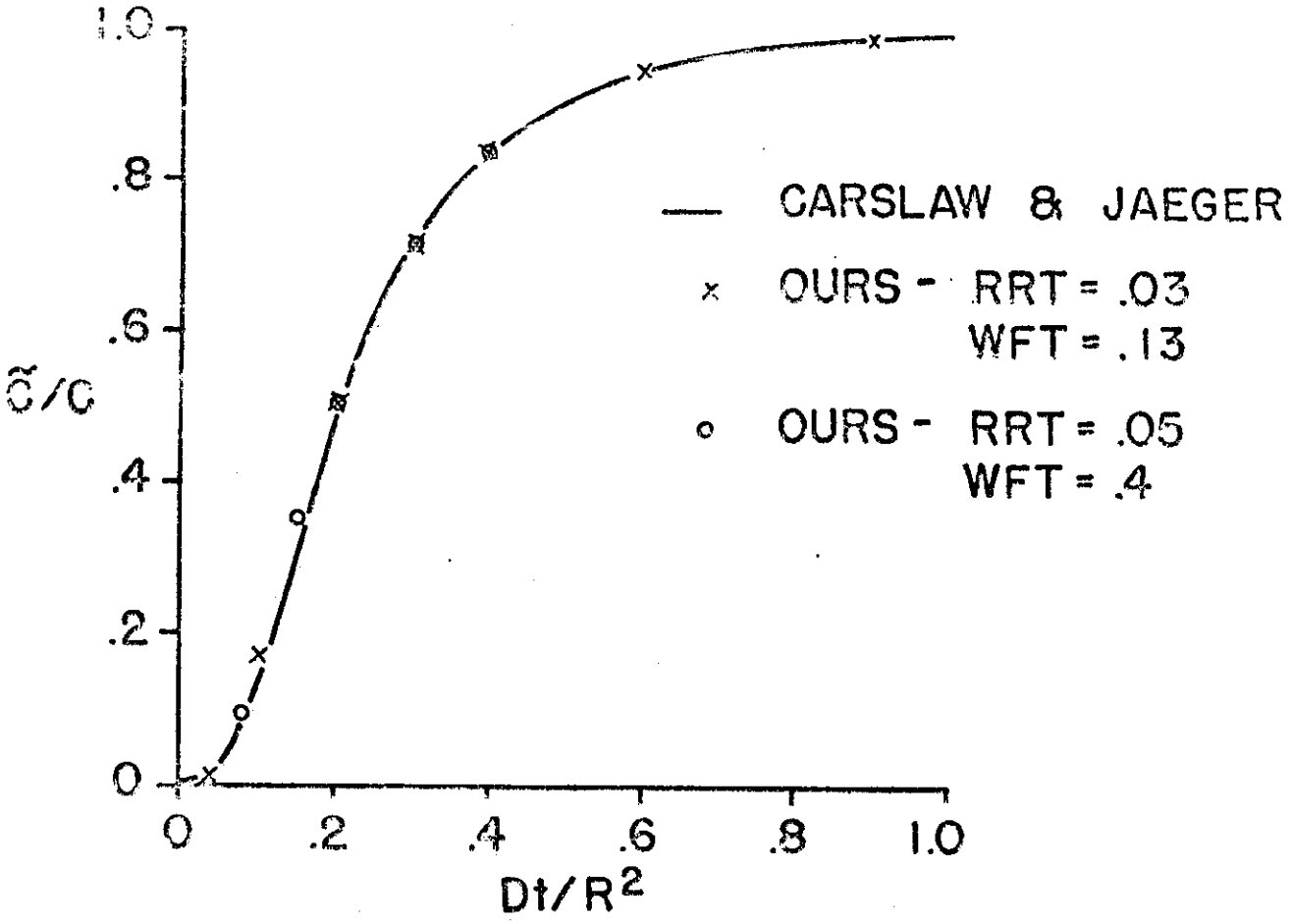

Figure 3. Normalized oxygen concentration versus normalized time at the root center for two sets of values of root radius and water film thickness calculated by this model. Solid line represents exact solution obtained from Carslaw and Jaeger (1947).

part of the model was functioning properly.

Results

A sensitivity analysis was performed by running the model with several values of the controlling parameters, which were found in the literature. In all cases except where noted a bulk density of 1.4 gm cm^{-3} was assumed. Since we were interested in simulating oxygen profiles when oxygen may become limiting, relatively high water contents (0.25 cm^3 cm^{-3} to 0.42 cm^3 cm^{-3}) were selected for the study. Values of root density, as indicated by Taylor and Klepper (1973) for cotton roots, were typically 5 to 6 cm cm^{-3}, and root radii ranged from .02 to .05 cm, corresponding to values tabulated by Lemon and Wiegand (1962) for a variety of root types. Root respiration rates used were in the range 10^{-8} to 10^{-7} gm cm^{-3} sec^{-1}, corresponding to values cited by Lemon and Wiegand for alfalfa roots, but much higher values than this were cited for some other plant roots. Finally, values used for microbial respiration were in the range 0.12 to 12.0 ulg^{-1} hr^{-1}, as indicated by Grable and Seimer (1968). (Table 1).

The initial concentrations for each simulation are shown as the zero time profile in figure 4. The program was run for each set of parameters until the changes between one time and another became small. Samples of the concentration profiles at times after the conditions were imposed are given in figures 4 and 5. The profiles typically stabilized after 10 to 25 hours of simulated time, those with low respiration rates (due to low root respiration, low root radii, or low root densities) requiring

Table 1. Values of model parameters used for simulations

	Medium	High	Low
Water Content	0.35 cm^3 cm^{-3}	0.42	0.25
Bulk Density	1.4 g cm^{-3}	1.59	---
Root Radius	0.05 cm	---	0.03
Root Density	4.0 cm cm^{-3}	---	2.0
Root Consumption Rate	5. x 10^{-8} g cm^{-3} sec^{-1}	10. x 10^{-8}	.1 x 10^{-8}
Microbial Respiration Rate	7.15 x 10^{-10} g cm^{-3} sec^{-1}	---	.715 x 10^{-10}
Temperature	23 °C (all cases)		

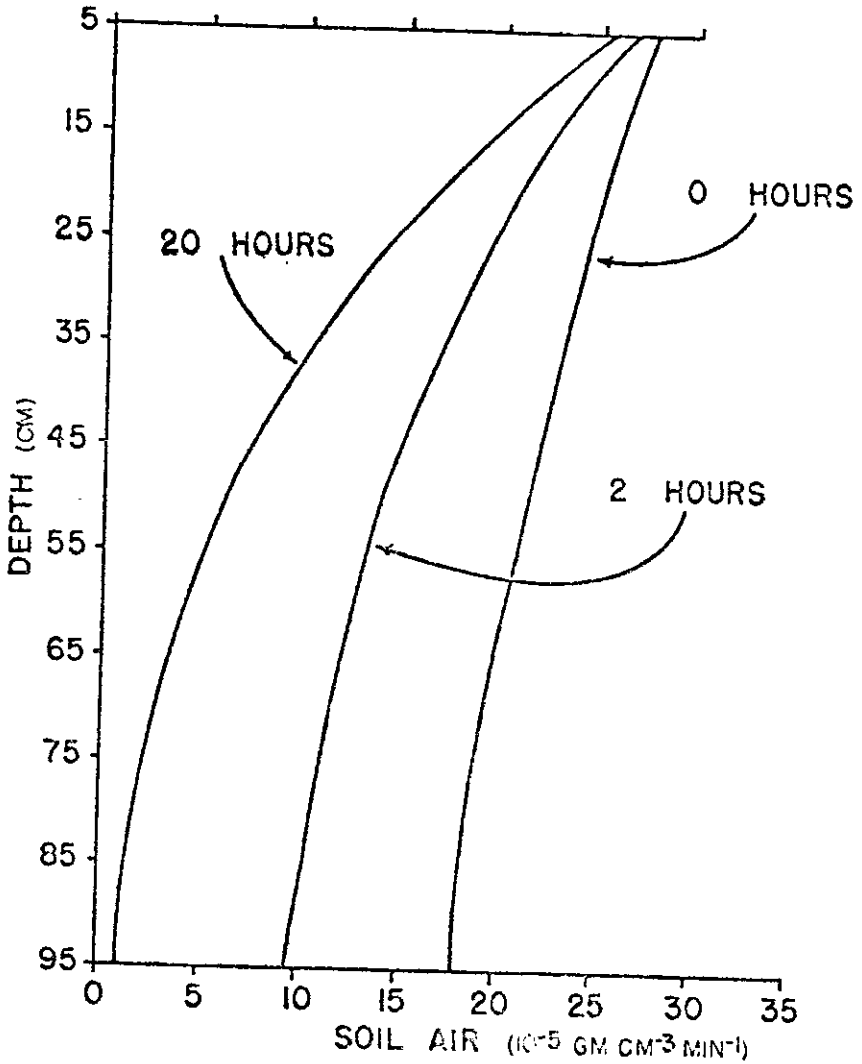

Figure 4. Soil air oxygen concentration profiles for different times, showing approach to equilibrium for medium values of the parameters.

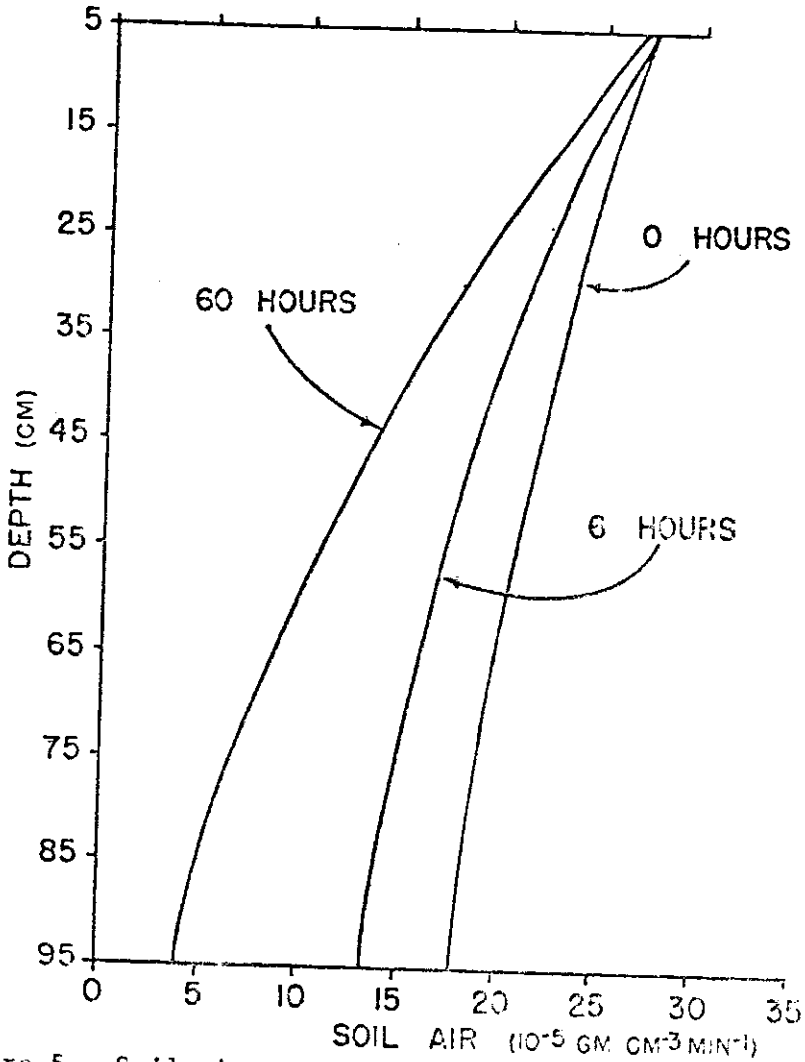

Figure 5. Soil air oxygen concentration profiles for different times, showing approach to equilibrium for low root consumption rate and medium values of the other parameters.

more time for equilibration. To simplify comparisons, only the equilibrium values will be considered, except where noted.

The results of the simulation are shown in figures 4 to 17. It was pointed out earlier that figures 4 and 5 typify how the soil concentration profiles change with time. Where medium limits of the parameters were used (figure 4) equilibration was essentially achieved after 8 hours, whereas with the low root consumption rate (figure 5), the profiles did not stabilize before 20 to 25 hours.

Equilibrium concentrations and rates for medium levels of the parameters are shown in figure 6. Root respiration was uniform to a depth of 30 cm, but below this depth it decreased due to the inability of diffusion across the water film and root to support the imposed root consumption rate. Oxygen concentration decreased from atmospheric near the surface to half this value at 27 cm. The oxygen concentration inside the root decreased with depth to nearly zero at 30 cm.

The results for the low water content (.25) are shown in figure 7. The lower water content allows oxygen to diffuse deeper into the soil, and induces a thin water film ($\simeq$ 0.01 cm) compared to the water content of .35 ($\simeq$ 0.1 cm). Thus root respiration is not curtailed above a depth of 55 cm. The similarity of soil air concentrations profiles probably indicates that the decreased water film thickness enhanced root respiration.

In the case of the high water content (Fig.8), only the roots at depths of 10 cm or less are able to respire to full capacity. Below this depth, root concentrations are zero and the soil concentration drops to one-half atmospheric at 20 cm. The effect of low soil oxygen concen-

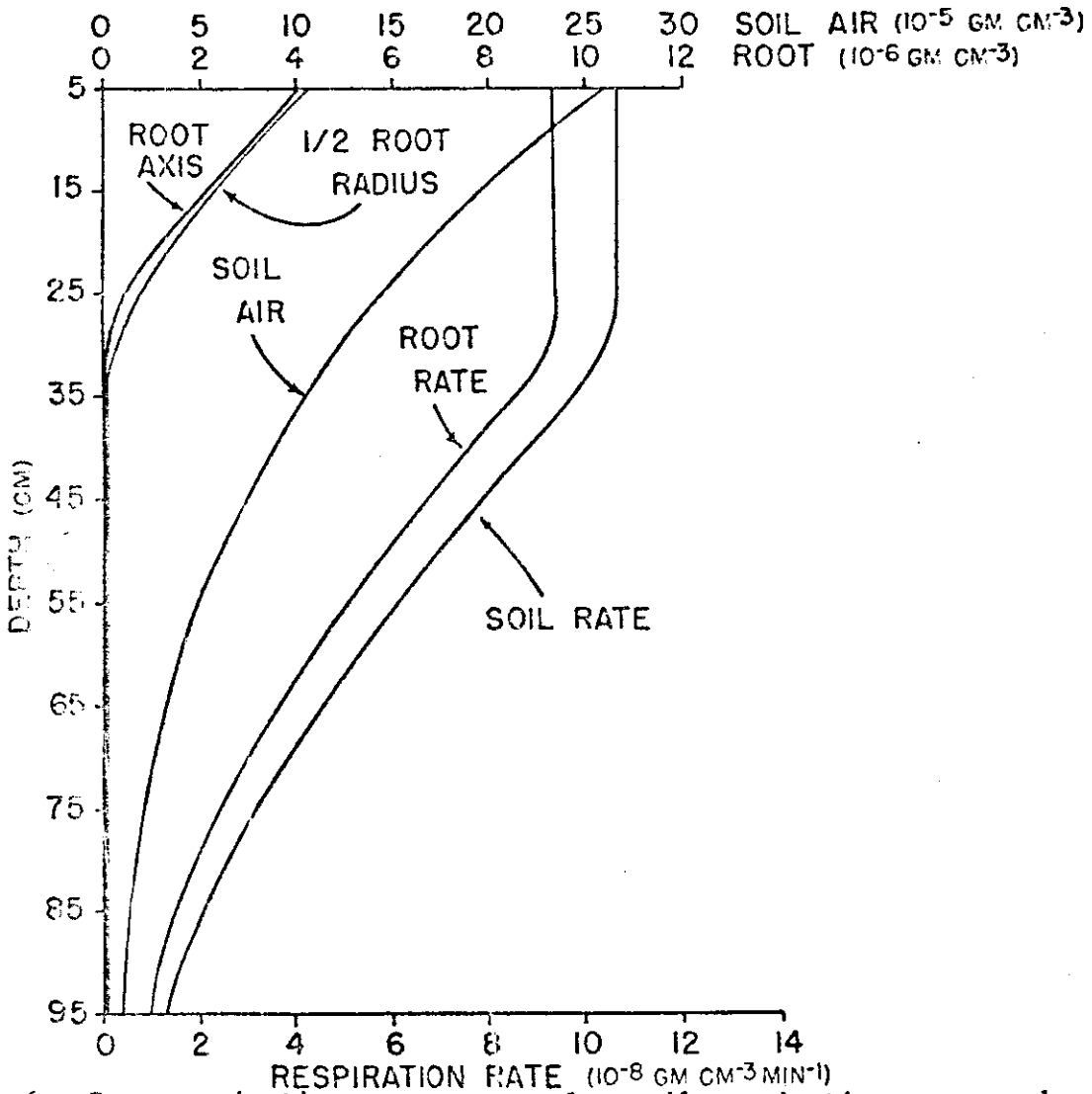

Figure 6. Root respiration rate, roots plus soil respiration rate, and oxygen concentration in the soil air, at half the radius of the root and at the root axis after equilibrium for the following set of conditions: bulk density of 1.4 gm cm^{-3}, root consumption of $3.x10^{-6}$ gm cm^{-3} min^{-1} microbial respiration of $4.32x10^{-8}$ gm cm^{-3} min^{-1}, root density 4.0 cm cm^{-3}, root radius of 0.05 cm, and water content of 0.35 cm^{3} cm^{-3}.

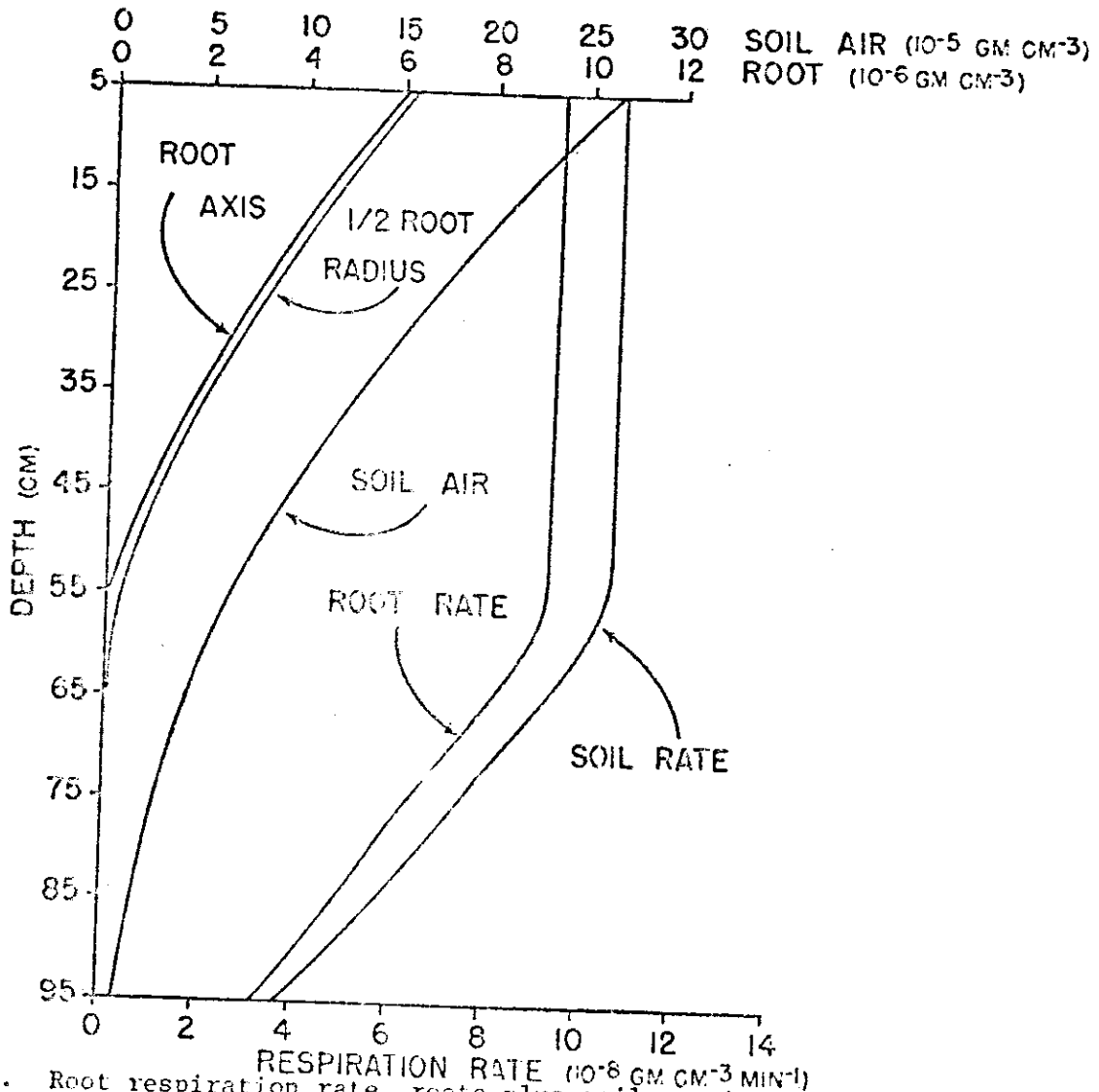

Figure 7. Root respiration rate, roots plus soil respiration rate, and oxygen concentration in the soil air, at half the radius of the root and at the root axis after equilibrium for the following set of conditions: bulk density of 1.4 gm cm^{-3}, root consumption of $3.x10^{-6}$ gm cm^{-3} min^{-1}, microbial respiration of $4.32x10^{-8}$ gm cm^{-3} min^{-1}, root density of 4.0 cm cm^{-3}, root radius of 0.05 cm, and water content of 0.25 cm^{3} cm^{-3}.

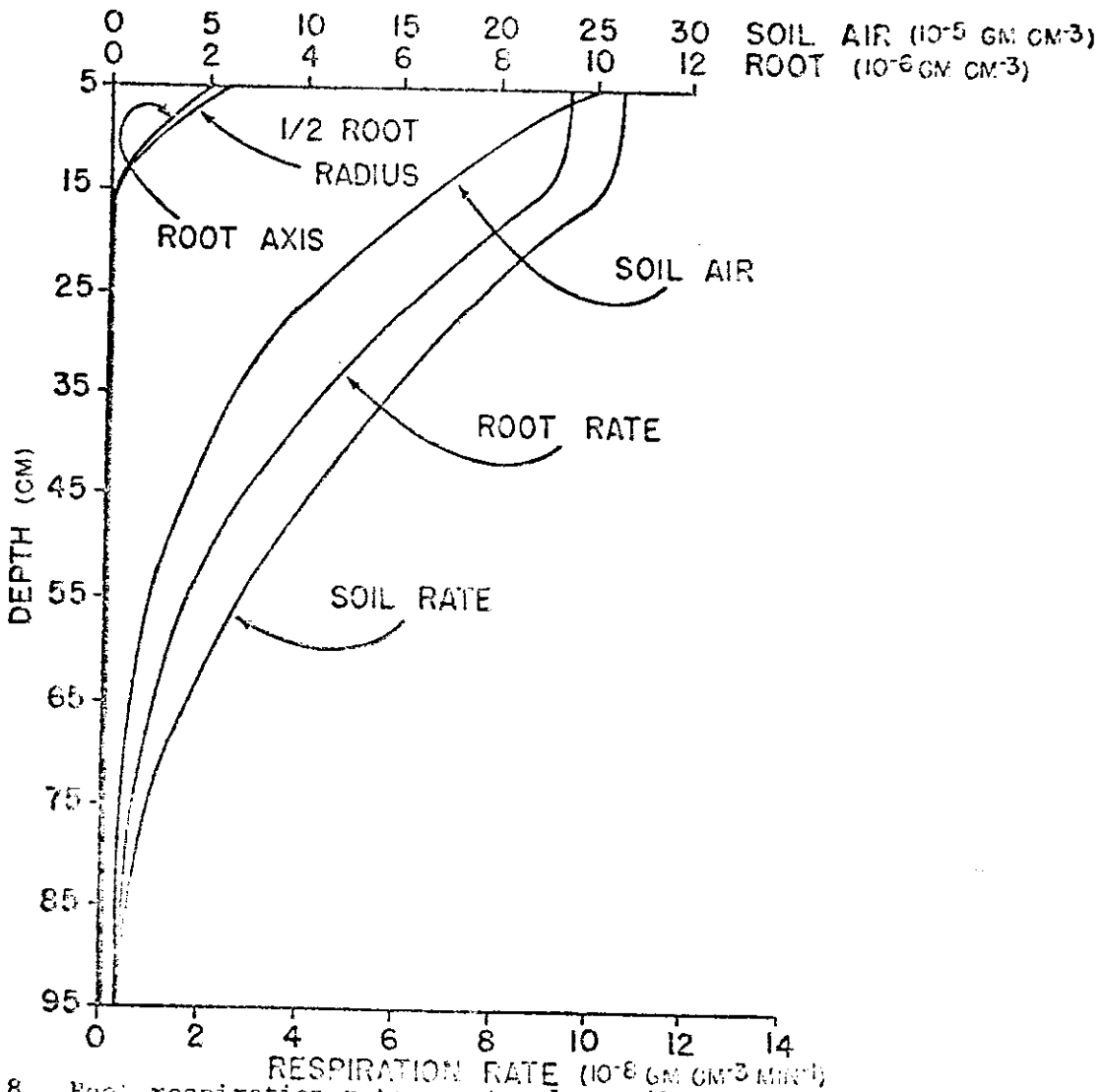

Figure 8. Root respiration rate, roots plus soil respiration rate, and oxygen concentration in the soil air, at half the radius of the root and at the root axis after equilibrium for the following set of conditions: bulk density of 1.4 gm cm^{-3}, root consumption of $3.x10^{-6}$ gm cm^{-3} min^{-1} microbial respiration of $4.32x10^{-8}$ gm cm^{-3} min^{-1}, root density of 4.0 cm cm^{-3}, root radius of 0.05 cm, and water content of 0.42 cm^{3} cm^{-3}.

tration on microbial respiration rate can be seen by comparing the soil respiration rate to the root respiration rate, as the difference between these two values is the microbial rate.

For a low water content and high root consumption rate (figure 9), root respiration is curtailed at a depth of 30 cm, where root concentrations go to zero. (Compare with figure 7, and note the similarities between figures 6 and 9.) Apparently, the low water content in this case just compensates the additional respiration load.

In the case of a low root consumption rate (figure 10), normal root respiration is indicated throughout the 95 cm profile. The concentration in the soil air drops to 50% atmospheric at about 45 cm (two times the corresponding value for the medium root consumption rate) and to 14% at 95 cm. Despite the low soil air concentration at the bottom of the profile, the small gradient in concentration across the root and water film is able to support the low root consumption rate.

For the low root radius (figure 11), root respiration is uninhibited to a depth of 70 cm, indicating the effect of decreased root volume on the soil air concentration (50% of atmospheric at 35 cm).

Perhaps more important is the effect of the decreased oxygen flow rate that must be supported by the concentration gradient across the root and water film. The validity of this statement is established by comparing with figure 12, which depicts the results for low root density. The soil air concentrations are essentially the same below 55 cm for these two cases, but in figure 12 root concentrations are zero and root respiration is inhibited at depths below 40 cm.

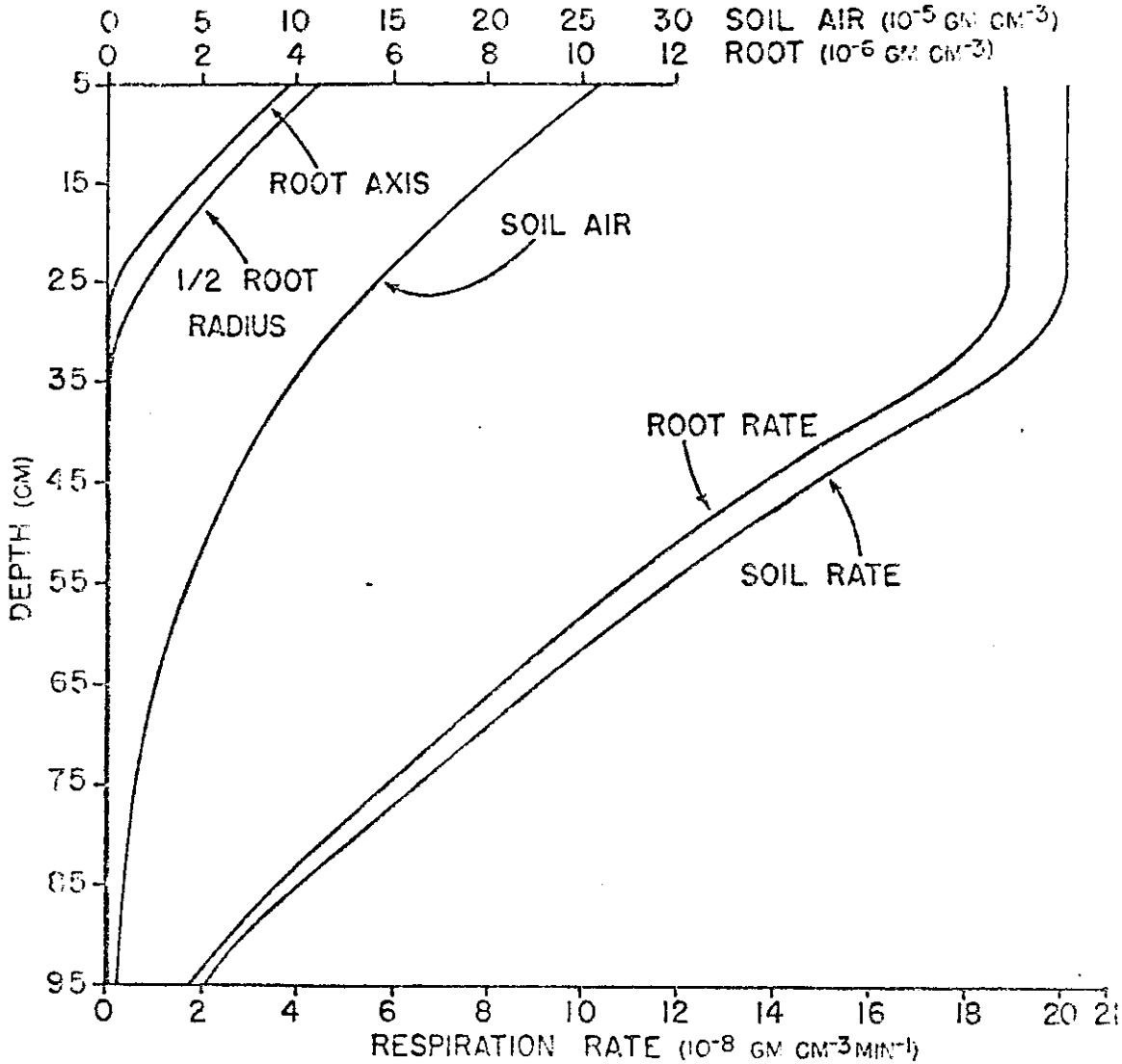

Figure 9. Root respiration rate, roots plus soil respiration rate, and oxygen concentration in the soil air, at half the radius of the root and at the root axis after equilibrium for the following set of conditions: bulk density of 1.4 gm cm^{-3}, root consumption of $6.x10^{-6}$ gm cm^{-3} min^{-1} microbial respiration of $4.32x10^{-8}$ gm cm^{-3} min^{-1}, root density of 4.0 cm cm^{-3}, root radius of 0.05 cm, and water content of 0.25 cm^{3} cm^{-3}.

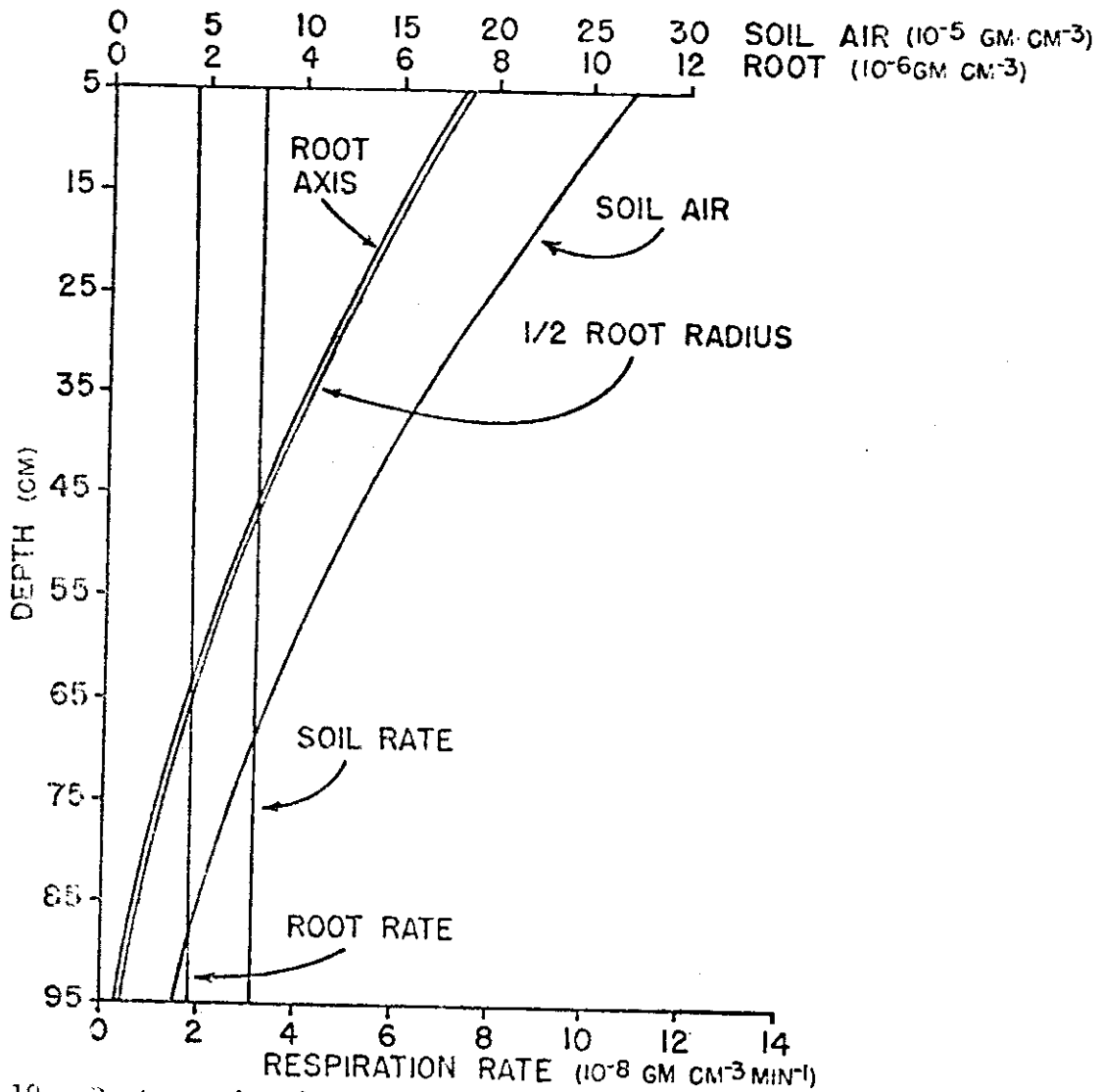

Figure 10. Root respiration rate, roots plus soil respiration rate, and oxygen concentration in the soil air, at half the radius of the root and at the root axis after equilibrium for the following set of conditions: bulk density of 1.4 gm cm $^{-3}$, root consumption of $6.x10^{-6}$ gm cm $^{-3}$ min $^{-1}$ microbial respiration of $4.32x10^{-8}$ gm cm $^{-3}$ min $^{-1}$, root density of 4.0 cm cm $^{-3}$, root radius of 0.05 cm, and water content of 0.35 cm ^{3} cm $^{-3}$.

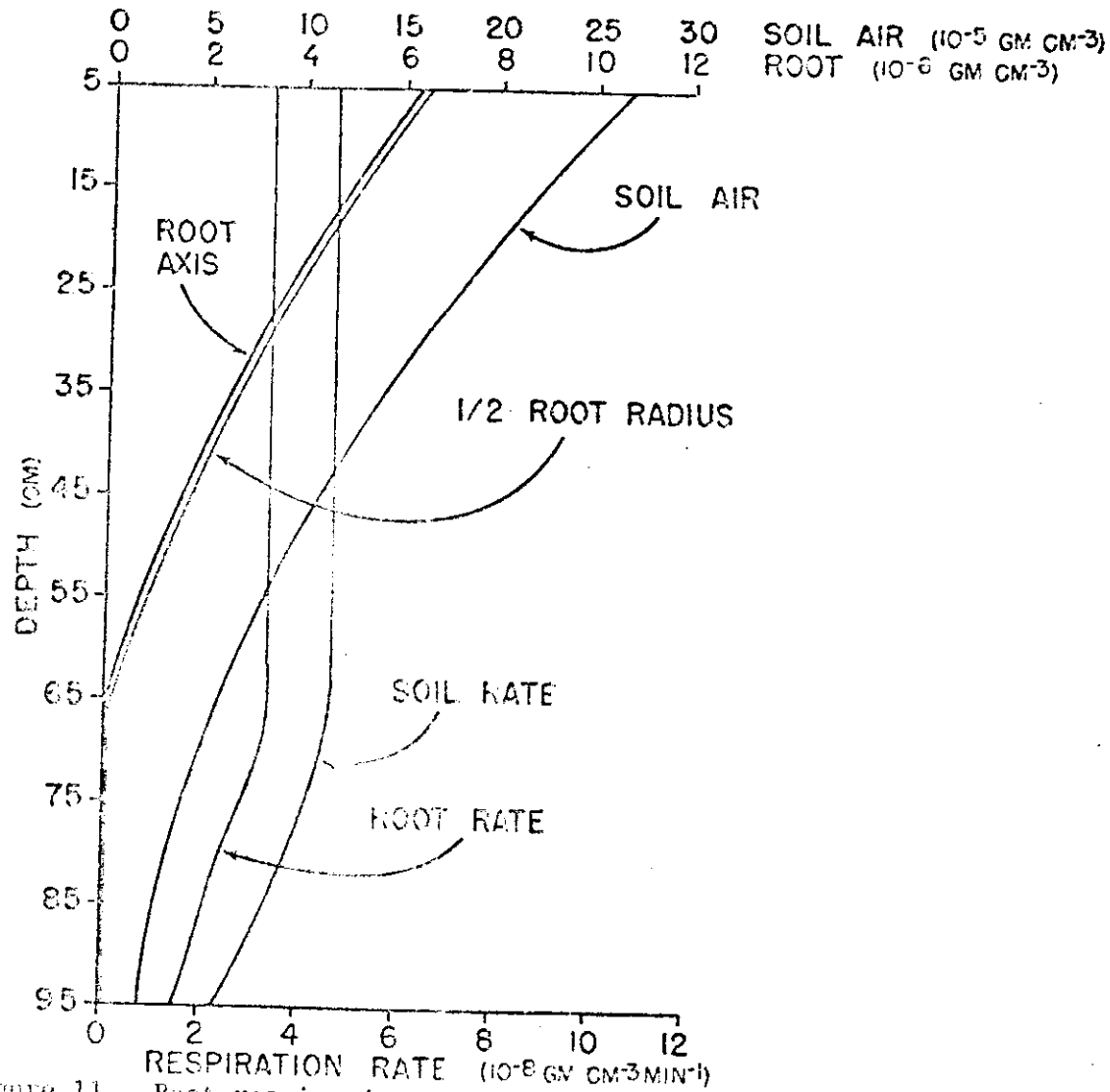

Figure 11. Root respiration rate, roots plus soil respiration rate, and oxygen concentration in the soil air, at half the radius of the root and at the root axis after equilibrium for the following set of conditions: bulk density of 1.4 gm cm $^{-3}$, root consumption of 3×10^{-6} gm cm $^{-3}$ min $^{-1}$ microbial respiration of 4.32×10^{-8} gm cm $^{-3}$ min $^{-1}$, root density of 4.0 cm cm $^{-3}$, root radius of 0.03 cm, and water content of 0.35 cm ^{3} cm $^{-3}$.

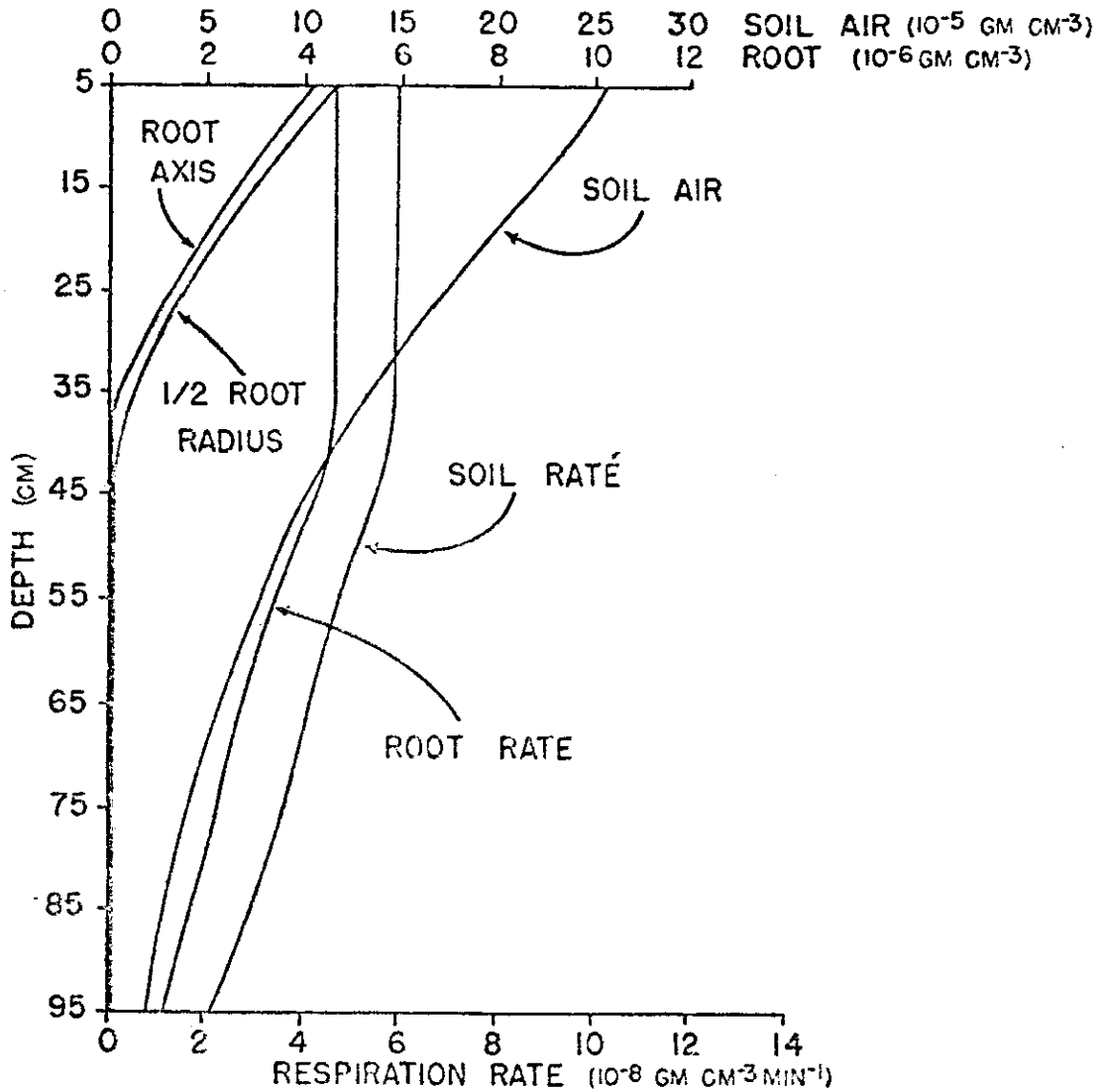

Figure 12. Root respiration rate, roots plus soil respiration rate, and oxygen concentration in the soil air, at half the radius of the root and at the root axis after equilibrium for the following set of conditions: bulk density of 1.4 gm cm^{-3}, root consumption of $3x10^{-6}$ gm cm^{-3} min^{-1} microbial respiration of $4.32x10^{-8}$ gm cm^{-3} min^{-1}, root density of 2.0 cm cm^{-3}, root radius of 0.05 cm, and water content of 0.35 cm^3 cm^{-3}.

Concentrations and respiration rates for a root density which decreases linearly (5 cm cm^{-3} at the 5 cm depth and -.5 cm cm^{-3} cm^{-1} slope) with depth is shown in figure 13. In this case the higher root densities in the 0 to 10 cm and 10 to 20 cm layers compensate the lower root densities at the lower depths. Thus the concentration profiles for both the soil air and roots are very similar to those for the case of medium root density (figure 6). The respiration rates (figure 13) decrease linearly with depth to 35 cm, where root concentrations are very nearly zero. At this depth an inflection point can be seen in the respiration rate curves. From this point on, the rates decrease more markedly due to the zero root concentrations in lower layers.

In figure 14, the effect of a ten-fold reduction in microbial respiration is somewhat obscured due to the fact that, at the temperature of 23 C at which the simulations were effected, the microbial respiration for the medium case is already somewhat low compared to normal root respiration. Nevertheless, the low microbial rate is evidenced by the decreased difference in root respiration rate and soil respiration rate (figure 14).

The results of imposing layers of soil of low aeration porosity are shown in figures 15, 16, and 17. For these simulations a root radius of 0.03 cm was used (compare with figure 11). In the case of a high bulk density in the surface layer (figure 15), the concentration in the soil air near the surface is reduced markedly over that for the case of medium bulk density in this layer. One-half atmospheric concentration is reached at 20 cm. The depth of unimpaired root respiration is reduced to 55 cm

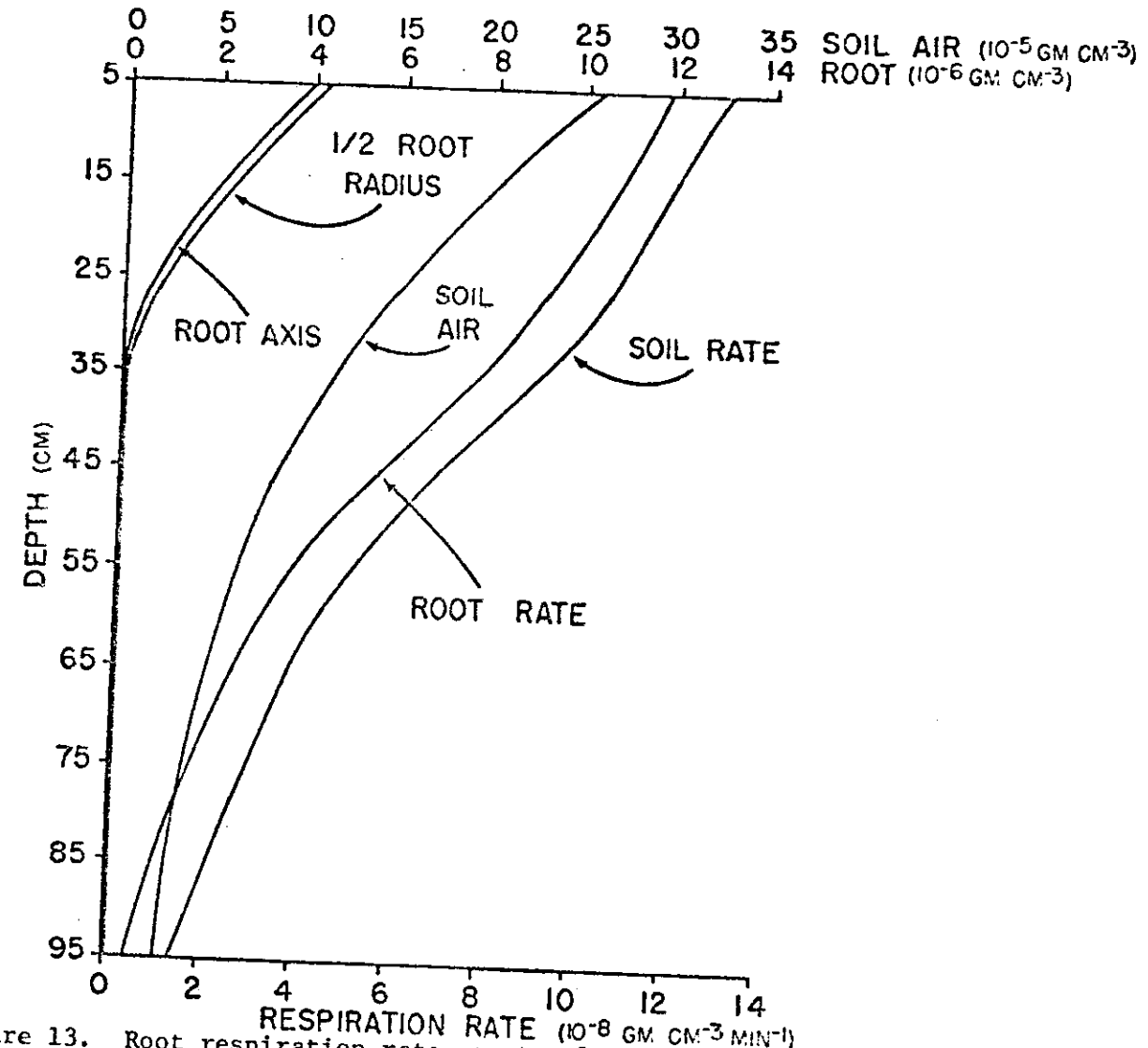

Figure 13. Root respiration rate, roots plus soil respiration rate, and oxygen concentration in the soil air, at half the radius of the root and at the root axis after equilibrium for the following set of conditions: bulk density of 1.4 gm cm^{-3}, root consumption of 3×10^{-6} gm cm^{-3} min^{-1} microbial respiration of 4.32×10^{-8} gm cm^{-3} min^{-1}, root density of verying linearly with depth from 5 cm cm^{-3} at 5 cm to 0.5 cm cm^{-3} at 95 cm, root radius of 0.05 cm, and water content of 0.35 cm^{3} cm^{-3}.

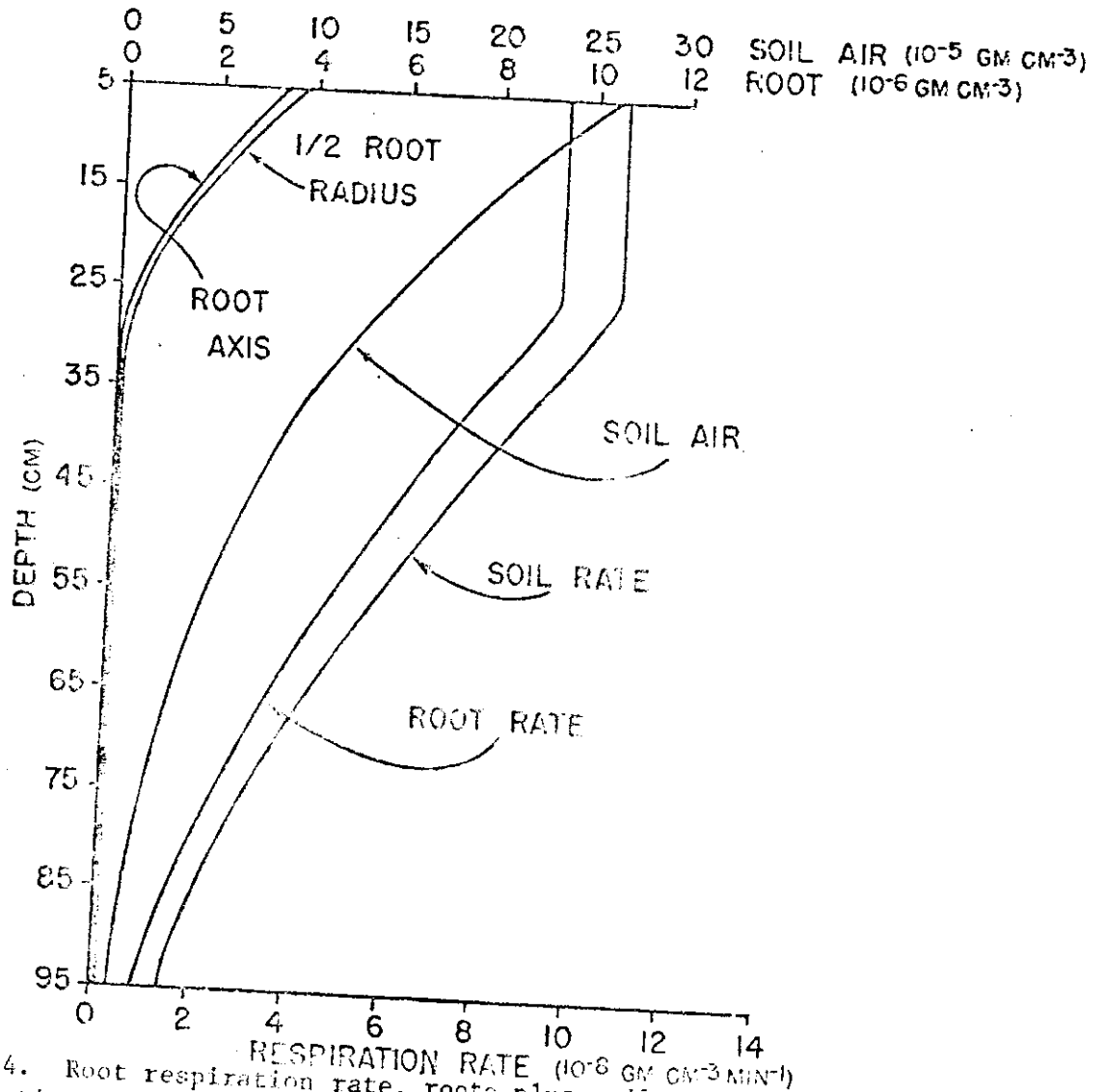

Figure 14. Root respiration rate, roots plus soil respiration rate, and oxygen concentration in the soil air, at half the radius of the root and at the root axis after equilibrium for the following set of conditions: bulk density of 1.4 gm cm $^{-3}$, root consumption of 3×10^{-6} gm cm $^{-3}$ min $^{-1}$, microbial respiration of 4.32×10^{-9} gm cm $^{-3}$ min $^{-1}$, root density of 4.0 cm cm $^{-3}$, root radius of 0.05 cm, and water content of 0.35 cm ^{3} cm $^{-3}$.

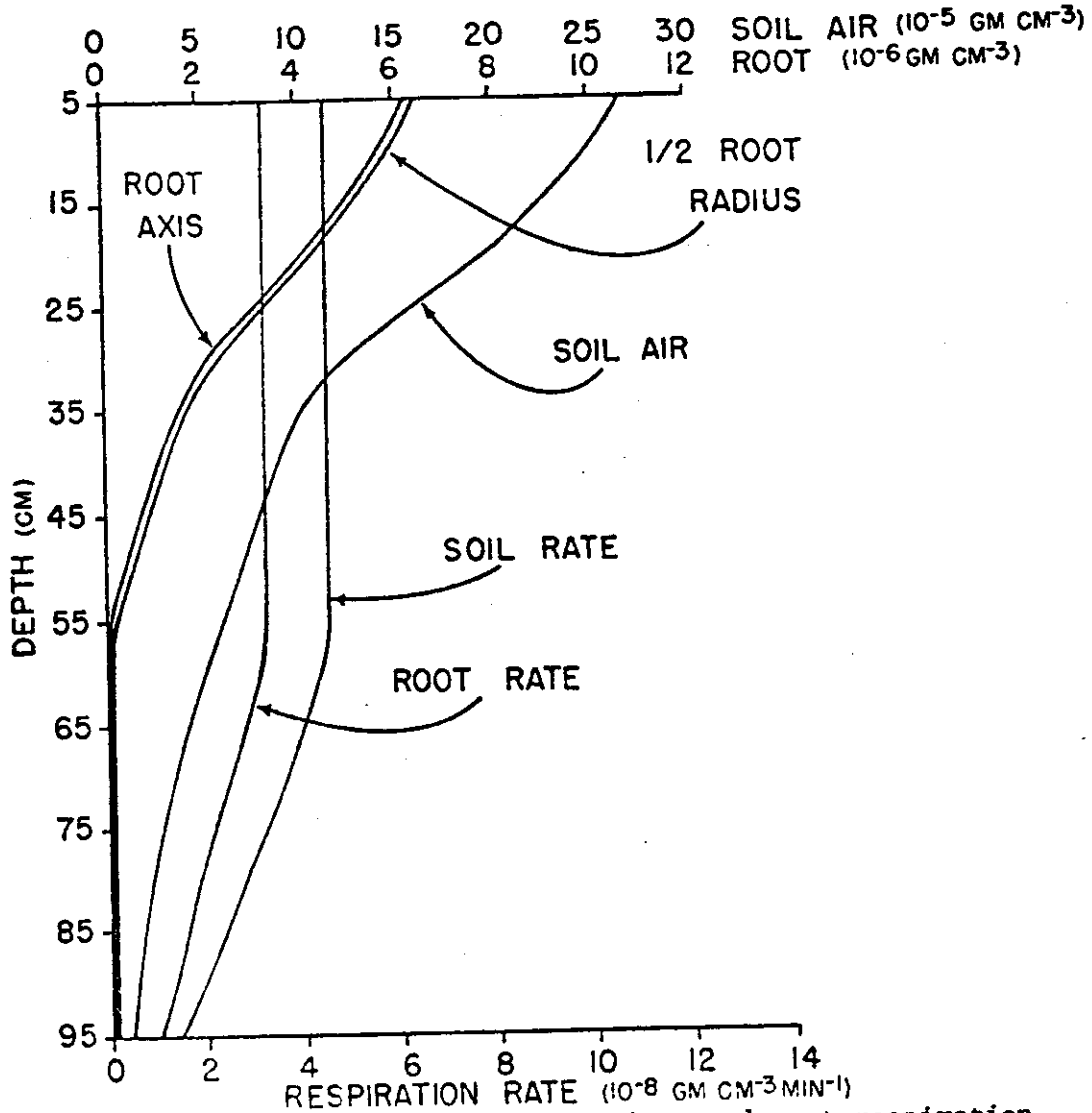

Figure 16. Soil air and root concentrations and root respiration and soil plus root respiration rates for a bulk density of 1.59 cm ^{3} cm $^{-3}$ at the 20 to 30 cm depths and 1.4 cm ^{3} cm $^{-3}$ at other depths with all other parameters medium.

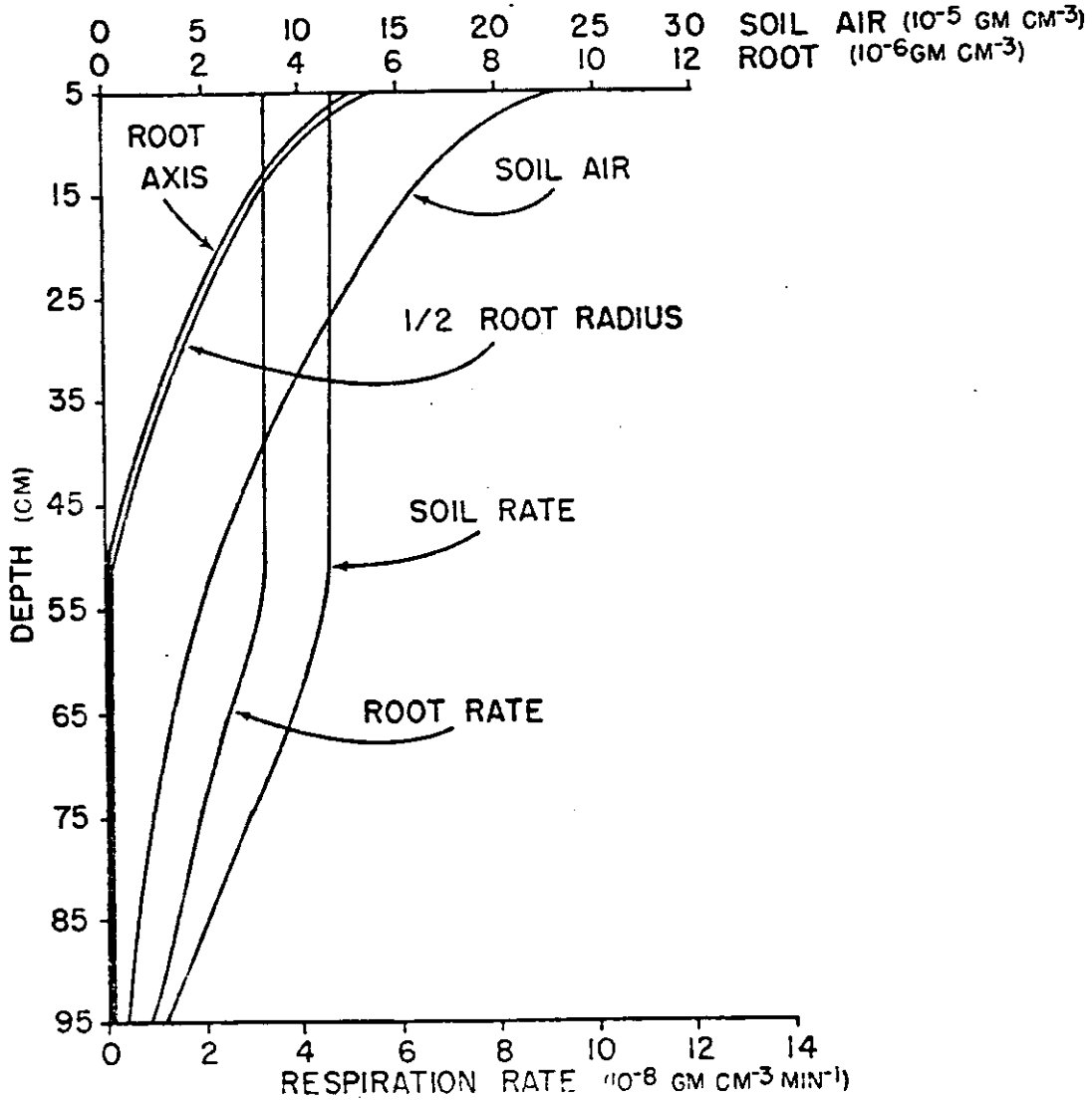

Figure 15. Soil air and root concentrations and root respiration and soil plus root respiration rates for a bulk density of 1.59 cm ^{3} cm $^{-3}$ in the 10 cm thick surface layer with all other parameters at the medium values and 1.4 cm ^{3} cm $^{-3}$ at lower depths.

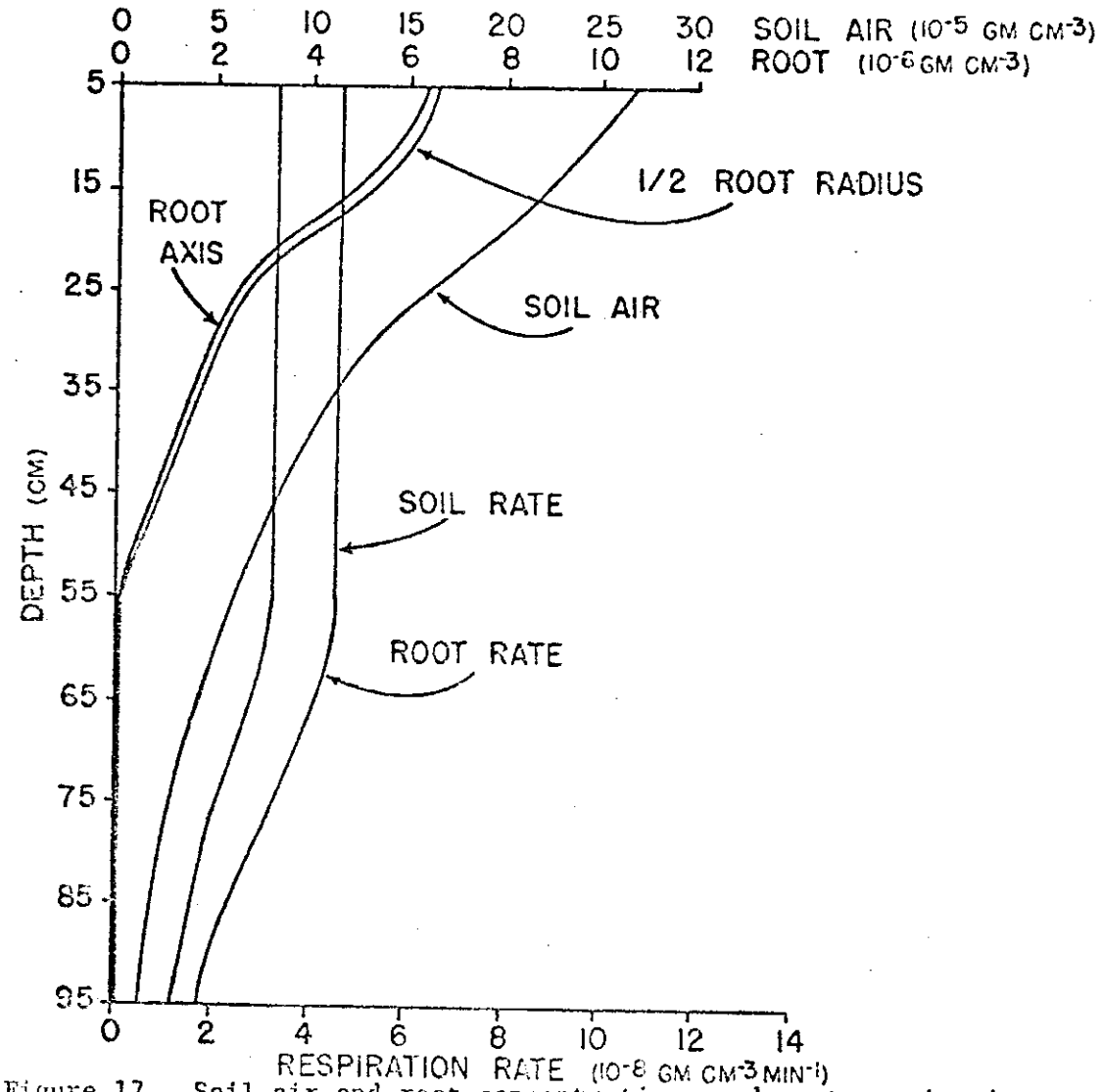

Figure 17. Soil air and root concentrations and root respiration and soil plus root respiration rates for a water content of 0.42 cm^3 cm^{-3} at the 20 to 30 cm depths and 0.35 cm^3 cm^{-3} at other depths with all other parameters at the medium values.

instead of 65 cm (medium case).

For the case of high bulk density in the 20-30 cm layer (figure 16), the profiles below 55 cm are similar to those of figure 15. Concentrations in the soil air and root are higher in the top 20 cm than for the medium case due to the insulating effect of the dense 20-30 cm layer. From 20 to 30 cm there is a marked reduction in concentrations, so at 55 cm there is essential agreement in the profiles of figures 15 and 16. Finally, the profiles of figure 17 (high water content in the 20-30 cm layer) are almost identical to those of figure 16. The sole exception is the lower root concentrations in the 20-30 cm layer of figure 17, due to the increased water film thickness around roots in this layer.

SYMBOLS

C = concentration of O_2 without regard to media (gm cm^{-3})

C_a = concentration of O_2 in atmosphere (g/cm^3)

C_s = concentration of O_2 in soil (gm/cm^3)

D_a = O_2 diffusivity in the air (cm^2/min)

D_i = O_2 diffusivity in root interior (cm^2/min)

D_s = O_2 diffusivity in soil (cm^2/min)

D_w = O_2 diffusivity in water-film (cm^2/min)

D_{w_t} = O2 diffusivity in water at temperature T

f = aeration porosity (cm^3/cm^3)

h = Henry's law constant (4.58×10^4 at 23°C)

k = unitless constant obtained from Henry's law

NO_2 = number of moles dissolved O_2 per cm^3 of solution

$[O_2]$ = molar concentration of O_2 in water (moles $liter^{-1}$)

PO_2 = partial pressure of O_2

q = consumption rate per unit volume of root (gm/cm^2-min)

q_r = consumption rate per unit volume of root (gm/cm^2-min)

q_m = microbial respiration rate (gm cm^{-3} min^{-1})

q_s = total rate of consumption/unit volume by roots and microbes (gm/cm^3-min)

q_{wfs} = O_2 flux across water film surface (gm/(cm root)min)

R = average root radius (cm)

R = root density (cm/cm^3)

r = radial distance from root axis (cm)

S = water-film thickness (cm)

T = temperature (°C)

t = time (min)

τ = normalized time variable for $g_{\tau} = f(t)$

U_1 = mean (optimal) microbial respiration rate

U_2 = amplitude (of optimal) microbial respiration rate

XO_2 = mole fraction of dissolved O_2

Z = depth in soil (cm)

LITERATURE CITED

Barber, S. A. 1966. The role of root interception, mass flow and diffusion in regulating the uptake of ions by plants from soil. Tech. Rept. Ser. Int. Atomic Energy Agency No.65:34-35.

Bakker, J. W. and A. P. Hidding. 1970. The influence of soil structure and air content on gas diffusion in soils. Neth. J. Agric. Sci. 18:37-48.

Brown, K. W. and N. J. Rosenberg. 1970. Effect of windbreaks and soil water potential on stomatal diffusion resistance and photosynthetic rate of sugar beets (Beta vulgaris). Agron. J. 62:4-8.

Carnahan, B., H. A. Luther and J. O. Wilkes. 1969. Applied numerical methods. John Wiley & Sons, Inc. New York. 604 p.

Carslaw, H. S. and J. C. Jaeger. 1947. Conduction of heat in soilids. Clarendon Press, Oxford. 386 p.

Covey, W. and E. R. Lemon. 1962. Soil aeration and plant root solutions; IV testing the cylindrical shell model in the transient case. Soil Sci. Soc. Amer. Proc. 26:526-530.

Grable, A. R. and E. G. Siemer. 1968. Effects of bulk density, aggregate size, and soil water suction on oxygen diffusion, redox potentials, and elongation of corn roots. Soil Sci. Soc. Amer. Proc. 32:180-186.

Griffin, D. M. 1972. Ecology of soil fungi. Syracuse Univ. Press, 193 p.

Hattori, T. 1973. Microbial life in the soil. Marcel Dekker, Inc., New York. 427 p.

Huck, M. G., R. H. Hageman, and J. B. Hanson. 1962. Diurnal variation in root respiration. Plant Physiol. 37:371-375.

Johnson, W. C. and R. G. Davis. 1973. Sugarbeet response to irrigation as measured with growth sensors. Agron. J. 65:789-794.

Lemon, E. R. 1962. Soil aeration and plant root relations. Agron. J. 54:167-170.

Lemon, E. R. and C. L. Wiegand. 1962. Soil Aeration and plant root relations II. Root respiration. Agron. J. 54:171-175.

Millington, R. J. 1959. Gas diffusion in porous media. Science 130:100-102.

Papendick, R. I. and J. R. Runkles. 1965. Transient-state oxygen diffusion in soil: I. The case when rate of oxygen consumption is constant. Soil Sci. 100:251-261.

Penman, H. L. 1940. Gas vapor movements in the soil: I. J. Agr. Sci. 30:437-462.

Taylor, H. M and B. Klepper. 1973. Rooting density and water extraction patterns for corn (Zea mays L.). Agron. J. 65:965-968.

Van Bavel, C. H. M. 1951. A soil aeration theory based on diffusion. Soil Sci. 72:33-46.

Wiegand, C. L. and E. R. Lemon. 1958. A field study of some plant-soil relations in aeration. Soil Sci. Soc. Amer. Proc. 22:216-221.

CHAPTER 5

BIOPHYSICAL MODEL OF SOIL NITROGEN METABOLISM

CONTRIBUTION

BY

PETER J. H. SHARPE

The N transformation rates are assumed to be in quasi-steady-state at any given time. For each change in the environment, a new quasi-steady-state can be calculated. Dynamic behavior of the soil-nitrogen system can be simulated by going from one steady-state to another over specified intervals of time.

To fully describe soil nitrogen transformations, the population dynamics of the microorganisms need also to be included. In this study, the population dynamics of the mineralizers, nitrifiers, and denitrifiers were linked to their respective biochemical energetics. A quasi-steady-state formulation was developed with the population of organisms determined by the environment at any given time. The resulting formulation was unstable due to the delayed feedback of decaying microorganisms, which essentially converts a population mortality loss to a growth substrate input, after degradation has been completed. The time delay involved depends upon the intervening environmental conditions.

A similar problem has been encountered in modeling the population dynamics of the boll weevil in cotton. In this case the population increase has an inherent time delay during to larval growth and development within the cotton square. This problem has been resolved by an in-

depth model of boll weevil development, reproduction and mortality. Insect physiology models were developed to describe the life cycle of the boll weevil and its interaction with the environment. A similar biophysical approach may be applicable to the micro-organisms involved in soil nitrogen transformations. To develop a biophysical model of soil nitrogen population dynamics, a combined experimental - computer modeling program needs to be established. The model would help in defining the experimental design as well as helping to overcome some of problems involved in monitoring a system of this complexity. The model could provide insight in the interrelations of the various competing or symbiotic reactions, thereby aiding in the interpretation of the experimental results. The complexity of the system suggests that an experimental or theoretical modeling approach taken in isolation from the other is unlikely to be successful.

INTRODUCTION

The current research interest in soil nitrogen transformations has gained impetus due to the need to control nitrate pollution of rivers and streams. A fundamentally based model of these transformations would enable management strategies to be tested on the computer for a wide range of soil conditions and environmental constraints. The model could also provide insight into the interrelations of the various competing or symbiotic reactions, thereby suggesting new management strategies to reduce nitrogen fertilizer costs while maintaining crop yield.

However, the development of a realistic model is not an easy task. The system has certain aspects which are difficult to describe mathematically; the numbers and variety of microorganisms is immense; and the microenvironmental conditions beneath the soil are difficult to measure. The complexity of the system coupled with its difficulty of observation lead naturally to a modeling approach. The success of a modeling program in this area will be dependent to a large extent upon the modeling approach followed.

Biological modeling can generally be broken into two categories, modeling from observed responses and modeling

from fundamental concepts. Modeling from observed responses involves stochastic approximations, regression analysis, and the use of polynomials to fit the behaviour of the system based on experimental data. This approach was used by Dutt et al. (1972) who developed rate equations governing four of the major soil N transformations based on a multiple regression analysis.

The second approach involves modeling from basic concepts. Models based upon this approach can be described as biophysical models. Biophysical models have the advantage that they give insight into the operation of the system and suggest ways in which the system may be manipulated. A 'best fit model' does not provide insight into the system; it only gives us back what we already know. The N transformation model of Mehran and Tanji (1973) follows a mechanistic or conceptual approach. They assume that the ion exchange process between the solution and exchangeable ammonium ions is reversible to reflect the dynamic nature of the exchange process. All other reactions are considered to be irreversible. It is also assumed that all transformations take place in aqueous media and obey first-order kinetics. Mehran and Tanji acknowledge that these rate constants vary with the energy source, oxygen level, soil water content, temperature and other variables. However, in their analysis, the rate con-

stants were estimated by empirical fitting, and the effect of the environmental factors upon the numerical value of these constants were not identified.

The analysis of Mehran and Tanji also assumes that the microbial population reaches a steady-state population. They point out that the development of functional relations between rate constants and environmental factors such as temperature, water content, aeration and other environmental variables is essential for better predictions of N transformations. However, they report that such functional relationships are not readily available at the present.

The intimate coupling of the biological N transformations to the soil environment predicates the use of biophysical models to describe the dynamics of the system. Although there is a scarcity of available data for developing microbial models, there is some information available at the molecular and enzymatic level to structure a biophysical model. However, due to the lack of fundamental data in some areas, a biophysical model such as this must contain some hypothetical components. The problems in using data from the literature to verify the model are as follows:

i) in using literature data, not all the input parameters required by the model are known; those not known must be assumed. It is therefore inevitable that in the first

phase of model development, the models will contain some hypothetical elements not directly validated by data;

ii) Published works on N transformations generally do not examine all the processes collectively. Consequently, a modeler is forced to use bits and pieces of experimental work.

An improvement in the data available for verification of the model is dependent upon a model defining the types of experiments required and the identification of the parameters to be measured.

BIOCHEMISTRY OF NITROGEN TRANSFORMATIONS

The purpose of this study is to describe a theoretical model of soil nitrogen metabolism appliable to organic nitrogen release, fertilizer nitrification, leaching of nitrate, and denitrification. The agriculturalist needs soil microbes as a means of converting organic nitrogenous materials into forms available for plant nutrition. The microbes on the other hand require nitrogenous substates as a material and energy input for growth and reproduction. These two orientations are shown schematically in Fig. 5.1 A biophysical model of the soil nitrogen system should include both aspects. However, as a simplification, the popu-

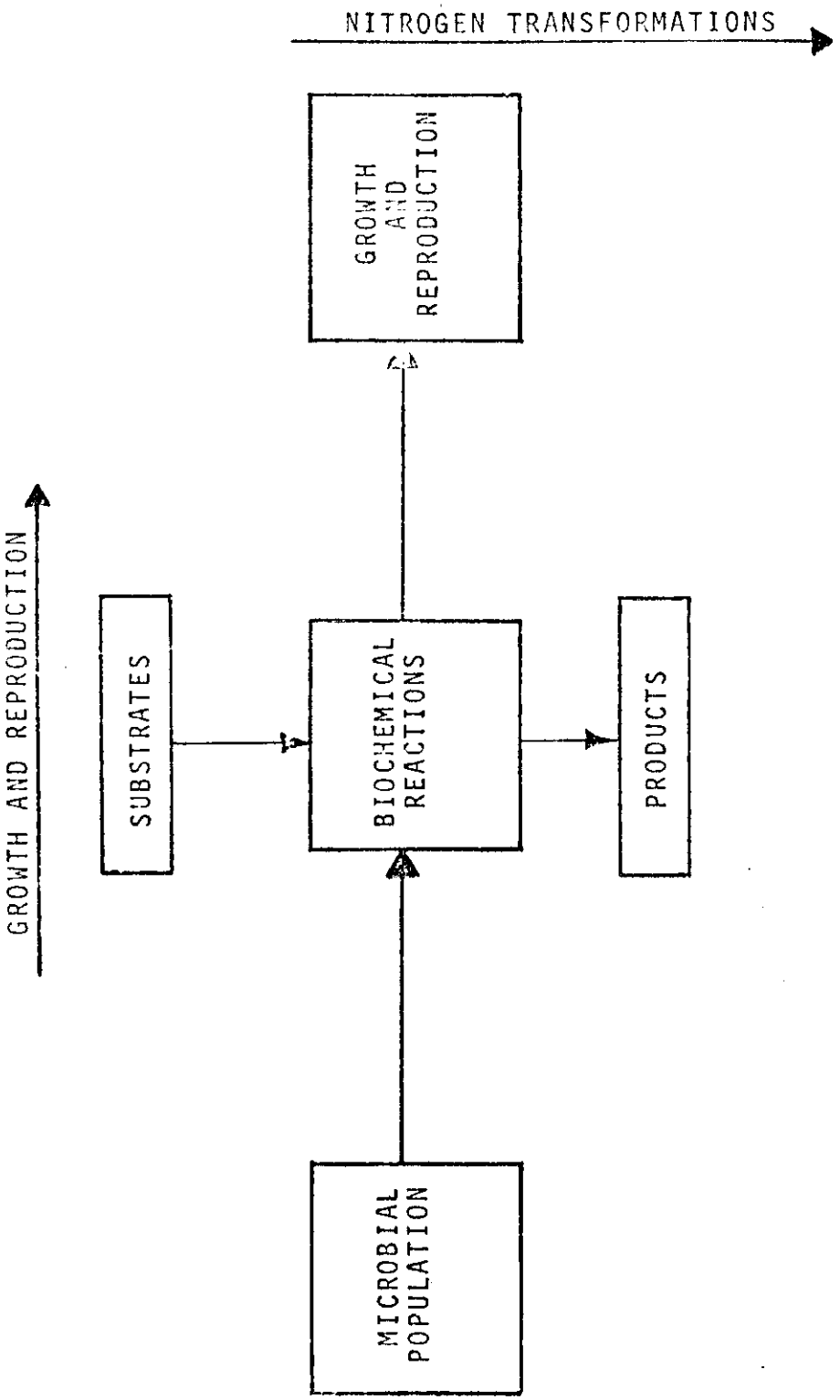

Fig. 5.1 Key Role of Biochemical Reactions in Nitrogen Transformations and Microbial Growth and Reproduction.

lation can be held constant and a model of the N transformation reactions developed. This can then be coupled to a growth and reproduction model.

The analysis described in this report is primarily oriented towards a nitrogen transformation model for populations at steady state. The equations describing the N transformations in the model are derived from the assumptions governing enzyme systems as outlined by Reiner (1969). These assumptions lead to reactions demonstrating enzyme saturation, substrate autoinhibition and substrate competition for reaction sites.

Essentials of Soil Nitrogen Cycle

In an irrigated non-leguminous crop production system, nitrogen fixation can be ignored as an immediate input and the residual organic nitrogen and nitrogen fertilizer can be considered the primary input terms. Figure 5.2 shows a simplified soil nitrogen cycle.

The preliminary model considers four functional microbes a) ammonifying microbes; b) *Nitrosomonas*; c) *Nitrobacter* and d) denitrifying bacteria.

Ammonification

In the soil, ammonium production is often the result

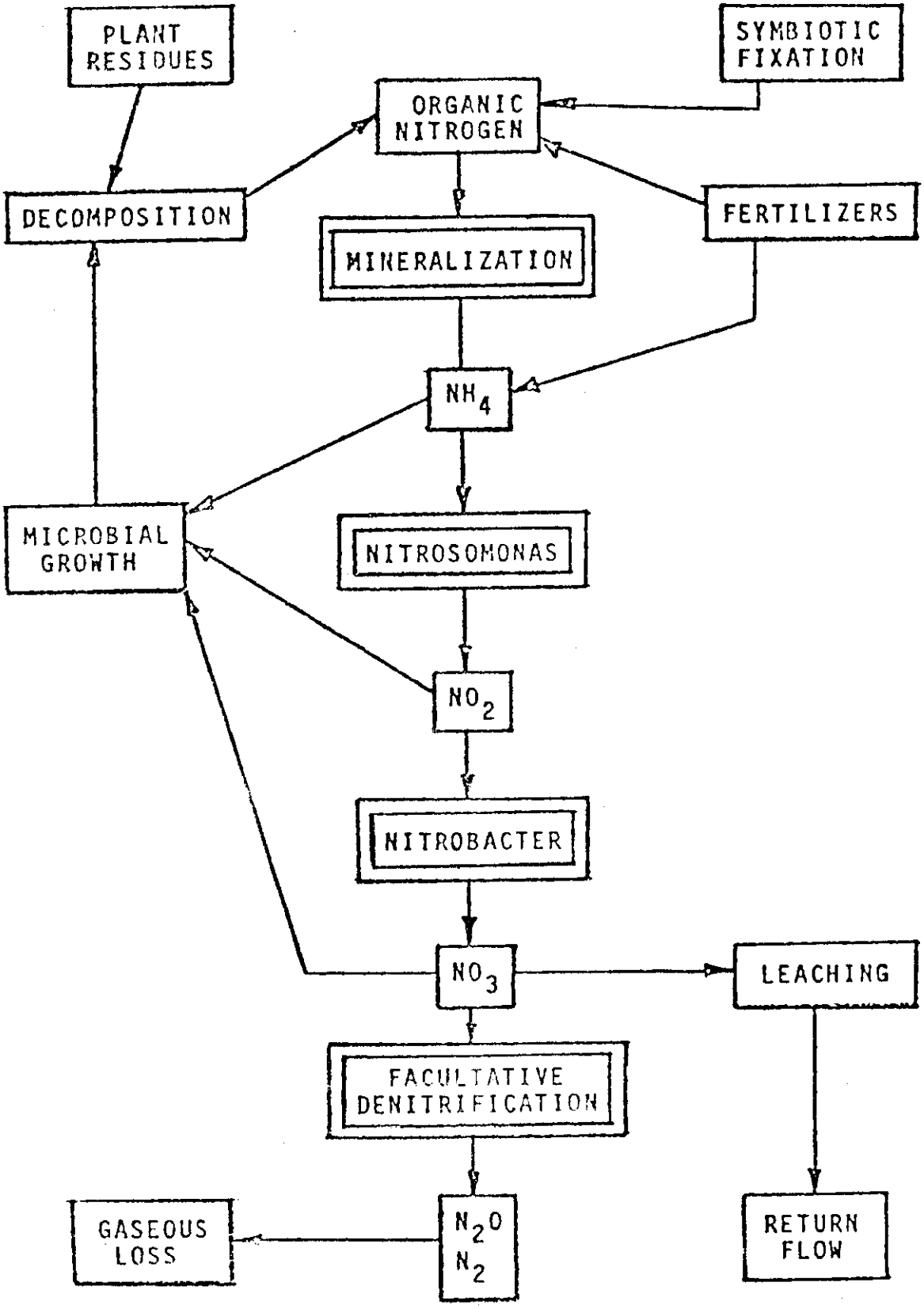

Figure 5.2 SIMPLIFIED SOIL NITROGEN CYCLE.

of interactions between different organisms; those responsible for the initial hydrolysis of the polymer proteins and aminopolysaccharides, and those which rapidly liberate ammonia from the resulting smaller molecules. Ammonification in the soil is essentially oxidation, with carbon dioxide and water being formed at the same time.

The overall reation can be summarized:

$$\text{ORGANIC N} + O_2 \xrightarrow{\text{Mineralizing Microbes}} NH_4 + CO_2 + H_2O. \qquad (1)$$

In this model, all forms of organic nitrogen (N) are considered to be mineralizable. Non-mineralizable organic nitrogen is not included. A recent study (Bremner, 1967) has confirmed that 20 to 50% of organic soil N occurs in the form of amino acids. Many of the amino acids and amino sugars are of bacterial or fungal origin. The breakdown of amino acids is complicated by reactions that do not yield ammonia and therefore reduce the rate of ammonification. The synthesis of bacterial and fungal protoplasm absorbes amino acids. Often, while some amino acids are being assimilated, others are being oxidized. The incorporation of bacterial growth into the model is necessary to describe this phenomena.

Nitrification

Biological oxidation of ammonium to nitrate is known as nitrification. Nitrification consists of two steps: ammonium is converted first to nitrite and then to nitrate. The first step is brought about by a group of autotrophic bacteria collectively called Nitrosomonas in keeping with the following overall reaction:

$$2NH_4^+ + 3O_2 \xrightarrow{\text{Nitrosomonas}} 2NO_2^- \; 2H_2O + 4H^+ \qquad (2)$$

The second step is affected largely by a collective group of autotropic bacteria called Nitrobacter. The overall reaction is:

$$2NO_2^- + O_2 \xrightarrow{\text{Nitrobacter}} 2NO_3^- \qquad (3)$$

These collective names include numerous species. Nitrification is also brought about by certain heterotrophs but the part these heterotrophic microbes play is not certain and therefore has been neglected.

Nitrification requires gaseous oxygen as it occurs only in well aerated soils. The reactions are also greatly influenced by the water content of the soil, by temperature and by pH. Nitrosomonas requires calcium for nitrification

to proceed. By contrast calcium is not necessary for Nitrobacter (Meyerhof, 1916).

Meyerhof (1916 a,b) found by measuring oxidation rates that the optimum pH of Nitrosomonas is 8.5 to 8.8, and that of Nitrobacter is about the same. This can be seen from the data points given in Figure 5.3. There has been some doubt cast on the steepness of the pH response of Nitrosomonas on the acid side and the optimum pH for Nitrobacter. As no clearly accepted experimental evidence for the pH and substrate responses of Nitrosomonas and Nitrobacter is comparable to that of Meyerhof (1916 a,b), the constants of the model have been determined from these results.

Nitrifying bacteria show sensitivity to excess substrate when in artificial culture. Nitrobacter is inhibited by excess nitrate and Nitrosomonas by ammonia. The inhibition may be slowly overcome, but it is powerful at first. The data of Meyerhof (1916a, b) has been recalculated as absolute concentrations and plotted on a logarithmic scale giving a substrate optimum for both bacteria as shown in Figure 3. This is unlike the behaviour of most other organisms with their substrates. Neither in pure nor enrichment cultures can any of the nitrifiers yet known grow at pH more acidic than 6. However, low rates of nitrifica-

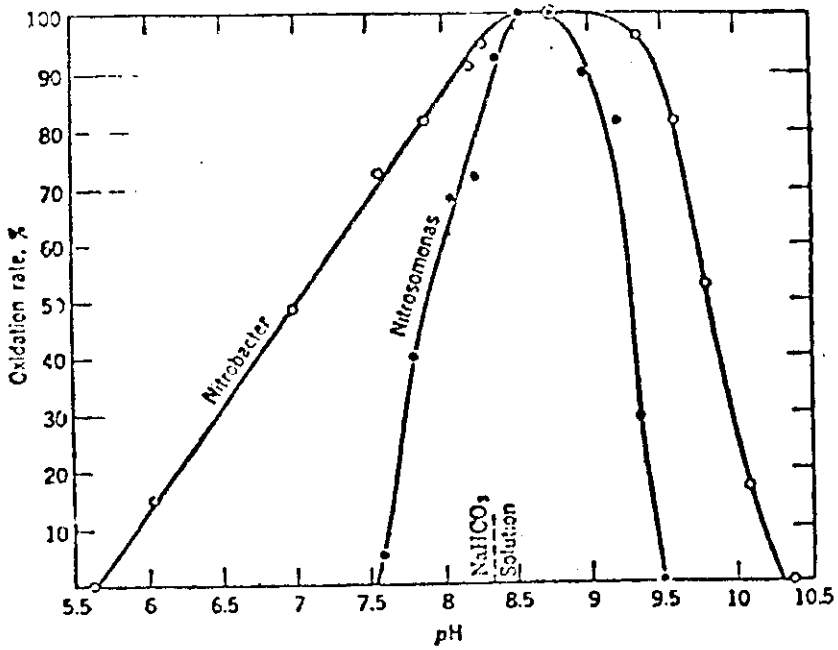

Dependence of oxidation of ammonia and nitrate upon pH. The substrates are NH_4^+ and $^-NO_2$, respectively. The oxidation rates are calculated as percentages of the maximum, which is reached at 8.5 to 8.7 in each case. (Plotted from data of O. Meyerhof, *Pflüger's Arch. ges. Physiol.*, 1916a and b.)

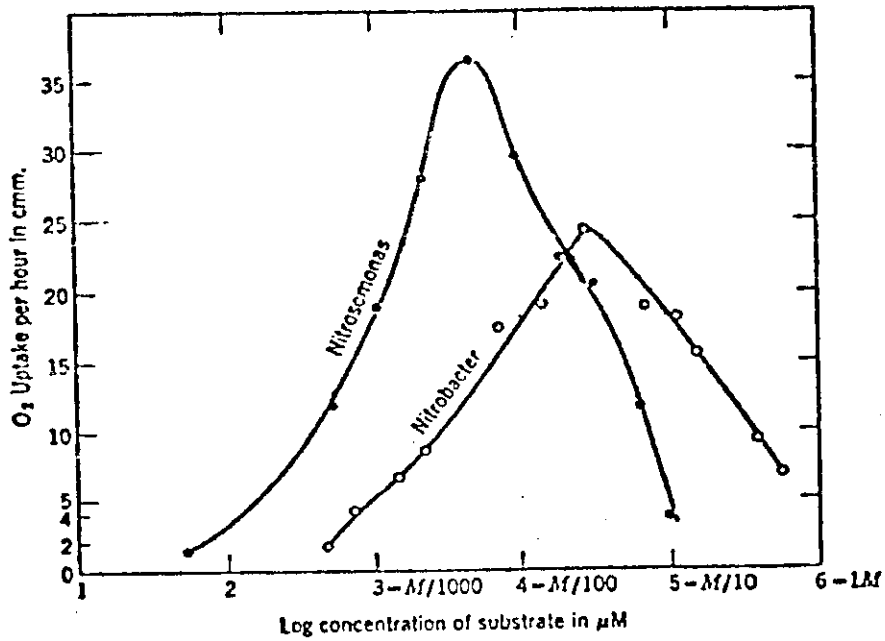

Dependence of oxidation of ammonia and nitrate upon substrate concentration. The substrates are NH_4^+ and $^-NO_2$, respectively. (Plotted from data of O. Meyerhof, *Pflüger's Arch. ges. Physiol.*, 1916a and b.)

Figure 5.3 Nitrification reaction rates as a function of pH and substrate concentration.

tion has been reported to occur in soils where the acidity is a low as pH 4.5. One explanation is that the nitrifying bacteria become attached to mineral particles where the pH is reported to be less acid.

Denitrification - Nitrate Respiration

Denitrification means the microbial reduction of nitrate and nitrite with liberation of gaseous nitrogen. Denitrification occurs by a respiratory mechanism termed nitrate respiration in which nitrate replaces molecular oxygen (Hattori, 1973). In normal respiration, molecular oxygen acts as an electron and hydrogen acceptor. Greenwood (1962) showed that when a soil is percolated anaerobically with a solution containing glucose and ammonium nitrate, the soil utilized nitrate at a rate similar to the oxygen uptake under air. Since the nitrogen output from the percolated soil was closely related to nitrate - N disappearing percolation, it was concluded that, under anaerobic conditions, nitrate was used solely as a hydrogen acceptor and was not assimulated or converted into ammonia.

Therefore depending on the relative concentrations of O_2 and NO_3, the electron transport chain can function as shown:

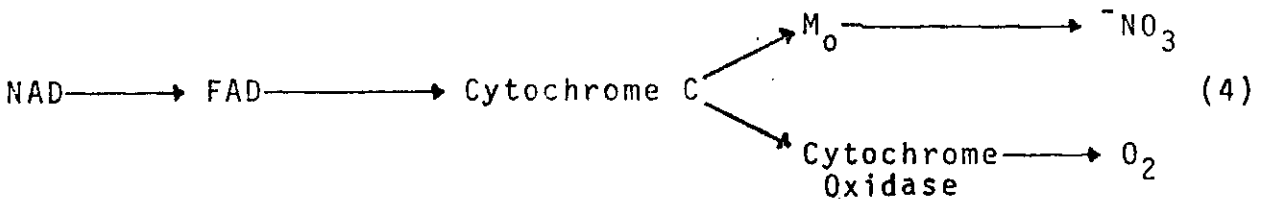

(4)

Consequently, a source of combined hydrogen and a limitation on the supply of free oxygen are needed for denitrification to occur. The inhibition of nitrate reduction by oxygen depends on the species of denitrifying bacteria present. Atmospheric oxygen can almost stop nitrate reduction by Aerobacter (Lewis and Hinshelwood, 1948), while with Pseudomonas denitrificans 2.5% O_2 gave 45% inhibition and air (21%) gave 73% inhibition (Sacks and Barker, 1949).

The denitrification reaction can be summarized as:

$$2HNO_3 + 10(H) \xrightarrow{\text{Denitrifier}} N_2 + 6H_2O. \qquad (5)$$

Alternatively, N_2O can be produced rather than N_2, but the N_2O breaks down to N_2 either microbially or physically. Various forms of carbohydrate can act as hydrogen sources giving the overall reaction:

$$2HNO_3^- + 2CH_2O \xrightarrow{\text{Denitrifier}} N_2O + 2CO_2 + 3H_2O \qquad (6)$$

MODEL DEVELOPMENT

The foundation of the model rests on the assumption that the biological transformations which occur are enzymatic in nature. The complexity of the enzyme systems themselves prohibits the modeling of the individual enzyme reactions. Therefore the approach used in this analysis is to define a multipurpose 'equivalent' enzyme for each microbial species. The concept of the equivalent enzyme has been developed by Sharpe and DeMichele (1973) and Sharpe (1973). An equivalent enzyme is taken to represent a complex enzyme pathway or cycle in much the same way that an equivalent resistor represents the overall resistance of a resistance network (see Fig. 5.4). Alternatively, the equivalent enzyme can be viewed as the rate-limiting enzyme in an enzyme network. Irregardless, an equivalent or functional enzyme can be defined for each biochemical process and appropriate rate constants defined for the overall process rates for the relevant microbes.

The assumptions underlying enzyme kinetics have been given by Reiner (1969). The primary assumption of enzyme kinetics is that the enzyme and the substrate form a complex, and this compound then undergoes internal rearrangement, after which the reaction product and the original

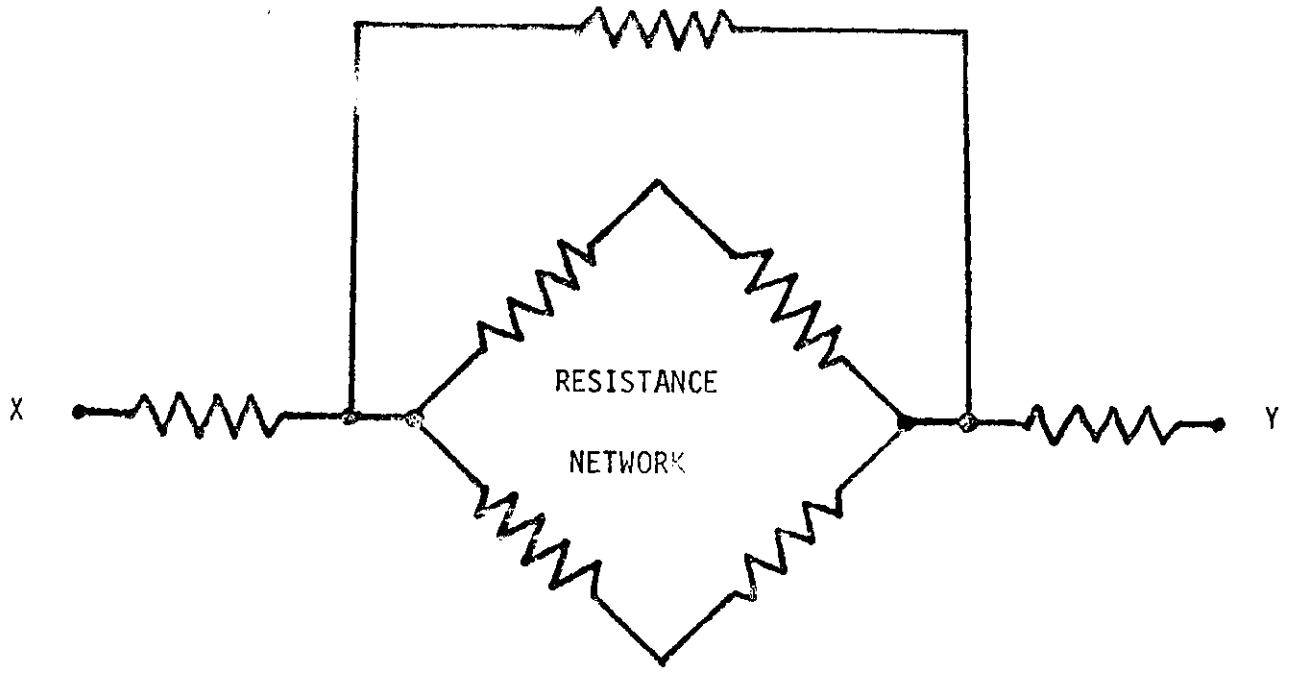

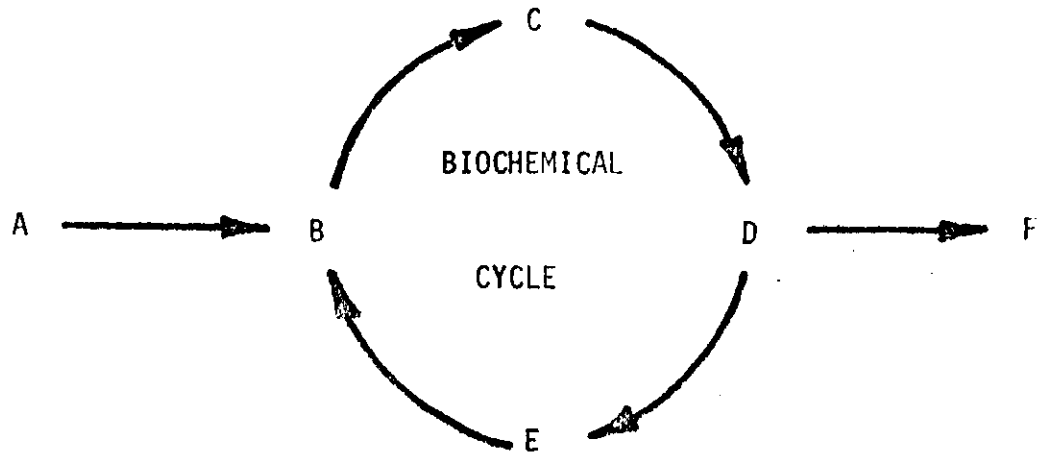

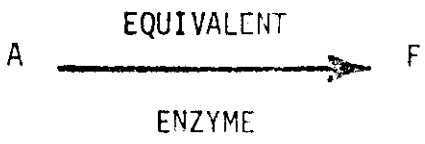

Figure 5.4 EQUIVALENT ENZYME CONCEPT

enzyme molecule are formed from the rearranged compound.

$$E + S \underset{\underline{k}_1}{\overset{k_1}{\rightleftharpoons}} C \qquad (7)$$

$$C \xrightarrow{k_2} E + P \qquad (8)$$

where E is the amount of free enzyme,

S is the amount of substrate,

C is the amount of complex,

P is the product formed, and

k_1, $\underline{k}_1$ and k_2 are the relevant rate constants.

As the total amount of enzyme is constant throughout the reaction period

$$E_t = E + C \qquad (9)$$

where E_t is the total amount of enzyme.

The rate reactions can be determined by applying the law of Mass Action which states that the rate of a reaction is proportional to the product of appropriate powers of the reactants' concentrations; the "appropriate powers" for each reactant is the number of molecules reacting according to the stoichiometric equation. For example, the rate of formation of C in equation (7) is:

$$\frac{\delta C}{\delta t} = k_1 . E . S . \qquad (10)$$

where K_1 is the proportionality or rate constant.

A number of enzyme schemes have been tried, and the following has been found applicable to the nitrogen model developed in this report. The enzyme systems used include:

a) a simple irreversible multi-complex scheme,

b) a complex reversible multi-valent, multi-complex scheme with two blind ends, and

c) a two substrate irreversible multi-complex scheme.

The general characteristics of the equivalent enzyme schemes given above and their assumptions will be reviewed before application to the actual nitrogen model.

a) Multiple Complexes

In this scheme, the following assumptions have been made:

i) A molecule of enzyme E and a molecule of substrate S_1 combine irreversibly to form a complex C_1.

ii) A molecule of complex C_1 combines irreversibly with a molecule of another substrate S_2 to form another complex C_2.

iii) Depending upon the enzyme system under study, more substrates S_i can irreversibly combine with complex C_{i-1} to form a higher complex C_i.

iv) The final complex C_n breaks up irreversibly, giving a molecule of product P and the original enzyme molecule E.

v) The forms of the enzyme are: free enzyme and enzyme incorporated into the various complexes.

vi) The amount of substrate which is bound to the enzyme is very small compared with the total amount of substrate present.

The stoichiometric scheme for the above system is:

$$E + S_1 \xrightarrow{k_1} C_1 \qquad (11)$$

$$C_1 + S_2 \xrightarrow{k_2} C_2 \qquad (12)$$

.....

$$C_{i-1} + S_i \xrightarrow{k_i} C_i \qquad (13)$$

.....

$$C_{n-1} + S_n \xrightarrow{k_n} C_n \qquad (14)$$

$$C_n \xrightarrow{k_{n+1}} E + P \qquad (15)$$

and $$E_t = E + \sum_1^n C_i \qquad (16)$$

This scheme can be solved for steady state conditions for n=2:

$$E + S_1 \xrightarrow{k_1} C_1 \qquad (17)$$

$$C_1 + S_2 \xrightarrow{k_2} C_2 \qquad (18)$$

$$C_2 \xrightarrow{k_3} E + P \qquad (19)$$

and $$E_t = E + C_1 + C_2 \qquad (20)$$

Solving for steady state:

$$\frac{\delta E}{\delta t} = k_3 C_2 - k_1 E S_1 = 0 \qquad (21)$$

$$\frac{\delta C_1}{\delta t} = k_1 E S_1 - k_2 C_1 S_2 = 0 \qquad (22)$$

$$\frac{\delta C_2}{\delta t} = k_2 C_1 S_2 - k_3 C_2 = 0 \qquad (23)$$

and $$E = Et - C_1 - C_2 \qquad (24)$$

Substituting equation (24) into (22),

$$k_1 S_1 E_t - K_1 S_1 C_1 - k_1 S_1 C_2 - k_2 C_1 S_2 = 0 \qquad (25)$$

$$C_2 = \frac{k_1 S_1 E_t - k_1 S_1 C_1 - k_2 C_1 S_2}{k_1 S_1} \qquad (26)$$

from equation (23)

$$C_1 = \frac{k_3 C_2}{k_2 S_2} \qquad (27)$$

Substituting (27) into (26),

$$C_2 = \frac{k_1 S_1 E_t - k_1 S_1 k_3 C_2 / k_2 S_2 - k_2 S_2 k_3 C_2 / k_2 S_2}{k_1 S_1} \qquad (28)$$

$$k_1 S_1 C_2 + \frac{k_1 S_1 k_3 C_2}{k_2 S_2} + \frac{k_2 S_2 k_2 C_2}{k_2 S_2} = k_1 S_1 E_t \qquad (29)$$

$$k_1 S_1 k_2 S_2 C_2 + k_1 S_1 k_3 C_2 + k_2 S_2 k_3 C_2 = k_1 S_1 k_2 S_2 E_t \qquad (30)$$

$$C_2 = \frac{k_1 k_2 S_1 S_2 E_t}{k_1 k_2 S_1 S_2 + k_1 k_3 S_1 + k_2 k_3 S_2} \qquad (31)$$

Now

$$\frac{\delta P}{\delta t} = k_3 C_2 \tag{32}$$

$$\frac{\delta P}{\delta t} = \frac{k_1 k_2 k_3 S_1 S_2 E_t}{k_1 k_2 S_1 S_2 + k_1 k_3 S_1 + k_2 k_3 S_2} \tag{33}$$

The steady state production rate is dependent upon the substrate concentrations, S_1 and S_2 and the total enzyme concentration E_t. The production rate is constant over time for any given input of S_1, S_2 and E_t.

b) Complex Multivalent Enzyme Scheme

In this scheme, the enzyme has more than one active site per molecule. The assumptions for the multiple complex scheme are applied to this enzyme scheme. A number of additional assumptions are also made:

a) The enzyme can combine with two molecules of substrates S_i at more than one site to give a double substrate - enzyme complex.

b) The second combination is reversible and the double substrate - enzyme complex does not engage in any other reactions. It forms a blind end.

$$C_{i-1} + S_i \xrightarrow{k_i} C_i \tag{34}$$

$$C_i + S_i \xrightarrow{k_i} C_{i+1} \qquad (35)$$

$$C_{i+1} \xrightarrow{k_{ni}} C_1 + S_i \qquad (36)$$

The simplest case of this enzyme scheme is as follows:

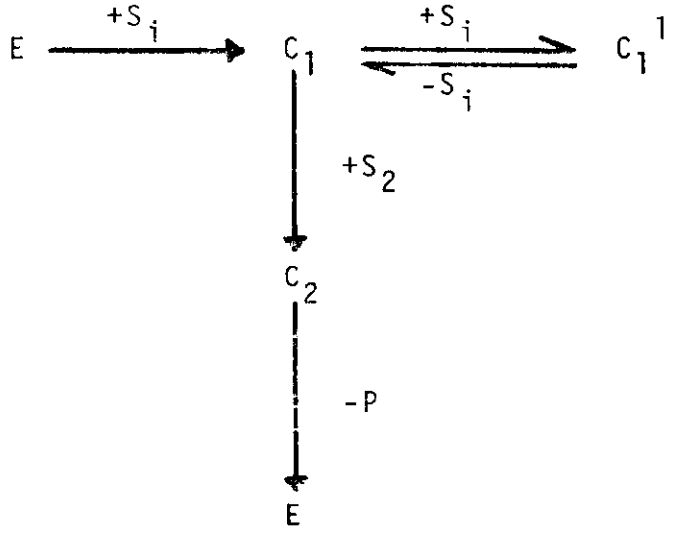

Writing the stoichiometric chemical equations:

$$E + S_1 \xrightarrow{k_1} C_1 \qquad (37)$$

$$S_1 + C_1 \xrightarrow{k_2} C_1^1 \qquad (38)$$

$$C_1^1 \xrightarrow{k_2^1} C_1 + S_1 \qquad (39)$$

$$C_1 + S_2 \xrightarrow{k_3} C_2 \qquad (40)$$

$$C_2 \xrightarrow{k_4} E + P \qquad (41)$$

and the conservation equation:

$$E_t = E + C_1 + C_1^1 + C_2 \qquad (42)$$

Solving these equations for steady state conditions:

$$\frac{\delta E}{\delta t} = k_4 C_2 - k_1 E S_1 = 0 \qquad (43)$$

$$\frac{\delta C_1}{\delta t} = k_1 E S_1 - k_2 S_1 C_1 + k_2^1 C_1^1 - C_1 K_3 S_2 = 0 \qquad (44)$$

$$\frac{\delta C_1^1}{\delta t} = k_2 S_1 C_1 - k_2^1 C_1^1 = 0 \qquad (45)$$

$$\frac{\delta C_2}{\delta t} = k_3 C_1 S_2 - k_4 C_2 = 0 \qquad (46)$$

and

$$E = E_t - C_1 - C_1^1 - C_2 \qquad (47)$$

Substituting (47) into (43):

$$k_4 C_2 - k_1 S_1 E_t + k_1 S_1 C_1 + k_1 S_1 C_1^1 + k_1 S_1 C_2 = 0 \qquad (48)$$

and from (45) and (46):

$$C_1^1 = \frac{k_2 S_1 C_1}{k_1^1} \tag{49}$$

and

$$C_1 = \frac{k_4 C_2}{k_3 S_2} \tag{50}$$

Substituting:

$$k_4 C_2 - k_1 S_1 E_t + \frac{k_1 S_1 k_4 C_2}{k_3 S_2} + \frac{k_1 S_1 k_2 S_1 k_4 C_2}{k_1^1 k_3 S_2} + k_1 S_1 C_2 = 0 \tag{51}$$

$$k_1^1 k_3 S_2 k_4 C_2 - k_1 S_1 E_t k_1^1 k_3 S_2 + k_1^1 k_1 S_1 k_4 C_2 + k_1 S_1 k_2 S_1 k_4 C_2$$

$$+ k_1^1 k_3 S_2 k_1 S_1 C_2 = 0 \tag{52}$$

$$C_2 = \frac{k_1 S_1 E_t k_1^1 k_3 S_2}{k_1^1 k_3 S_2 k_4 + k_1^1 k_1 S_1 k_4 + k_1 S_1 k_2 S_1 k_4 + k_1^1 k_3 S_2 k_1 S_1} \tag{53}$$

$$= \frac{k_1 k_1^1 k_3 S_1 S_2 E_t}{k_1^1 k_3 k_4 S_2 + k_1 k_1^1 k_4 S_1 + k_1 k_2 k_4 (S_1)^2 + k_1 k_1^1 k_3 S_1 S_2} \tag{54}$$

$$\frac{\delta P}{\delta t} = k_4 C_2 \tag{55}$$

$$= \frac{k_1 k_1^{1} k_3 k_4 S_1 S_2 E_t}{k_1 k_2 k_4 (S_1)^2 + k_1 k_1^{1} k_4 S_1 + k_1^{1} k_3 k_4 S_2 + k_1 k_1^{1} k_3 S_1 S_2} \quad (56)$$

This rate equation contains a second power of S_1 as well as the first.

Let $A = k_1 k_1^{1} k_3 k_4 S_2 E_t$ (57)

$B = k_1 k_2 k_4$ (58)

$C = k_1 k_1^{1} k_4$ (59)

$D = k_1^{1} k_3 k_4 S_2$ (60)

$E = k_1 k_1^{1} k_3 S_2$ (61)

Taking the derivative of the velocity equation; $v = \frac{\delta P}{\delta t}$, with respect to S:

$$v = \frac{AS_1}{B(S_1)^2 + (C+E)S_1 + D} \quad (62)$$

$$\frac{\delta v}{\delta S_1} = \frac{AD - AB(S_1)^2}{(B(S_1)^2 + (C+E)S_1 + D)^2} \quad (63)$$

Testing this equation for a maximum. The condition for a maximum is $\frac{\delta v}{\delta S} = 0$. One way for this equation to equal zero is for the numerator to be zero while the denominator remains finite.

Setting the numerator equal to zero

$$AD - AB(S_1)^2 = 0 \tag{64}$$

therefore

$$S_1 = \pm\sqrt{\frac{D}{B}} \tag{65}$$

Only the positive root need be considered as a negative concentration of S_1 has no meaning, thus

$$S_1 = \sqrt{\frac{k_1{}^1 \; k_3 S_2}{k_1 k_2}} \tag{66}$$

This equation indicates that the location of the maximum depends upon the ratio of $k_1{}^1$, k_3, k_1 and k_2 as well as the second substrate S_2 concentration. The fact that it is a function of the square root of S_2 is novel and was not expected. This is a case of autoinhibition - the inhibition of the enzyme by its own substrate. Reference to Figure 5.3 shows that autoinhibition occurs for both Nitrosomonas and Nitrobacter reactions of nitrification.

c) Two Substrate Irreversible Multi-complex Scheme

In this scheme, an equivalent enzyme can catalyse two competing reactions. A stoichiometric scheme for this system is as follows:

$$E + S_1 \xrightarrow{k_1} C_1 \tag{67}$$

$$C_1 + S_2 \xrightarrow{k_2} C_2 \tag{68}$$

$$C_2 \xrightarrow{k_3} E + P_1 \tag{69}$$

$$E + S_3 \xrightarrow{k_4} C_3 \tag{70}$$

$$C_3 + S_2 \xrightarrow{k_5} C_4 \tag{71}$$

$$C_4 \xrightarrow{k_6} E + P_2 \tag{72}$$

Solving these equations for steady state condition, the following is obtained:

$$\frac{\delta E}{\delta t} = k_3C_2 + k_6C_4 - k_1ES_1 - k_4ES_3 = 0 \tag{73}$$

$$\frac{\delta C_1}{\delta t} = k_1ES_1 - k_2C_1S_2 = 0 \tag{74}$$

$$\frac{\delta C_2}{\delta t} = k_2C_1S_2 - k_3C_2 = 0 \tag{75}$$

$$\frac{\delta C_3}{\delta t} = k_4 E S_3 - k_5 C_3 S_2 = 0 \qquad (76)$$

$$\frac{\delta C_4}{\delta t} = k_5 C_3 S_2 - C_4 k_6 = 0 \qquad (77)$$

and

$$E = E_t - C_1 - C_2 - C_3 - C_4 \qquad (78)$$

From equation (75) and (77):

$$C_1 = \frac{k_3 C_2}{k_2 S_2} \qquad (79)$$

$$C_3 = \frac{k_6 C_4}{k_5 S_2} \qquad (80)$$

Substituting into equation (78):

$$E = E_t - \frac{k_3 C_2}{k_2 S_2} - C_2 - \frac{k_6 C_4}{k_5 S_2} - C_4 \qquad (81)$$

$$E = E_t - C_2 \left(1 + \frac{k_3}{k_2 S_2} \right) - C_4 \left(1 + \frac{k_6}{k_5 S_2} \right) \qquad (82)$$

Substituting into equation (76):

$$k_4 S_3 E_t - k_4 S_3 C_2 \left(1 + \frac{k_3}{k_2 S_2} \right) - k_4 S_3 C_4 \left(1 + \frac{k_6}{k_5 S_2} \right)$$

$$- \frac{k_5 S_2 k_6 C_4}{k_5 S_2} = 0 \qquad (83)$$

$$C_2\left(k_4S_3 + \frac{k_3k_4S_3}{k_2S_2}\right) = k_4S_3E_t - C_4\left(k_4S_3 + \frac{k_4k_6S_3 - k_5S_2k_6}{k_5S_2}\right) \quad (84)$$

$$C_2 = \frac{k_4S_3E_t - C_4\left(k_4S_3 + \frac{k_4k_6S_3 - k_5S_2k_6}{k_5S_2}\right)}{k_4S_3 + \frac{k_3k_4S_3}{k_2S_2}} \quad (85)$$

Substituting into equation (74):

$$k_1S_1E_t - C_4\left(1 + \frac{k_6}{k_5S_2}\right)\Big) - \frac{k_2S_2k_3}{k_2S_2}C_2 - k_1S_1C_2\left(1 + \frac{k_3}{k_2S_2}\right) = 0 \quad (86)$$

$$k_1S_1E_t - k_1S_1C_4\left(1 + \frac{k_6}{k_5S_2}\right) - C_2\left(k_3 + k_1S_1\left(1 + \frac{k_3}{k_2S_2}\right)\right) = 0 \quad (87)$$

$$k_1S_1E_t - k_1S_1C_4\left(1 + \frac{k_6}{k_5S_2}\right) - \frac{\left[k_4S_3E_t + C_4\left(1 + \frac{k_6}{k_5S_2}\right)k_4S_3 + C_4k_6\right]\left(k_3 + k_1S_1\left(1 + \frac{k_3}{k_2S_2}\right)\right)}{k_4S_3 + \frac{k_3k_4S_3}{k_2S_2}} = 0 \quad (88)$$

$$k_1S_1E_tk_4S_3\left(1 + \frac{k_3}{k_2S_2}\right) - k_1S_1C_4k_4S_3\left(1 + \frac{k_3}{k_2S_2}\right)\left(1 + \frac{k_6}{k_5S_2}\right)$$

$$- k_4 S_3 E_t \left(k_3 + k_1 S_1 \left(\frac{1+k_3}{k_2 S_2} \right) + C_4 \left(\frac{1+k_6}{k_5 S_2} \right) k_4 S_3 \left(k_3 + k_1 S_1 \left(\frac{1+k_3}{k_2 S_2} \right) \right) + C_4 k_6 k_3 \right.$$

$$\left. + C_4 k_6 k_1 S_1 \left(\frac{1+k_3}{k_2 S_2} \right) \right) = 0 \qquad (89)$$

$$\cancel{k_1 S_1 k_4 S_3 E_t \left(\frac{1+k_3}{k_2 S_2} \right)} - \underline{k_1 S_1 C_4 k_4 S_3 \left(\frac{1+k_6}{k_5 S_2} \right) \left(\frac{1+k_3}{k_2 S_2} \right)}$$

$$- k_4 S_3 E_t k_3 - \underline{k_4 S_3 E_t k_1 S_1 \left(\frac{1+k_3}{k_2 S_2} \right)} + C_4 k_6 k_3$$

$$+ C_4 k_6 k_1 S_1 \left(\frac{1+k_3}{k_2 S_2} \right) + C_4 k_4 S_3 k_3 \left(\frac{1+k_6}{k_5 S_2} \right)$$

$$+ \underline{C_4 k_4 S_3 k_1 S_1 \left(\frac{1+k_6}{k_5 S_2} \right) \left(\frac{1+k_3}{k_2 S_2} \right)} = 0 \qquad (90)$$

$$k_4 S_3 E_t k_3 = C_4 \left(k_6 k_3 + k_6 k_1 S_1 \left(\frac{1+k_3}{k_2 S_2} \right) + k_4 k_3 S_3 \left(\frac{1+k_6}{k_5 S_2} \right) \right) \qquad (91)$$

$$C_4 = \frac{k_3 k_4 S_3 E_t}{k_6 k_3 + k_6 k_1 S_1 \left(\frac{1+k_3}{k_2 S_2} \right) + k_4 k_3 S_3 \left(\frac{1+k_6}{k_5 S_2} \right)} \qquad (92)$$

$$\frac{\delta P_2}{\delta t} = \frac{k_3 k_4 k_6 S_3 E_t}{k_6 k_3 + k_6 k_1 S_1 \left(1 + \frac{k_3}{k_2 S_2}\right) + k_4 k_3 S_3 \left(1 + \frac{k_6}{k_5 S_2}\right)} \quad (93)$$

A similar equation can be derived to describe the rate of production of P_1.

SUMMARY OF SECTION:

The enzyme rate equations have been applied to the nitrogen microbial metabolism reactions in the soil. Four equivalent enzymes have been defined: a) an Ammonifying equivalent enzyme, b) a Nitrosomonas equivalent enzyme, c) a Nitrotracter equivalent enzyme and d) a denitrifying equivalent enzyme. These equivalent enzymes have the following characteristics.

(a) they can interact with more than one substrate,

(b) they form multiple complexes,

(c) only some of the reactions are reversible, and

(d) the total amount of enzyme is conserved, i.e. the total amount of enzyme is equal to the amount of free enzyme plus the various complexes.

RESPONSES OF THE MODEL

The equations derived in this study were programmed in FORTRAN. The computer code has not been included in this report as the model is still developmental and requires adjustment and validation before it can be used as a management tool. The FORTRAN equations have been included in the report for those who

wish to include these segments of code in their soil computer models.

The FORTRAN equations and the responses of the model to varying environmental conditions are presented herein:

A) Ammonification

$$E1 + ORGN \xrightarrow{K1} C11 \quad (94)$$

$$O2 + C11 \xrightarrow{K2} C21 \quad (95)$$

$$C21 \xrightarrow{K3} NH4 + CO2 + H2O + E1 \quad (96)$$

$$E1 + C11 + C21 = E1T \quad (97)$$

where E1 represents the amount of uncomplexed equivalent enzyme,

ORGN is the concentration of organic nitrogen capable of enzymatic breakdown,

C11 is the amount of complex formed between E1 and ORGN,

O2 is the gaseous oxygen concentration adjacent to the microbe,

C21 is the amount of complex formed between C11 and O2,

and E1T is the total amount of equivalent enzyme per microbe.

Solving these sets of rate equations for steady state conditions, the rate of ammonium formation per microbe is equal to:

$$RNH4(1) = C21 * K3 * E1T \quad (98)$$

$$C21 = K1 * K2 * O2 * ORGN/D1 \quad (99)$$

$$D1 = K2 * K3 * O2 + K1 * K3 * ORGN + K1 * K2 * O2 * ORGN \quad (100)$$

The rate of ammonium formation DNH4 is:

$$DNH4(1) = RNH4(1)*B1 \quad (101)$$

where B1 is the number of microbes per unit volume of soil.

The response of equations (94-101) for varying oxygen and organic nitrogen concentrations is shown in Figures 5

and 6. The inputs to the equations are shown in Table 5.1 Variations in the constants K1, K2, K3 and E1T will change the position of these curves. Experimental data is needed to determine the values of these constants for various mineralizer species.

B) Nitrosomonas

$$INSOM + CA \xrightarrow{K4} NSOMAS \quad (102)$$

$$NSOMAS \xrightarrow{K5} CA + INSOM \quad (103)$$

$$NSOMAS + H \xrightarrow{K6} C12 \quad (104)$$

$$C12 + NH4 \xrightarrow{K7} C22 \quad (105)$$

$$C22 + O2 \xrightarrow{K8} C32 \quad (106)$$

$$C32 \xrightarrow{K9} NO2 + NSOMAS \quad (107)$$

$$C22 + H \xrightarrow{K10} C42 \quad (108)$$

$$C42 \xrightarrow{K11} C22 + H \quad (109)$$

$$C22 + NH4 \xrightarrow{K12} C52 \quad (110)$$

$$C52 \xrightarrow{K13} C22 + NH4 \quad (111)$$

$$NH4 \rightleftharpoons NH3 + H \qquad pK = 9.24 \quad (112)$$

$$INSOM + NSOMAS + C12 + C22 + C32 + C42 + C52 = E2T \quad (113)$$

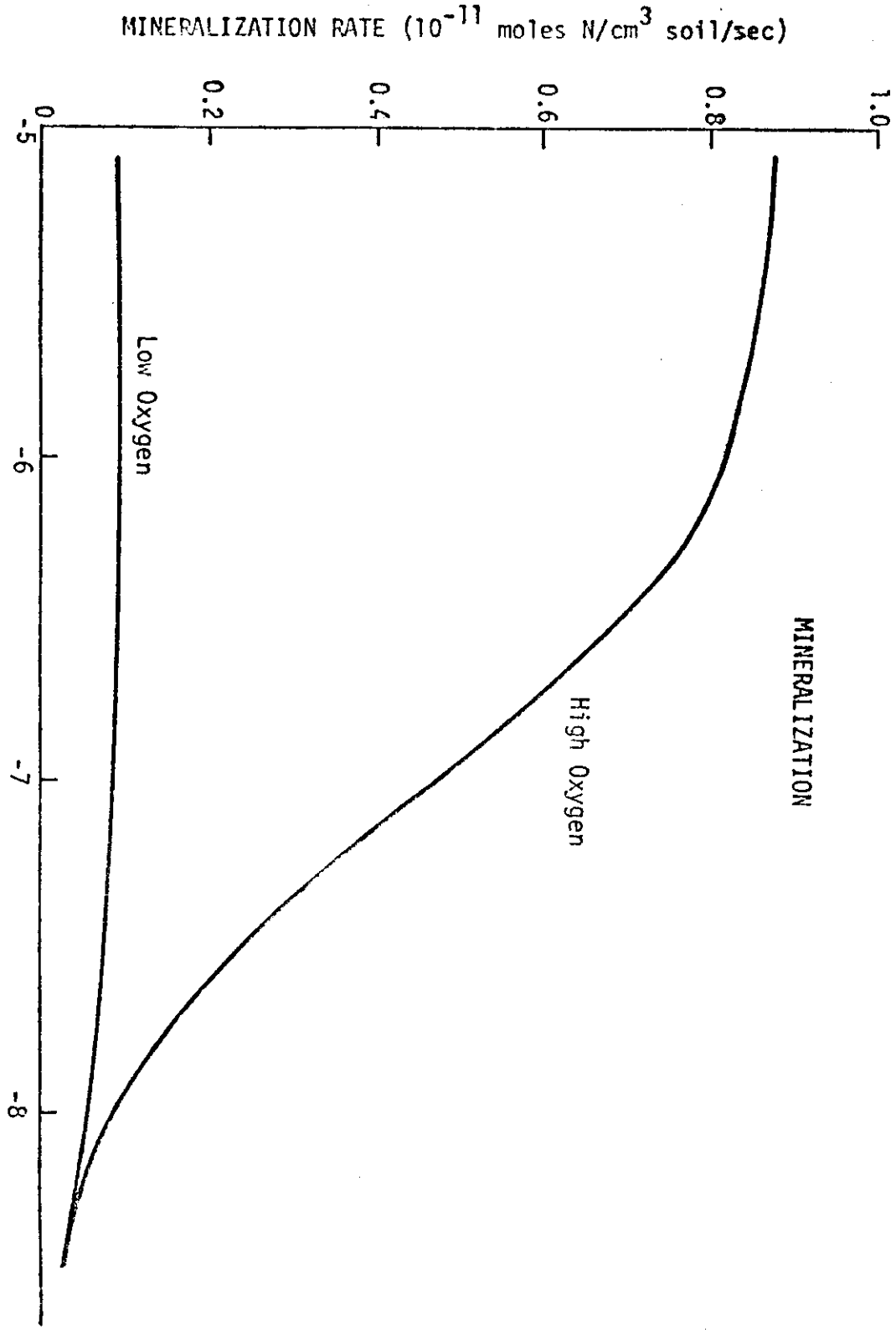

Figure 5.5 MINERALIZATION RATE AS A FUNCTION OF ORGANIC NITROGEN SUBSTRATE CONCENTRATION

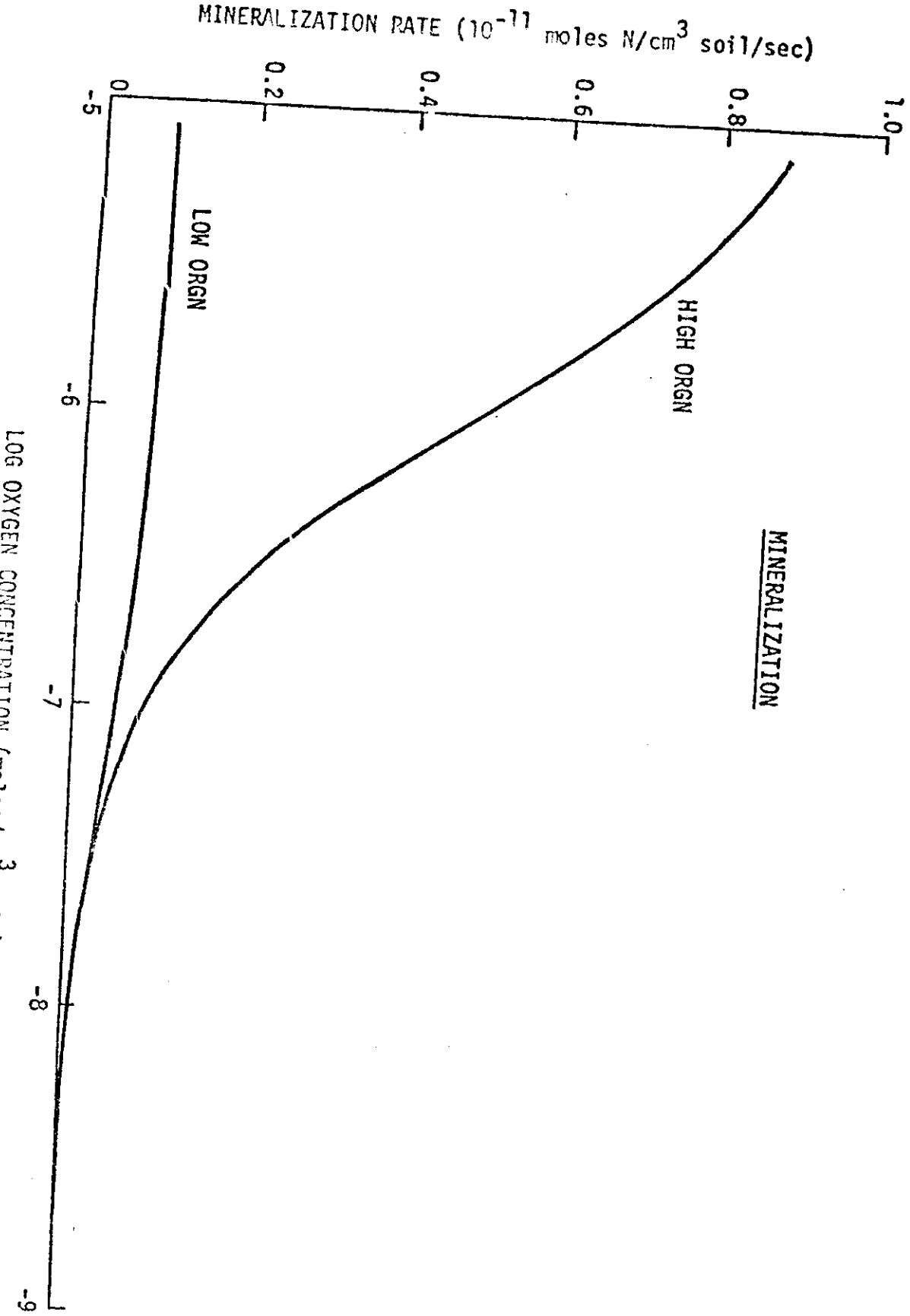

Figure 5.6 MINERALIZATION RATE AS A FUNCTION OF OXYGEN CONCENTRATION

Table 5.1 Values Of Constants Used In Mineralization Model

Symbol	Constant	Value	Units
K1	Rate constant	10^{+7}	$cm^3 moles^{-1} sec^{-1}$
K2	Rate constant	10^{+6}	$cm^3 moles^{-1} sec^{-1}$
K3	Rate constant	1	sec^{-1}
EIT	Equivalent Enzyme Conc.	10^{-19}	moles microbe^{-1}
ORGN	Organic Nitrogen Conc.	variable	moles cm^{-3}
High	--	$8X10^{-6}$	moles cm^{-3}
Low	--	10^{-8}	moles cm^{-3}
O2	Gaseous Oxygen Conc.	variable	moles cm^{-3}
High	--	$8X10^{-6}$	moles cm^{-3}
Low	--	10^{-8}	moles cm^{-3}
B1	Number of Mineralizing microbes	10^{+8}	microbes cm^{-3}

where

CA is calcium concentration,

NH4 is ammonium concentration,

H is hydrogen ion concentration,

INSOM is the inactive form of the equivalent enzyme,

NSOMAS is the active form of the equivalent enzyme,

C12 to C52 are the various enzyme - multiple substrate complexes,

NO2 is the amount of nitrite produced,

E2T is the total amount of microbial equivalent enzyme.

Solving these rate equations for steady state conditions where E2T does not increase (assuming no microbial growth or death), the result is:

```
NH4 = A*H*TOTAMN/(1.+A*H)                                    (114)
```

where A is a constant

and TOTAMN is the total amount of ammonia in either gaseous or ion form.

```
D2 = K5*K8*NH4*O2/(K4*K6)+K8*NH4*CA*O2/K6
   + K8*CA*H*O2/K7+NH4*CA*H+K8*NH4*CA*H*O2/K9
   + K10*NH4*CA*H*H/K11+K12*NH4*NH4*CA*H/K13                 (115)

C32 = K8*NH4*CA*H*O2/(D2*K9)                                 (116)
```

The rate of Nitrite formation per microbe, RNO2(1) is:

```
RNO2(1) = K9*C32*E2T                                         (117)
```

The total rate of nitrite formation DNO2(1) is:

$$DNO2(1) = RNO2(1) * B2 \qquad (118)$$

where B2 is the total number of Nitrosomonas organisms.

The output of the model of Nitrosomonas represented by these equations is shown in Figures 5.7 to 5.10. The inputs to these equations are shown in Table 5.2. H is calculated as a function of pH as follows:

$$H = 10.**(-3.-pH) \quad \text{moles cm}^{-3} \qquad (119)$$

The rate constants K_4 to K_{13} were set by taking a least squares difference between the experimental points of Meyerhof shown in Figures 5.7 and 5.8 and the values calculated from equation (116) normalized to its maximum.

The least squares difference has been optimized by using an optimization code developed by D.W. DeMichele. This code makes it possible to determine all the constants for both pH and total ammonium N simultaneously. As shown in the theoretical section the location of the maximum is dependent upon the concentration of the other substrates.

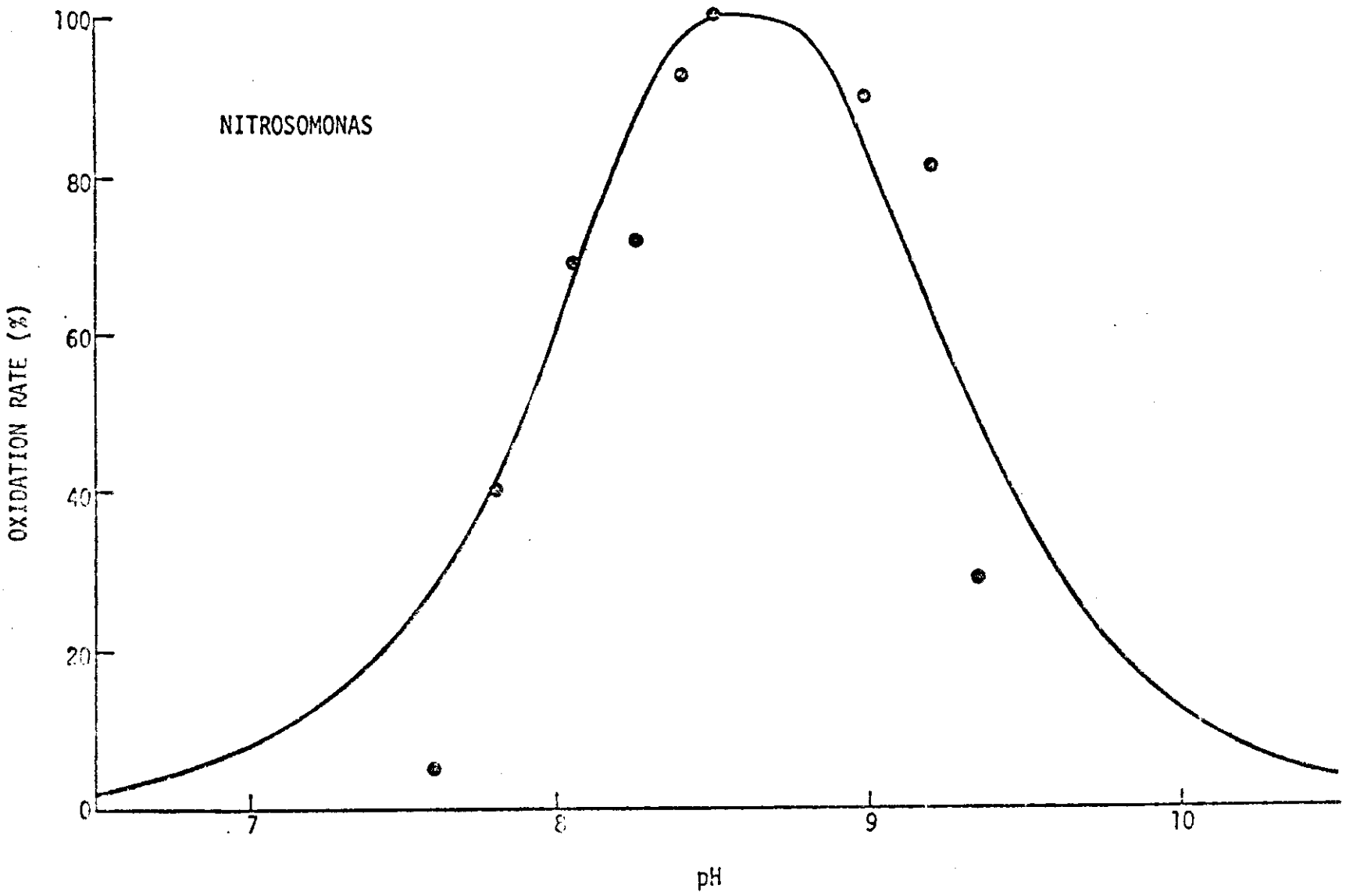

Figure 5.7 AMMONIUM OXIDATION RATE AS A FUNCTION OF pH. EXPERIMENTAL DATA OF MEYERHOF (1916).

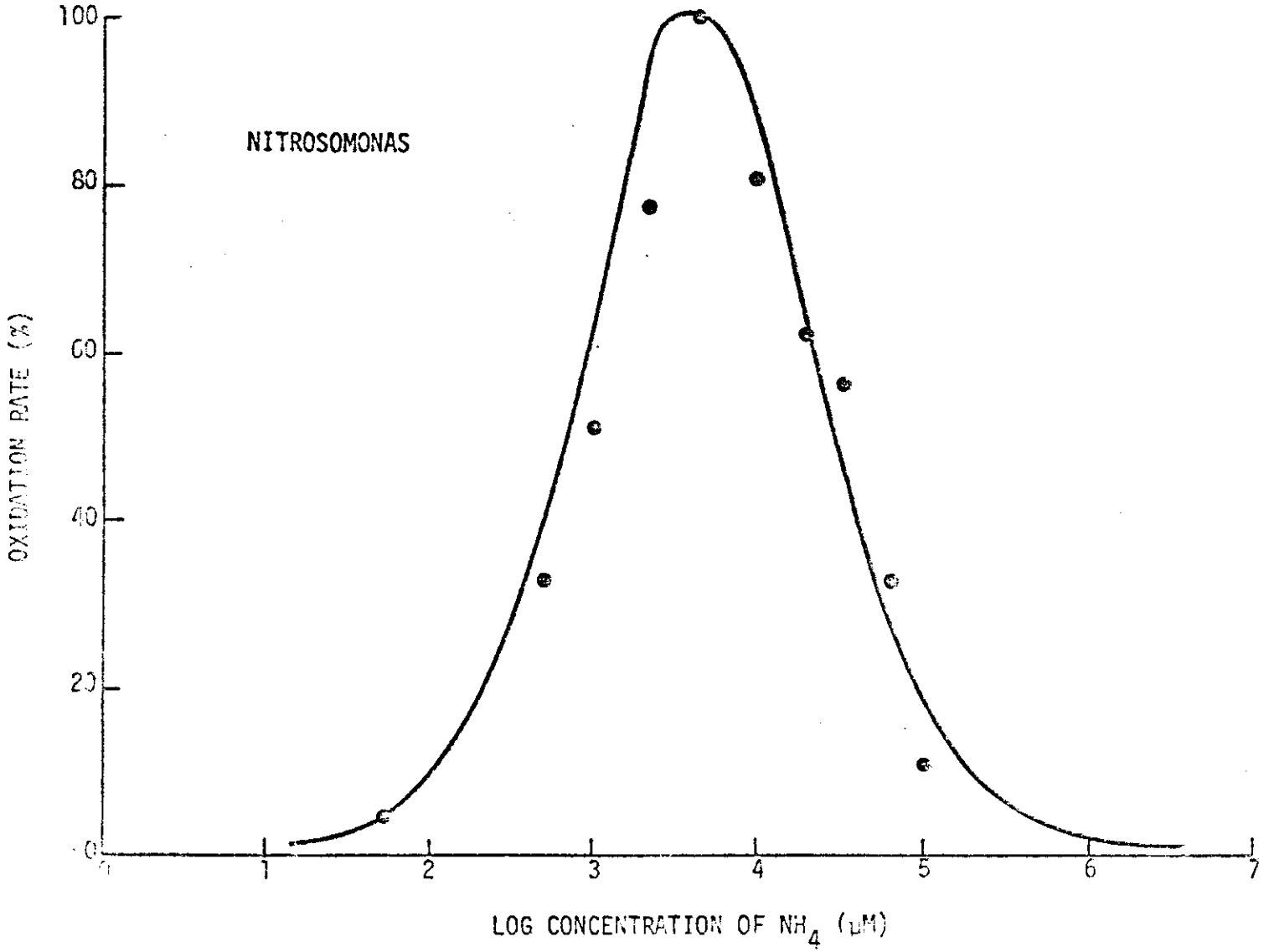

Figure 5.8 AMMONIUM OXIDATION RATE AS A FUNCTION OF AMMONIUM ION CONCENTRATION. EXPERIMENTAL DATA OF MEYERHOF (1916).

Table 5.2 Values Of Constants Used In Nitrosomonas Model

Symbol	Constant	Value	Units
K4	Rate constant	1.	$cm^3 moles^{-1} sec^{-1}$
K5	Rate constant	$.49 \times 10^{-5}$	sec^{-1}
K6	Rate constant	$.22 \times 10^{13}$	$cm^3 moles^{-1} sec^{-1}$
K7	Rate constant	10^6	$cm^3 moles^{-1} sec^{-1}$
K8	Rate constant	10^7	$cm^3 moles^{-1} sec^{-1}$
K9	Rate constant	$.17 \times 10^5$	sec^{-1}
K10	Rate constant	$.98 \times 10^{13}$	$cm^3 moles^{-1} sec^{-1}$
K11	Rate constant	1.	sec^{-1}
K12	Rate constant	$.41 \times 10^7$	$cm^3 moles^{-1} sec^{-1}$
K13	Rate constant	1.	sec^{-1}
A	Proportionality constant	1.7×10^{12}	--
E2T	Equivalent Enzyme Concentration	10^{-14}	moles microbe^{-1}
B2	Nitrosomonas density	10^3	microbes cm^{-3}
TOTAMN	Total Ammonium N concentration	variable	moles cm^{-3}
High		$.44 \times 10^{-6}$	moles cm^{-3}
Low			moles cm^{-3}

Table 5.2 Values Of Constants Used In Nitrosomonas Model

(CONTINUED)

Symbol	Constant	Value	Units
O2	Gaseous Oxygen concentration	variable	moles cm^{-3}
High		$8X10^{-6}$	moles cm^{-3}
Low			moles cm^{-3}
CA	Calcium ion concentration	variable	moles cm^{-3}
High		$1.2X10^{-3}$	moles cm^{-3}
Low		$1.2X10^{-5}$	moles cm^{-3}
pH	-Log 10 Hydrogen ion concentration	variable	-log moles $liter^{-1}$
optimum		8.5	-log moles $liter^{-1}$
H	Hydrogen ion concentration	calculated	moles cm^{-3}

The model response to oxygen and calcium ions is given in Figures 5.9 and 5.10. It can be seen that, for the given concentrations, the response to oxygen decrease is much more pronounced than that for calcium.

C) Nitrobacter

$$NBACTR + 2H \xrightarrow{K14} C13 \quad (120)$$

$$C13 + NO2 \xrightarrow{K15} C23 \quad (121)$$

$$C23 + O2 \xrightarrow{K16} C33 \quad (122)$$

$$C23 + H \xrightarrow{K17} C43 \quad (123)$$

$$C43 \xrightarrow{K18} C23 + H \quad (124)$$

$$C23 + NO2 \xrightarrow{K19} C53 \quad (125)$$

$$C53 \xrightarrow{K20} C23 + NO2 \quad (126)$$

$$C33 \xrightarrow{K21} NO3 + NBACTR \quad (127)$$

$$NBACTR + C13 + C23 + C33 + C43 + C53 = E3T \quad (128)$$

where

NBACTR is the active form of the equivalent enzyme

C13 to C53 are the various enzyme - multiple substrate complexes

NO2 is the concentration of nitrite

H is the hydrogen ion concentration, and

O2 is the gaseous soil oxygen concentration.

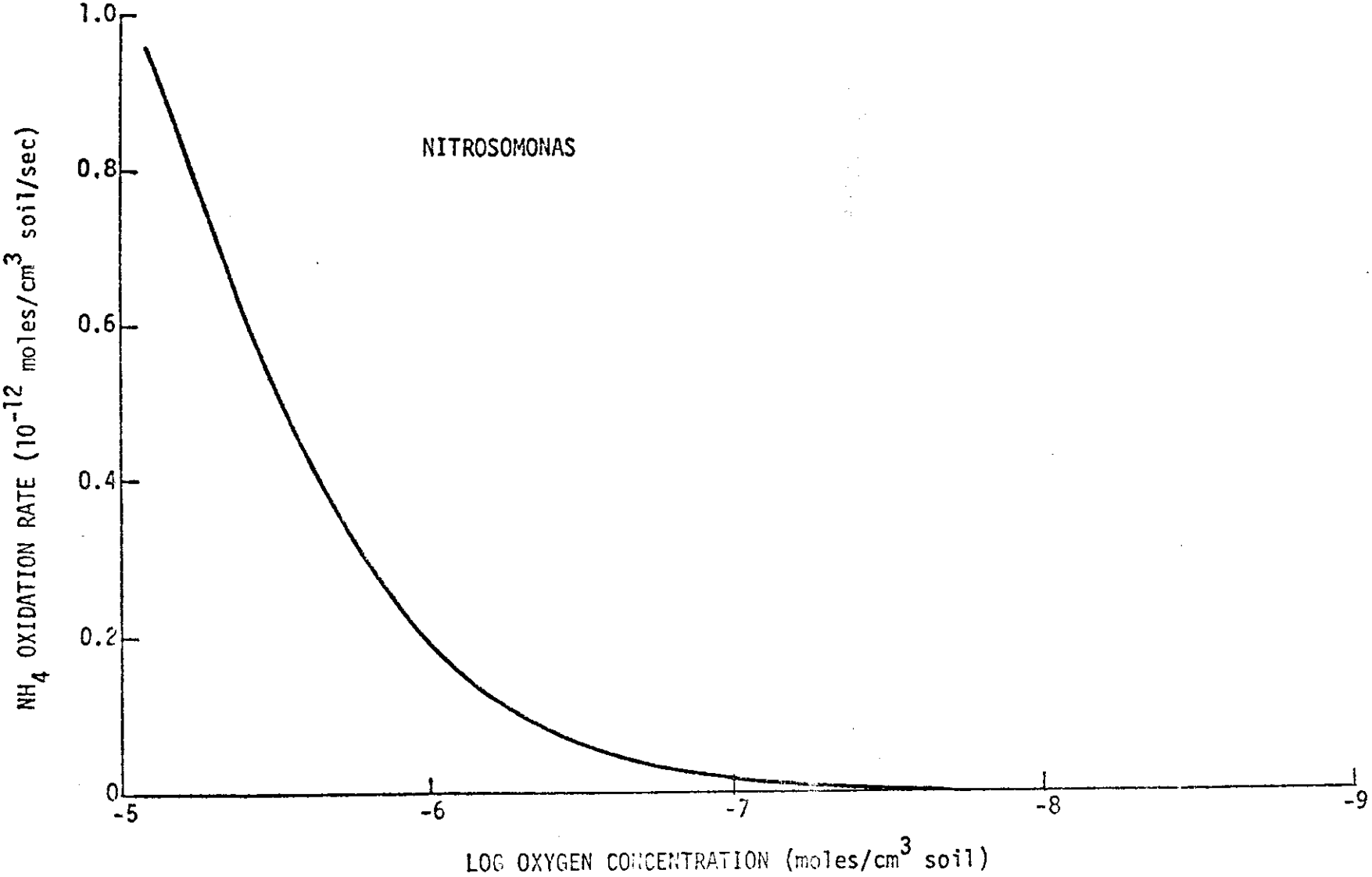

Figure 5.9 AMMONIUM OXIDATION RATE AS A FUNCTION OF OXYGEN CONCENTRATION.

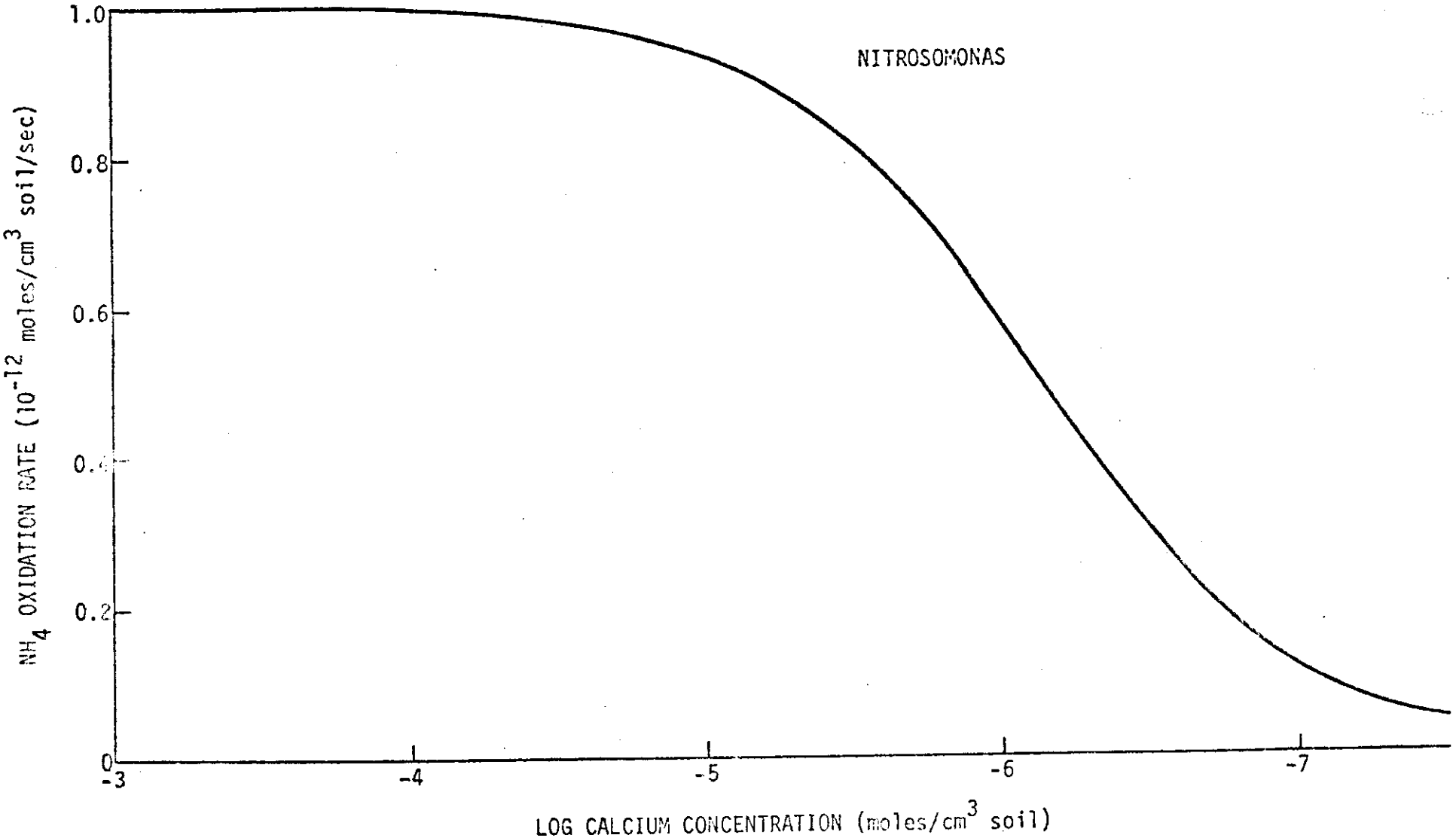

Figure 5.10 AMMONIUM OXIDATION RATE AS A FUNCTION OF CALCIUM CONCENTRATION.

The constants were optimized as described for Nitrosomonas using one hydrogen molecule in equation (120). It was not possible to obtain a good least squares fit between the model function and the experimental data of Meyerhof (1916 a,b) for pH sensitivity. When two molecules of H^+ in equation (120) were tried, a much better fit was obtainable. Reference to Figure 5.3 shows that the Nitrobacter response to pH is not symmetrical. Figure 5.11 shows the model response for both one and two hydrogen ions in reaction (120). The dotted line represents a one proton C13 complex and does not fit the data as well as the line representing a two proton C13 complex. In this case, attempting to model the system from a rather basic level has enabled a choice to be made between possible mechanisms.

The solution of equations (120) to (128) for steady state conditions (no growth or death) is:

```
D3=K16*O2*NO2/K14+K16*O2*H**2/K15
+NO2*H**2+K16*NO2*O2*H**2/K21
+K17*NO2*H**2/K18+K19*H**2*NO2**2/K20                    (129)

C33=K16*NO2*O2*H**2/(D3*K21)                             (130)

RNO3(1)=K21*C33*E2T                                      (131)

DNO3(1)=B3*RNO3(1)                                       (132)
```

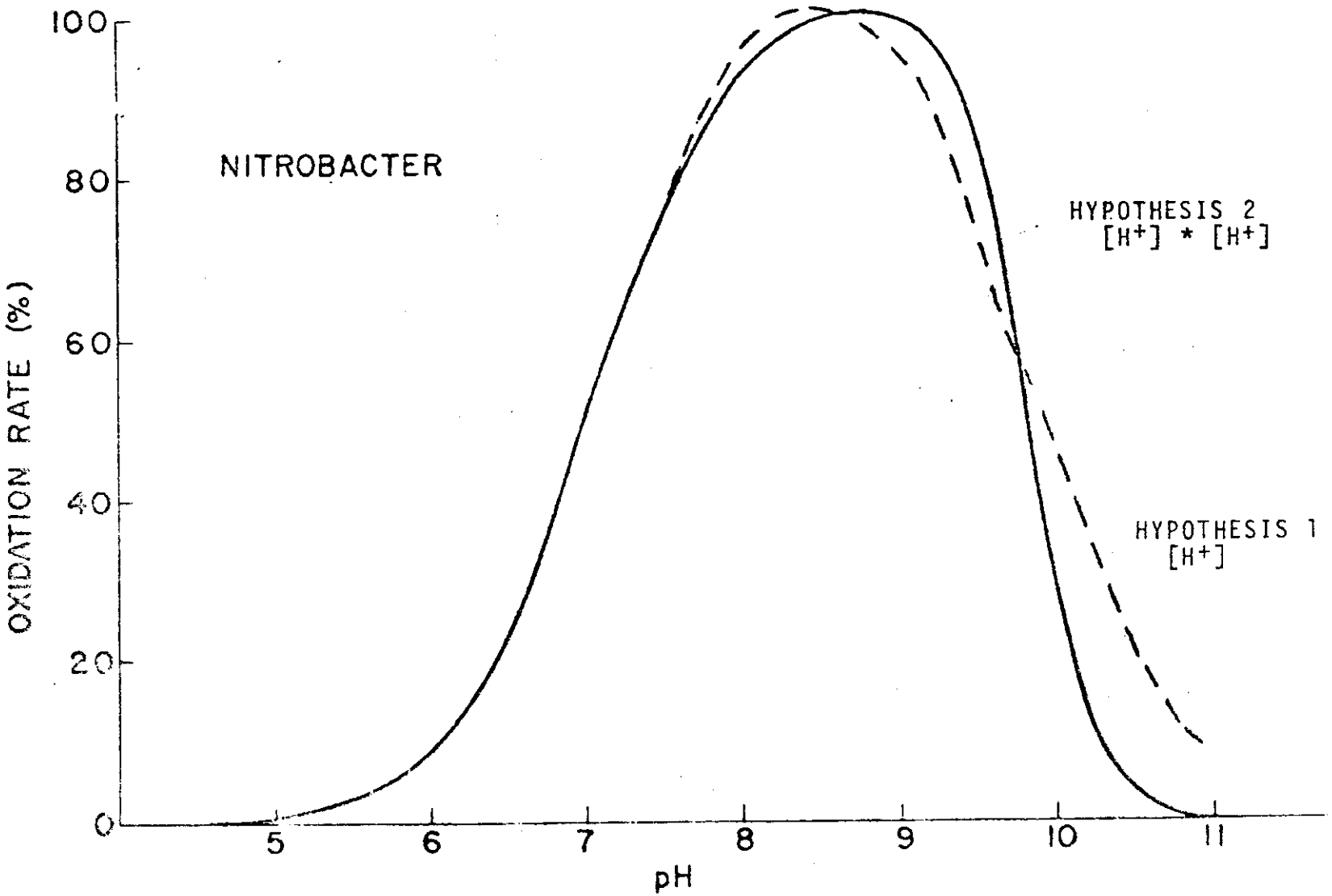

Figure 5.11 NITRITE OXIDATION RATE AS A FUNCTION OF pH FOR HYPOTHESES 1 AND 2.

where

B3 is the number of nitrobacter microbes per cubic centimeter of soil.

RNO3 is the rate of NO3 formation per nitrobacter microbe, and

DNO3 is the total rate of NO2 production per cm^3 of soil.

The model of Nitrobacter represented by these equations is shown in Figures 5.12 to 5.14. The inputs and constants for these equations are shown in Table 3. The hydrogen ion concentration is calculated using equation (119). The rate constants K14 to K21 were set using a least squares fit to Meyerhof's data. The fit to Meyerhof's data for pH and NO2 is shown in Figures 5.12 and 5.13, normalized to their maximum. It can be seen that there is good approximation between the experimental and model predictions. Figure 5.14 shows the hypothetical oxygen response resulting from using the values given in Table 5.3 This graph needs experimental verification for the inputs given.

D) Denitrification

In this system, the microbes are facultative anaerobes and can use NO3 in place of O2 as an electron acceptor. In this case, an equivalent enzyme system exists with effectively two substrates, the oxygen having a

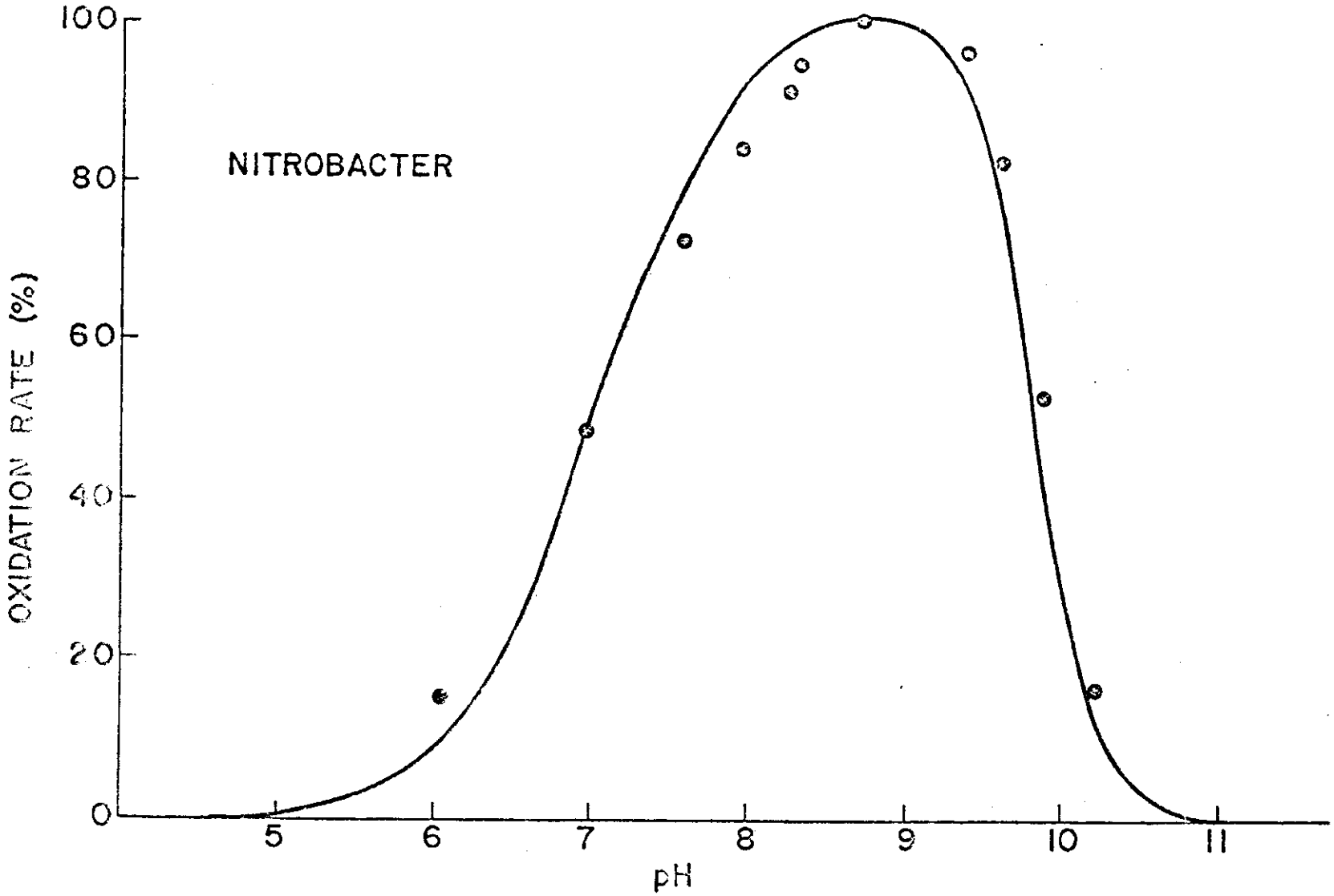

Figure 5.12 NITRITE OXIDATION RATE AS A FUNCTION OF pH.

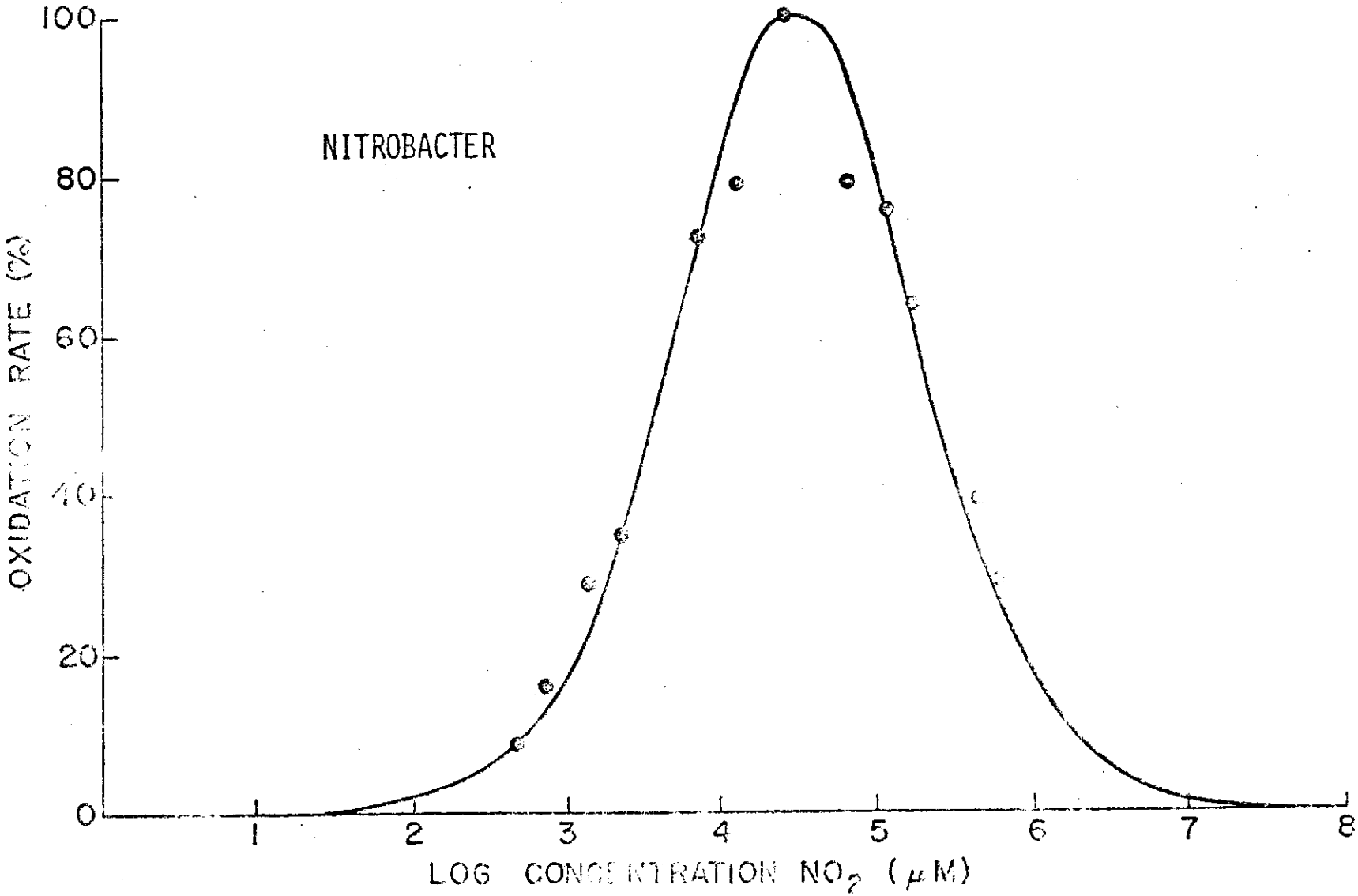

Figure 5.13 NITRITE OXIDATION RATE AS A FUNCTION OF NITRITE SUBSTRATE CONCENTRATION.

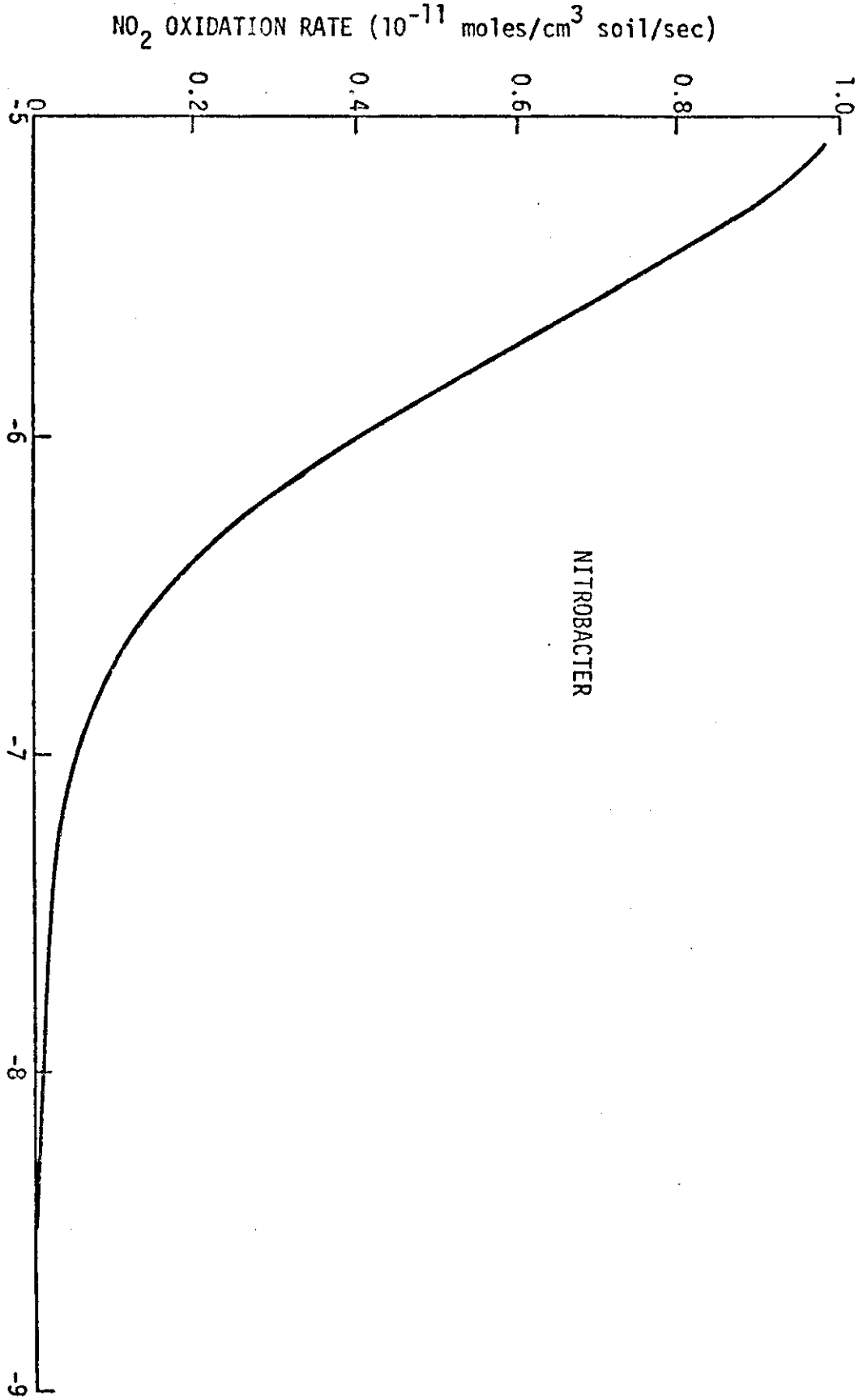

Figure 5.14 NITRITE OXIDATION RATE AS A FUNCTION OF OXYGEN CONCENTRATION

Table 5.3 Values Of Constants Used In Nitrobacter Model

Symbol	Constant	Value	Units
K14	Rate constant	$.4X10^{26}$	$cm^3 moles^{-1} sec^{-1}$
K15	Rate constant	$.2X10^{6}$	$cm^3 moles^{-1} sec^{-1}$
K16	Rate constant	$.3X10^{7}$	$cm^3 moles^{-1} sec^{-1}$
K17	Rate constant	$.25X10^{12}$	$cm^3 moles^{-1} sec^{-1}$
K18	Rate constant	1.	sec^{-1}
K19	Rate constant	$.12X10^{6}$	$cm^3 moles^{-1} sec^{-1}$
K20	Rate constant	1.	sec^{-1}
K21	Rate constant	1.6	sec^{-1}
E3T	Equivalent Enzyme Concentration	10^{-14}	moles microbe^{-1}
B2	Nitrobacter density	10^{3}	microbes cm^{-3}
NO2	Nitrite concentration	variable	moles cm^{-3}
High		$.27X10^{-4}$	moles cm^{-3}
Low			
pH	-Log 10 Hydrogen Ion Concentration	variable	-log moles liter^{-1}
optimum		8.7	-log moles liter^{-1}
H	Hydrogen Ion Concentration	calculated	moles cm^{-3}
O2	Gaseous Oxygen Concentration	variable	moles cm^{-3}
High		8X10	moles cm^{-3}
Low			

greater affinity for the enzyme than NO3. The stoichiometric equations used in the model were as follows:

ANAEROBIC

$$\text{DENITR} + \text{NO3} \xrightarrow{K22} \text{C14} \quad (133)$$

$$\text{C14} + \text{CARB} \xrightarrow{K23} \text{C24} \quad (134)$$

$$\text{C24} \xrightarrow{K24} \text{N2} + \text{O2} + \text{DENITR} \quad (135)$$

AEROBIC

$$\text{DENITR} + \text{O2} \xrightarrow{K25} \text{CC14} \quad (136)$$

$$\text{CC14} + \text{CARB} \xrightarrow{K26} \text{CC24} \quad (137)$$

$$\text{CC24} \xrightarrow{K27} \text{CO2} + \text{DENITR} \quad (138)$$

$$\text{E4T} = \text{DENITR} + \text{C14} + \text{C24} + \text{CC14} + \text{CC24} \quad (139)$$

where

DENITR is the concentration of free enzyme

NO3 is the nitrate concentration

C14 and C24 are the anaerobic enzyme - substrate complexes

CC14 and CC24 are the aerobic enzyme - substrate complexes

CARB is the carbohydrate concentration, and

E4T is the equivalent facultative denitrification enzyme concentration.

Table 5.4 Values Of Constants Used In Denitrification Model

Symbol	Constant	Value	Units
K22	Rate constant	10^{-6}	$cm^3 moles^{-1} sec^{-1}$
K23	Rate constant	10^{-6}	$cm^3 moles^{-1} sec^{-1}$
K24	Rate constant	10^{-6}	sec^{-1}
K25	Rate constant	10^{-4}	$cm^3 moles^{-1} sec^{-1}$
K26	Rate constant	10^{-6}	$cm^3 moles^{-1} sec^{-1}$
K27	Rate constant	10^{-11}	sec^{-1}
E4T	Equivalent Enzyme concentration	10^{-7}	moles $microbe^{-1}$
B4	Facultative Denitrifier Density	10^{+7}	microbes cm^{-3}
NO3	Nitrate concentration	variable	moles cm^{-3}
High		$8X10^{-6}$	moles cm^{-3}
Low		10^{-7}	moles cm^{-3}
O2	Soil Air Oxygen concentration	variable	moles cm^{-3}
High		$8X10^{-5}$	moles cm^{-3}
Low		10^{-12}	moles cm^{-3}
CARB	Soil Carbohydrate concentration	variable	moles cm^{-3}
High		$8X10^{-6}$	moles cm^{-3}
Low		10^{-7}	moles cm^{-3}

The constants were chosen to give reasonable responses. These constants are shown in Table 5.4 The greater affinity of the equivalent enzyme to oxygen over nitrate is shown by the ratio of K22 to K25. The affinity for oxygen is 500 times greater. Due to the other reactions however, the maximum rate of aerobic respiration is three and a half times greater than the anaerobic NO3 respiration for equivalent concentrations of substrate. The change over from aerobic respiration to anaerobic NO3 respiration as oxygen concentration is decreased is shown in Figure 5.15 The higher maximum rate of aerobic respiration is the result of the greater enzyme affinity for oxygen over nitrate. Figure 5.14 shows the denitrification response to NO3 concentration for low oxygen - high carbohydrate concentrations. Also shown are the responses for high O2 - high carbohydrate and high O2 - low carbohydrate. These responses need experimental refinement to accurately adjust the constants. The overall response of facultative use of NO3 in place of O2 in respiration is shown by the model.

Total System Response

The individual components of the model have been described, but the model lacks immobiliation of nitrogen

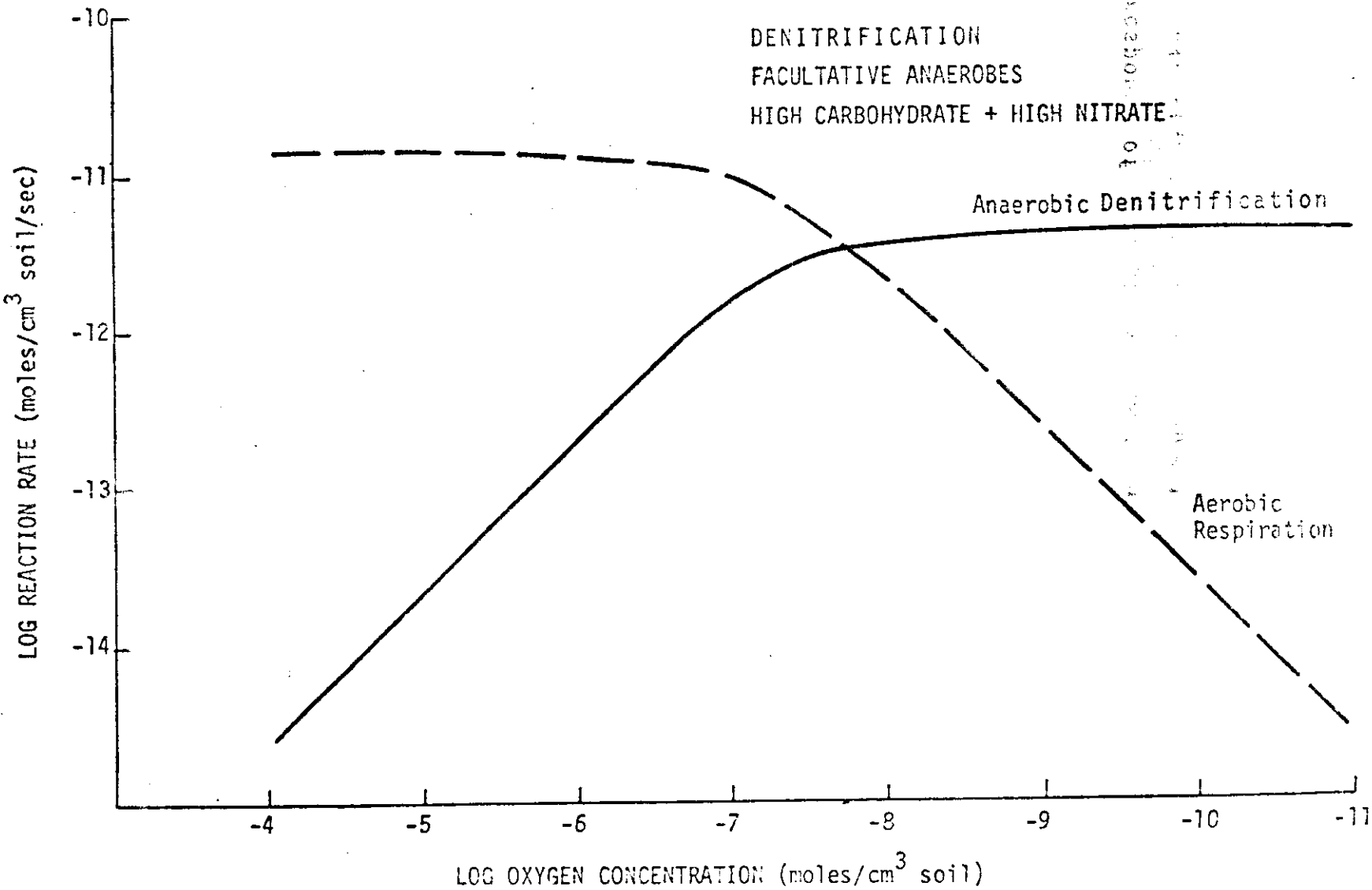

Figure 5.15 DENITRIFICATION RATE OF FACULTATIVE ANAEROBES AS A FUNCTION OF OXYGEN CONCENTRATION.

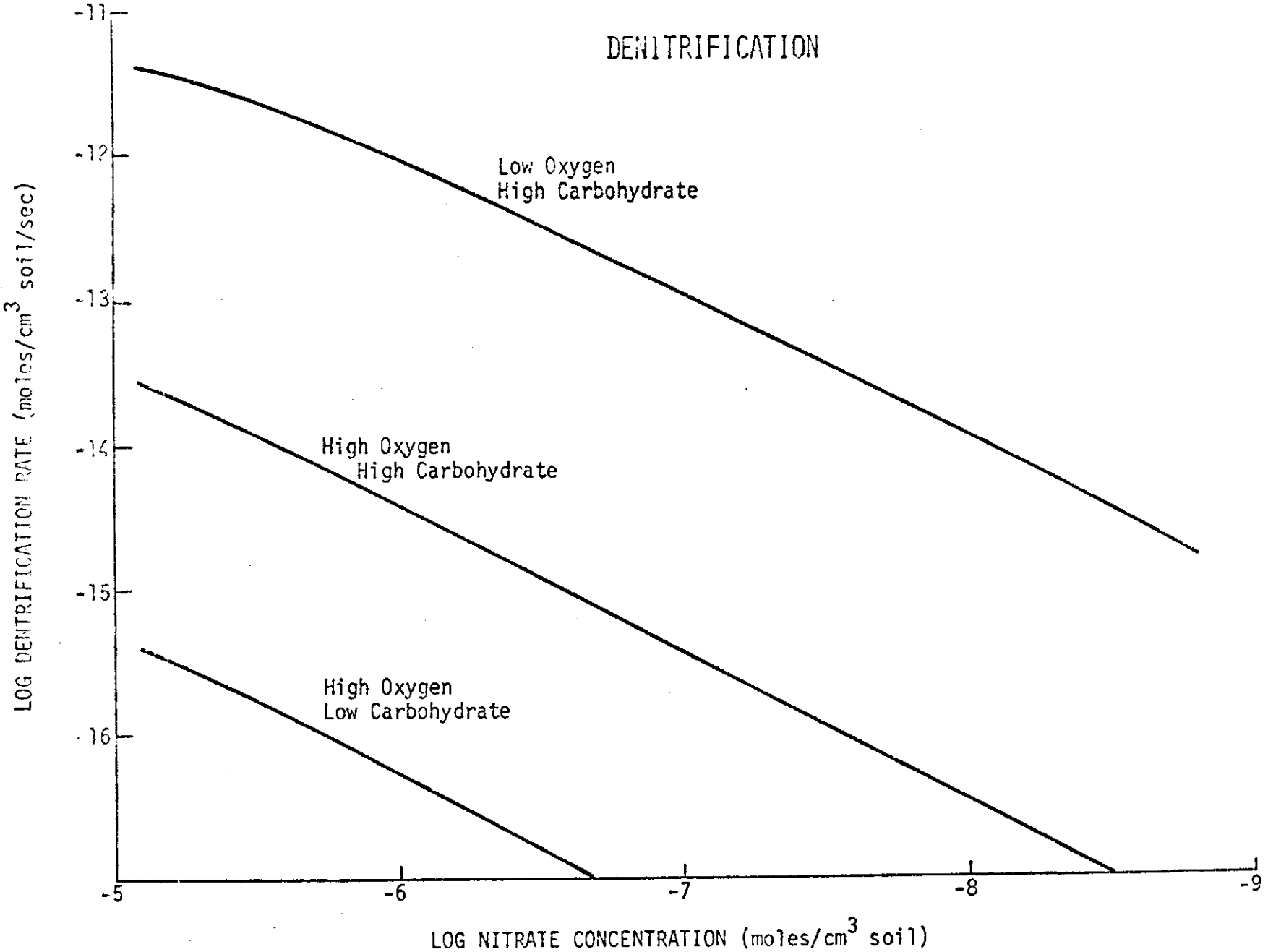

Figure 5.16 DENITRIFICATION RATE OF FACULTATIVE ANEROBES AS A FUNCTION OF NITRATE CONCENTRATION.

which is an important aspect of the model. For this reason the response of the total system has not been incorporated in this report. The model needs revision to include microbial growth, death, and decomposition. This addition will create the possiblity of immobilization of nitrogen during parts of the growing season. An additional feature which could be included into the revised model is the temperature sensitivity of the rate constants to follow the Arnhenius equation together with the thermal stability of the equivalent enzymes. The catalytic properties of the enzymes are sensitive to reversible and irreversible thermal denaturation. The equations describing the thermal properties of enzyme kinetics have been developed by Sharpe and DeMichele (1974) and are available in an unpublished manuscript.

Other aspects which need to be incorporated into the model are microbes' sensitivity to low soil water potentials. Below -8 bars, Seifert (1969) found that the rate of nitrification decreased significantly. It would be possible in the code to render an increasing number of enzymes inactive as the soil water potential decreases. However, it is difficult to incorporate into the model the exact mechanism of water potential inhibition of nitrification when no conceptual framework exists.

CONCLUSIONS AND RECOMMENDATIONS

This study formulates the theoretical structure of a model to describe the reaction kinetics of interlocking Nitrogenous transformations in the soil. To further advance the modeling of soil nitrogen metabolism, an indepth experimental program needs to be established to determine the temperature dependent rate constants of the competing reactions. After these rate constants have been established, a combined modeling-experimental program should be established to explore the dynamics of the system. The model will help to overcome some of the experimental difficulties while at the same time the experimental program will help to validate the model. A realistically structured model would help to identify the parameters which are critical and therefore should be monitored or measured, and which parameters are of minor significance. The model can provide insight into the interrelations of the various competing symbiotic reactions, thereby giving greater significance to some measurements than would be immediately obvious. The experimental program would in turn reinforce parts of the model and cast light on the underlying mechanisms involved.

The current research interest in the soil nitrogen transformations has gained impetus due to the need to reduce nitrate pollution of rivers and streams. A realistic model of these

transformations would enable management strategies to be tested on the computer for a wide variety of conditions and restraints. However, the development of a realistic model is not an easy task. The system has certain aspects which are difficult to describe mathematically; the numbers of organisms involved are immense; and the environmental conditions beneath the soil are difficult to measure. This complexity suggests that an experimental or theoretical approach taken in isolation for the other is unlikely to be successful.

During the development of the model, the population dynamics of the microorganisms were linked to the biochemical energetics of the mineralizers, nutrifiers and denitrifiers. The resulting mathematical model was unstable due to the delayed feedback of decaying microorganisms from a population mortality term to a substrate growth factor. Fig. 5.17 shows a schematic of the population dynamics of soil nitrogen microorganisms. The solid lines show the parts of the system which can be mathematically described as being in quasi-steady-state with the soil environment. The dashed line portion however, has an inbuilt time delay which distorts a quasi-steady state formulation. A similar problem has been encountered in modeling the population dynamics of the boll weevil in cotton. In this case, popu-

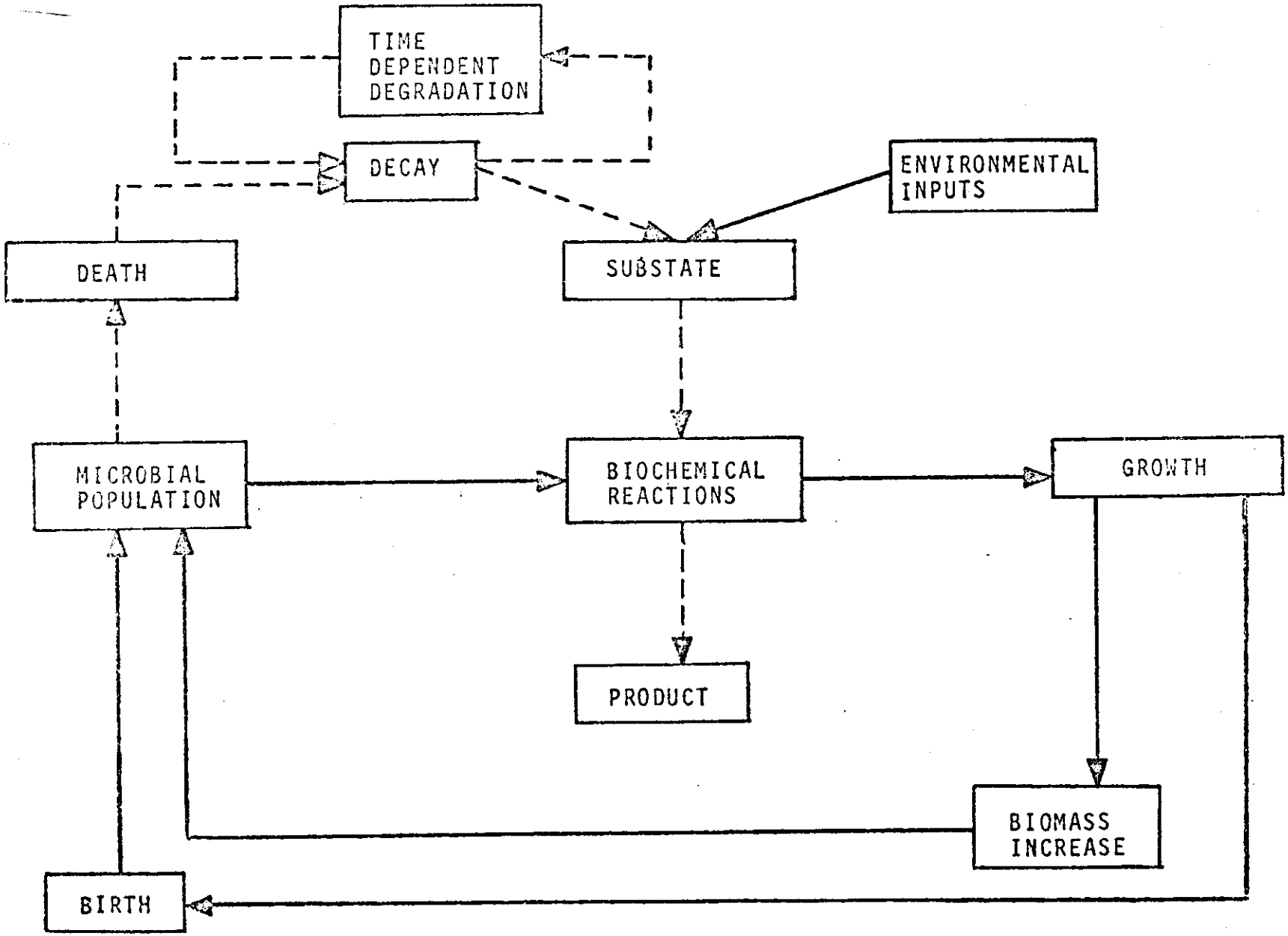

Figure 5.17 SCHEMATIC OF POPULATION DYNAMICS OF SOIL NITROGEN MICROORGANISMS

lation increase has a time delay during the larval growth period within the cotton bud. This problem has been resolved by an indepth model of boll weevil development, reproduction and mortality. (Curry, DeMichele and Sharpe, 1973-4). Equations of the Lofka-Volterra (1916) type were found unsuitable to describe this system. Instead, models of boll weevil metabolism and physiology were developed to describe the life cycle of the boll weevil and its interaction with the environment. A similar biophysical approach may be applicable to the organisms involved in nitrogen mineralization, nitrification and demtrification.

Acknowledgements

Thanks are due to Dr. Wally Curtis who helped with the programming and Dr. Aubrey Harvey for helpful discussions on population dynamics.

REFERENCES

Bingham, F.T., Davis, S., and Shade, E. 1971. Water Relations, salt balance and nitrate leaching losses of a 900-acre citrus watershed. Soil Science 112: 410-418.

Bremner, J.S., 1967. Nitrogenous compounds. In. Soil Biochemistry (Ed. McLaren, A.D. and Peterson, G.H.) Marcel Dekker N.Y. p. 19-66.

Buckman, H.O., and Brady, N.C. 1961. The Nature and Properties of Soils. MacMillan Company, N.Y.

Curry, G. L., D. W. DeMichele and P. J. H. Sharpe, 1973, Annual Report Biosystems Resaech Group, Texas A&M University College Station, Texas, 77843.

Dutt, G.R., and Shaffer, M.J. 1972. A computer model for predicting nitrate and other solutes of agricultural drain water. Final Report on Contract No. 14-06-D-7328 To: U.S. Dept. Interior. Bureau of Reclamation. June 1972.

Dutt, G.R., and Shaffer, M.J., and Moore, W.J. 1972. Computer simulation model of dynamic bio-physicochemical processes in soil. Tech. Bull. 196, Agr. Exp. Station. University of Arizona. 101 pp.

Greenwood, D. J., 1962, Plant Soil, Vol. 17, p. 365.

Huttori, Tsutomu. 1973. Microbial Life in the Soil. Marcel Dekker Inc., N.Y.

Lewis, P.R., and Kinshelwood, C.N. 1948. J. Chem. Soc. pp. 824-847.

Mehran, M., and Tanji, K.K. 1973. Computer modeling of nitrogen transformations in soils. Presented at American Society of Agronomy, Nov. 14, 1973. Las Vegas, Nevada.

Meyerhof, O. 1916. Pfluger's Arch. ges. Physiol., 164: 353-427; 165: 229-284.

Reiner, J.M. 1969. Behaviour of Enzyme Systems. Van Nostrand Reinhold Co., N.Y.

Sacks, L.E., and Barker, H.A. 1949. J. Bact., 58: 11-22

Seifert, J. 1969. Acta Univ. Carol., Biol., 353

Sharpe, P.J.H., and DeMichele, D.W. 1974. A Morphological and Physiological Model of the Leaf. Trans. ASAE (in press).

Sharpe, P.J.H. 1973. A Cellular Model of Leaf and Stomatal Metabolism. Symposium on application of systems methods to crop production, sponsored by Mississippi Agricultural and Forestry Experiment Station and Mississippi Departments of Agronomy and Entomology. Mississippi State. June 7-8, 1973.

Viets, F.G., and Hageman, R.H. 1971. Factors affecting the accumulation of nitrate in soil, water and plants. Agriculture Handbook No. 413. ARS-USDA.